FREQUENCY RESPONSE IN SHORT THERMOCOUPLE WIRES

Final Report
April 1989 - June 1992

L. J. Forney
E. L. Meeks
J. Ma

Georgia Institute of Technology
Atlanta, Georgia 30332

G. C. Fralick

NASA - Lewis Research Center
Cleveland, Ohio 44135

Sponsored by

ARNOLD ENGINEERING DEVELOPMENT CENTER
Arnold Air Force Base, Tennessee 37389

under

NASA Cooperative Agreement NCC 3-135

Georgia Institute of Technology
October, 1992

Frequency Response in Short Thermocouple Wires

L. J. Forney [1]

E. L. Meeks [2]

J. Ma [3]

Georgia Institute of Technology

Atlanta, Georgia 30332

G. C. Fralick

NASA - Lewis Research Center

Cleveland, Ohio 44135

[1] School of Chemical Engineering

[2] Microelectronics Research Center

[3] School of Mechanical Engineering

ABSTRACT

Theoretical expressions are derived for the steady-state frequency response of a thermocouple wire. In particular, the effects of axial heat conduction are demonstrated for a non-uniform wire with unequal material properties and wire diameters across the junction. The amplitude ratio at low frequency $\omega \to 0$ agrees with the results of Scadron and Warshawsky (1952) for a steady-state temperature distribution. Moreover, the frequency response for a non-uniform wire in the limit of infinite length $l \to \infty$ is shown to reduce to a simple expression that is analogous to the classic first order solution for a thermocouple wire with uniform properties.

Theoretical expressions are also derived for the steady-state frequency response of a supported thermocouple wire. In particular, the effects of axial heat conduction are demonstrated for both a supported one material wire and a two material wire with unequal material properties across the junction. For the case of a one material supported wire, an exact solution is derived which compares favorably with an approximate expression that only matches temperatures at the support junction. Moreover, for the case of a two material supported wire, an analytical expression is derived that closely correlates numerical results.

Experimental measurements are made for the steady-state frequency response of a supported thermocouple wire. In particular, the effects of axial heat conduction are demonstrated for both a supported one material wire (type K) and a two material wire (type T) with unequal material properties across the junction. The data for the amplitude ratio and phase angle are correlated to within 10% with the theoretical predictions of Forney and Fralick (1991). This is accomplished by choosing a natural frequency ω_n for the wire data to correlate the first order response at large gas temperature frequencies. It is found that a large bead size, however, will increase the amplitude ratio at low frequencies but decrease the natural frequency of the wire. The phase angle data are also distorted for imperfect junctions.

PREFACE

The work reported herein was sponsored by the Air Force Systems Command (AFSC) under NASA cooperative agreement NCC 3-135 for the Arnold Engineering Development Center (AEDC), AFSC, Arnold Air Force Station, Tennessee. The contract officers are Ms. Marjorie Collier and Captain Hal Martin for the Directorate of Technology (DOT), AFSC. The authors also wish to acknowledge the support of Dr. W. D. Williams, head of the Research Sensor Technology Branch of NASA-Lewis.

TABLE OF CONTENTS

1.0 UNSUPPORTED THERMOCOUPLE WIRE: THEORY

Theoretical expressions are derived for the steady-state frequency response of a thermocouple wire. In particular, the effects of axial heat conduction are demonstrated for a non-uniform wire with unequal material properties and wire diameters across the junction. The amplitude ratio at low frequency $\omega \to 0$ agrees with the results of Scadron and Warshawsky for a steady-state temperature distribution. Moreover, the frequency response for a non-uniform wire in the limit of infinite length $l \to \infty$ is shown to reduce to a simple expression that is analogous to the classic first order solution for a thermocouple wire with uniform properties.

1.1 INTRODUCTION

The measurement of fluctuating temperatures in the high speed exhaust of a gas turbine engine combustor is required to characterize the local gas density gradients or convective heat transfer (Fralick, 1985). Although thermocouples are suitable for the measurement of high frequency temperature fluctuations (< 1 KHz) in a flowing gas or liquid, the measured signal must be compensated since the frequency of the time dependent fluid temperature is normally much higher than the corner frequency of the thermocouple probe (Scadron and Warshawsky, 1952). Moreover, the amplitude and phase angle of the thermocouple response may be attenuated by axial heat conduction for rugged thermocouples of finite length (Elmore, et al.; 1983, 1986).

In the present chapter, the theoretical steady-state frequency response of a thermocouple wire has been calculated to include the effects of axial heat conduction. Solutions are derived for a non-uniform wire with unequal properties across the junction (e.g., different wire diameter, thermoconductivity, etc.). Solutions are presented in the form of the amplitude ratio and phase angle for both the uniform the non-uniform thermocouple wires. In both configurations, the results are presented for thermocouple wires of either finite length where the effects of axial heat conduction are demonstrated or wires of infinite length for which the neglect of axial conduction is justified. For the case of the uniform wire, the theroetical results are compared with the series solution of Scadron and Warshawsky (1952). Moreover, for non-uniform wires the results are compared in the limit of low frequency with the steady-state temperature solution of Scadron and Warshawsky.

1.2 THEORY

The steady-state frequency response of a thermocouple wire will be developed in the following sections with the following assumptions: (a) the amplitude of the fluctuating fluid temperature is small relative to the mean absolute temperature (b) the thermocouple dimensions are small relative to the size of the turbulent eddies or enclosure dimensions (c) radial temperature gradients in a wire cross section can be neglected and (d) radiative heat transfer can be neglected relative to conduction and convection.

1.2.1 Uniform Wire

In this section the geometry of Fig. 1 is considered where the material properties of thermal conductivity k, specific heat c and wire density ρ are assumed to be equal on both sides of the thermocouple junction. If the probe is subjected to a flowing fluid, whose temperature fluctuates about its mean, the expression for the local conservation of energy in the thermocouple wire becomes (Scadron and Warshawsky, 1952)

$$\frac{\partial T_w}{\partial t} = \alpha \frac{\partial^2 T_w}{\partial x^2} + \frac{4h}{\rho c D}(T_g - T_w) \qquad (1.1)$$

where $\alpha = k/\rho c$ is the thermal diffusivity of the wire, T_g is the ambient fluid temperature, h is the convective heat transfer coefficient, D is the wire diameter and T_w is the local wire temperature measured along the axis at a distance x from the centerline of Fig. 1.

If the wire and fluid temperatures are measured relative to the support and mean fluid temperature T_0, the variation in the ambient fluid temperature can be written in the complex form

$$T_g(t) = T_0 + T_f e^{i\omega t} \qquad (1.2)$$

where ω is the angular frequency of the ambient fluid. Since Eq. (1.1) is linear, we now seek a solution for the local wire temperature of the form (Hildebrand, 1976)

$$T_w = T_0 + \vec{T}_\omega(x) e^{i\omega t}. \qquad (1.3)$$

Referencing all temperatures with respect to the steady-state temperature T_o and normalizing with respect to the amplitude of the fluctuating ambient fluid

temperature T_f, one defines a local normalized steady-state frequency response $\vec{T}(x)$ for the thermocouple wire of the form

$$\frac{T_w - T_0}{T_f} = \frac{\vec{T}_\omega(x)e^{i\omega t}}{T_f} = \vec{T}(x)e^{i\omega t}. \tag{1.4}$$

Substituting Eqs. (1.2) and (1.3) into Eq. (1), one obtains an ordinary differential equation of the form

$$i\omega T = \alpha \frac{d^2T}{dx^2} + \omega_n(1-T) \tag{1.5}$$

where $T = \vec{T}(x)$ is the frequency response and the vector notation will be dropped for simplicity. Thus for the geometry of fig. 1, one seeks a solution to the non-homogeneous linear second order differential equation for the dependent variable T of the form

$$\gamma T'' - G(\omega)T = -1 \tag{1.6}$$

subject to the boundary conditions

$$T(l) = T(-l) = 0. \tag{1.7}$$

Here, the parameters in Eqs. (1.5) and (1.6) are defined as

$$\omega_n = \frac{4h}{\rho cD}, \qquad \gamma = \frac{\alpha}{\omega_n}, \qquad G(\omega) = 1 + i(\frac{\omega}{\omega_n}) \tag{1.8}$$

where ω_n is the natural frequency of the uniform wire of fig. 1.

The general solution to Eq. (1.6) can be written in the form (Hildebrand, 1976)

$$T = A \sinh qx + B \cosh qx + \frac{1}{G(\omega)} \tag{1.9}$$

where the constants A and B are complex, $1/G(\omega)$ represents the particular solution and the parameter

$$q = \sqrt{\frac{G(\omega)}{\gamma}}$$

Substituting $x = \pm 1$ in Eq. (1.9), the boundary condition Eq. (1.7) yields values for the constants

$$A = 0, \; B = \frac{-1}{G(\omega)\cosh ql}. \tag{1.10}$$

Hence, one obtains a steady-state frequency response for the simple uniform wire of Fig. 1 in the form (Forney, 1988)

$$T = \frac{1}{G(\omega)}\left(1 - \frac{\cosh qx}{\cosh ql}\right) \tag{1.11}$$

The steady-state frequency response at the junction $x = 0$ of fig. 1 now becomes

$$T(0) = \frac{1}{G(\omega)}(1 - \operatorname{sech} ql). \tag{1.12}$$

The term 1 - sech (ql) in Eq. (1.12) corresponds to the steady-state temperature distribution for a constant ambient fluid temperature $T_f > T_o$ derived by Scadron and Warshawsky (1952). It is also interesting to note that the first order response can be derived from Eq. (1.12) in the limit of large wire length l or

$$\lim_{l \to \infty} T(0) = \frac{1}{G(\omega)} \tag{1.13}$$

where Eq. (1.13) represents the frequency response of a uniform thermocouple wire with no axial heat conduction.

The steady-state frequency at the thermocouple junction x = 0 is normally characterized graphically in the form

$$T(0) = |T(0)|e^{i\Phi} \tag{1.14}$$

where $|T(0)|$ is the amplitude ratio and Φ is the phase angle. in the latter case, the phase angle in degrees is

$$\Phi = 57.3 \ \tan^{-1}\left[\frac{\text{Im } T(0)}{\text{Re } T(0)}\right] \tag{1.15}$$

where Im[T(0)] and Re[T(0)] are the imaginary and real parts of T(0), respectively.

1.2.2 Previous Work

Scadron and Warshawsky (1952) in their pioneering work considered the frequency response of a uniform thermocouple wire as shown in fig. 1. Introducations for the dependent variable T_w in Eq. (1.1) as suggested by Carslaw (1945), Scadron and Warshawsky obtained expressions for the steady-state frequency response in the form of the amplitude ratio

$$|T(0)| = \frac{\sqrt{S_1^2 + \left(\frac{\omega}{\omega_n}\right)^2 S_2^2}}{\sqrt{1 + \left(\frac{\omega}{\omega_n}\right)^2}} \tag{1.16}$$

and phase angle

$$\Phi \tan^{-1}\left(\frac{\omega S_2}{\omega_n S_1}\right) - \tan^{-1}\left(\frac{\omega}{\omega_n}\right). \tag{1.17}$$

Here, the infinite series S_1 and S_2 that appear in Eqs. (1.16) and (1.17) are

$$S_1 = 1 - \sum_{j=1}^{\infty} c_j \left[\frac{d_j(d_j - 1)}{d_j^2 + \left(\frac{\omega}{\omega_n}\right)^2} \right] \tag{1.18a}$$

and

$$S_2 = \sum_{j=1}^{\infty} c_j \left[\frac{d_j - 1}{d_j^2 + \left(\frac{\omega}{\omega_n}\right)^2} \right] \tag{1.18b}$$

where the constant that appear in the terms of S_1 and S_2 are

$$c_j = \frac{2}{j\pi}[1 - \cos(j\pi)]\sin\left(\frac{j\pi(1-x)}{2l}\right) \tag{1.19a}$$

and

$$d_j = 1 + \frac{(j\pi)^2\gamma}{4l^2}. \tag{1.19b}$$

Properties of these solutions derived by Scadron and Warshawsky are discussed in Sec. III.

1.2.3 Non-Uniform Wire

If the wire diameters or the physical properties such as thermoconductivity are different across the thermocouple junction as shown in fig.2, Eq.(1.6) must be solved in the separate regions 1 and 2 on both sides of the junction. This solution is subject to the boundary conditions of continuous temperature and equal rates of conductive heat transfer at the junction x = 0 or

$$T_1(-l) = T_2(l) = 0 \tag{1.20a}$$

$$T_1(0) = T_2(0) \tag{1.20b}$$

$$k_1 D_1^2 \frac{dT_1(0)}{dx} = k_2 D_2^2 \frac{dT_2(0)}{dx}. \qquad (1.20c)$$

In region 1, the general solution to Eq. (1.6) for the frequency response can be written in the form

$$T_1(x) = A_1 \sinh q_1(l+x) + B_1 \cosh q_1(l+x) + \frac{1}{G_1(\omega)} . \qquad (1.21)$$

Since $T_1(-l) = 0$ from boundary condition Eq. (1.20a), one finds for the constant B_1

$$0 = B_1 + \frac{1}{G_1(\omega)} .$$

Substituting for B_1 into Eq. (1.21), one obtains

$$T_1(x) = A_1 \sinh q_1(l+x) + \frac{1}{G_1(\omega)}\left[1 - \cosh q_1(l+x)\right] \qquad (1.22)$$

where the parameters in Eq. (1.22) reflect the material properties and wire diameter of region 1 or

$$\omega_1 = \frac{4h_1}{\rho_1 c_1 D_1}, \quad \gamma_1 = \frac{\alpha_1}{\omega_1}, \quad G_1(\omega) = 1 + i\left(\frac{\omega}{\omega_1}\right), \quad q_1 = \sqrt{\frac{G_1(\omega)}{\gamma_1}} .$$

Similarly in region 2, the frequency response can be shown to be of the form

$$T_2(x) = A_2 \sinh q_2(l-x) + \frac{1}{G_2(\omega)}\left[1 - \cosh q_2(l-x)\right] \qquad (1.23)$$

where the constants A_1 and A_2 in Eqs. (1.22) and (1.23) above must be determined by the simultaneous solution to the boundary conditions Eqs. (1.20b) and (1.20c).

Substituting Eqs. (1.22) and (1.23) into boundary condition (1.20b), one obtains a linear equation for the constants of integration A_1, A_2 or

$$A_1 \sinh q_1 l - A_2 \sinh q_2 l = R_1 . \qquad (1.24)$$

Similarly, substituting Eqs. (1.22) and (1.23) into boundary condition (1.20c), one obtains a second linear equation for A_1, A_2 or

$$A_1 Q \cosh q_1 l + A_2 \cosh q_2 l = R_2 . \tag{1.25}$$

Here, the complex constant

$$Q = \left(k_1 D_1^2 q_1\right) / \left(k_2 D_2^2 q_2\right) \tag{1.26}$$

and the complex constants R_1, R_2 are equal to

$$R_1 = \left(\frac{1}{G_2} - \frac{1}{G_1}\right) + \frac{1}{G_1} \cosh q_1 l - \frac{1}{G_2} \cosh q_2 l \tag{1.27}$$

and

$$R_2 = \frac{Q}{G_1} \sinh q_1 l + \frac{1}{G_2} \sinh q_2 l. \tag{1.28}$$

Solving Eqs. (1.24) and (1.25) for A_1 and A_2, one obtains the determinate system

$$A_1 = \frac{\begin{vmatrix} R_1 & -\sinh q_2 l \\ R_2 & \cosh q_2 l \end{vmatrix}}{DET} \tag{1.29}$$

$$A_2 = \frac{\begin{vmatrix} \sinh q_1 l & R_1 \\ Q \cosh q_1 l & R_2 \end{vmatrix}}{DET} \tag{1.30}$$

where the determinate in the denominator is equal to

$$\text{DET} = \sinh q_1 l \cosh q_2 l + Q \cosh q_1 l \text{ and } q_2 l \tag{1.31}$$

Thus, the constants A_1 and A_2 in Eqs. (1.22) and (1.23) become

$$A_1 = \frac{\frac{\sinh q_1 l}{G_1}\left(\tanh \frac{q_1 l}{2} + Q \tanh q_2 l\right) + \frac{\sinh q_2 l}{G_2}\left(-\tanh \frac{q_2 l}{2} + \tanh q_2 l\right)}{\sinh q_1 l + Q \cosh q_1 l \tanh q_2 l} \tag{1.32}$$

and

$$A_2 = \frac{\frac{\sinh q_1 l}{G_1}\left(\tanh q_1 l - \tanh\frac{q_1 l}{2}\right) + \frac{\sinh q_2 l}{G_2}\left(\tanh\frac{q_2 l}{2} + Q'\tanh q_1 l\right)}{\sinh q_2 l + Q'\cosh q_2 l \tanh q_1 l} \quad (1.33)$$

where the complex constant in A_2 is

$$Q' = 1/Q.$$

Finally, the steady-state frequency response at the thermocouple junction x = 0 can be determined by substituting the value for A_1 above or Eq. (1.32) into the general solution for $T_1(0)$ given by Eq. (1.22). One obtains after simplification

$$T_1(0) = \frac{\frac{Q\sinh q_1 l}{G_1}\left(1 - \coth q_1 l \tanh\frac{q_1 l}{2}\right) + \frac{\sinh q_2 l}{G_2}\left(1 - \coth q_2 l \tanh\frac{q_2 l}{2}\right)}{Q\coth q_1 l + \coth q_2 l} \quad (1.34)$$

where it can be shown that $T_1(0) = T_2(0)$ at the thermocouple junction.

It is interesting to note that one can determine a frequency response for a non-uniform wire of infinite length from Eq. (1.34) in a manner similar to the derivation of Eq. (1.13). Taking the limit of infinite wire length in $T_1(0)$ above, one obtains the simple expression

$$\lim_{l\to\infty} T_1(0) = \frac{\frac{Q}{G_1} + \frac{1}{G_2}}{Q+1} \quad . \quad (1.35)$$

Equation (1.35) represents the frequency response for a non-uniform wire which is1. analogous to the well known first order response given by Eq. (1.13) for a uniform wire of infinite length.

1.3 RESULTS

The amplitude ratio and phase angle of the thermocouple frequency response were plotted graphically for the case of a uniform wire with the geometry shown in fig. 1. In this case, average properties of a type B or $Pt/6\%\ Rh - Pt/30\%\ Rh$ were used since the material properties were nearly equal across the thermocouple junction. The wire dimensions, properties and gas conditions are listed in table 1(Touloukian et al., 1970).

The amplitude ratio and phase angle were also plotted for a composite or non-uniform thermocouple wire with the geometry shown in fig. 2. In this case, different wire diameters and material properties were used including a type B thermocouple described in Table 1 in addition to a type T or copper - constantan described in table 2 (Touloukian et al., 1970).

The form of the convective heat transfer coefficient h that appears in the computation of the natural frequency ω_n defined in Eq. (1.8) was determined from the expression (Scadron and Warshawsky 1952)

$$Nu = .431\ \mathrm{Re}^{1/2} \tag{1.36}$$

where $Nu\ (= hD/k_f)$ is the Nusselt number, k_f is the thermal conductivity of the ambient fluid and $\mathrm{Re}\ (= v\,D/\upsilon_f)$ is the Reynolds number of the thermocouple wire. Here, v and υ_f are the fluid velocity and kinematic viscosity, respectively. It should be noted that the convective heat transfer coefficient $h\ \alpha\ D^{1/2}$ and the natural frequency of a thermocouple wire for given material properties $\omega_n\ \alpha\ D^{-3/2}$.

1.3.1 Uniform Wire

The amplitude ratio $|T(0)|$ at the wire junction for the steady-state frequency response Eq. (1.12) is computed in fig. 3. This assumes a type B thermocouple wire with the dimensions listed in table 1. In this case, the average material properties listed in table 1 were used since the theory assumes that the thermocouple is uniform across the junction. In fig. 3 the amplitude ratio $|T(0)|$ $\rightarrow .54$ for low frequencies $\omega \rightarrow 0$. This lower limit corresponds to the attenuation expected for a thermocouple wire exposed to a steady ambient gas temperature T_f $> T_0$ as derived by Scadron and Warshawsky (1952).

The amplitude ratio Eq. (1.16) predicted by Scadron and Warshawsky (1952) is also graphed in fig. 3. It was found that the series Eqs. (1.18a) and (1.18b) converged slowly such that the final result was in error by ~ 11% at low frequencies after retaining the first 10 terms. The first 50 terms of the series expressions for $S_1$and S_2 reduced the error to 2.3% while retaining 100 terms as was done in fig. 3 limited the error to 1%. The final result is identical, however, to the amplitude ratio predicted by Eq. (1.12) and derived in the present chapter.

The amplitude ratio for a type B thermocouple wire of infinite length from the first order response Eq. (1.13) is also indicated in fig. 3. As expected, the first order response or Eq. (1.13) asymptotically approaches the amplitude ratio predicted for a wire of finite length in the limit of large frequencies $\omega / \omega_n >> 1$ where the time scale of the ambient temperature fluctuation is too small for axial heat conduction to occur.

The phase angle Φ for all three theories is computed in fig. 4. The phase angle varies over the range $0 \geq \Phi \geq -\pi/2$ and approaches the lower limit of $-\pi/2$ for large frequencies $\omega/\omega_n >> 1$. It is apparent that the effect of axial heat conduction is to reduce the magnitude of the phase angle.

The spacial variation of the amplitude ratio $|T(x)|$ derived from Eq. (1.11) is graphed in fig. 5. The present theory approaches the correct limit of $|T(\pm l)| = 0$. However, the theory of Scadron and Warshawsky oscillates near the end of the wire $x \rightarrow \pm l$. In the latter case the amplitude ratio equals the value $1/\sqrt{1+(\omega/\omega_n)^2}$ for $x = \pm l$ since $S_1 = 1$ and $S_2 = 0$ in Eqs. (1.18a) and (1.18b), respectively. An incorrect value for the amplitude ratio near the ends of the wire would not ordinarily present a problem unless one wished to adapt the theory to the common configuration of a supported thermocouple wire with heat transfer down the support legs (Forney and Fralick, 1991).

1.3.2 Non-Uniform Wire

The amplitude ratio $|T_1(0)|$ from the steady-state frequency response Eq. (1.34) is graphed in fig. 6. This plot assumes a type T thermocouple wire with the dimensions listed in table 2 . An important parameter that affects the relative magnitude of the terms in Eq. (1.34) and thus the relative importance of the thermocouple wire segments in regions 1 or 2 in the schematic of fig. 2 is the complex dimensionless ratio $Q = k_1 D_1^2 q_1 / k_2 D_2^2 q_2$. We note here that Q assumes different values in the limit of either low or high frequencies. Given that the Nusselt number is related to the wire Reynolds number by Eq. (1.36), one obtains

for low frequencies

$$Q(\omega = 0) \;=\; Q_0 \;=\; \left(\frac{k_1}{k_2}\right)^{.5}\left(\frac{D_1}{D_2}\right)^{1.25} \tag{1.37}$$

while for high frequencies

$$Q(\omega = \infty) \;=\; Q_\infty \;=\; \left(\frac{k_1}{k_2}\right)^{.5}\left(\frac{D_1}{D_2}\right)^{2} . \tag{1.38}$$

The amplitude ratio $|T_1(0)| \rightarrow .228$ for low frequencies $\omega \rightarrow 0$ in fig. 6. The lower limit corresponds to the attenuation predicted by Scadron and Warshawsky (1952) for a non-uniform thermocouple wire as shown in fig. 2 that is exposed to a steady-state ambient gas temperature $T_f > T_o$. The real expression for the temperature distribution developed by Scadron and Warshawsky for this case is

$$\frac{T_w(0) - T_0}{T_f} \;=\; 1 - \psi \tag{1.39}$$

where

$$\psi = \operatorname{sech}\frac{l\gamma^+}{2}\cosh\frac{l\gamma^-}{2}\left[\frac{1 - m_{12}\tanh\dfrac{l\gamma^-}{2}\coth\dfrac{l\gamma^+}{2}}{1 - m_{12}\sinh l\gamma^- \operatorname{csch} l\gamma^+}\right] . \tag{1.40}$$

Here, the parameters γ^+ and γ^- are defined as

$$\gamma^+ = \frac{1}{\sqrt{\gamma_1}} + \frac{1}{\sqrt{\gamma_2}} , \qquad \gamma^- = \frac{1}{\sqrt{\gamma_1}} - \frac{1}{\sqrt{\gamma_2}} \tag{1.41a}$$

and

$$m_{12} \;=\; \frac{Q_0 - 1}{Q_0 + 1} . \tag{1.41b}$$

The amplitude ratio $|T_1(0)|$ from Eq. (1.35) for a type T thermocouple wire with the same wire dimensions $D_2 / D_1 = 2$ as the solid curve in fig. 6 but of infinite length $l \to \infty$ is also computed. As indicated, the amplitude ratio at low frequencies $\omega \to 0$ for a non-uniform thermocouple wire of infinite length approaches $|T_1(0)| \to 1$. This result is identical to the first order frequency response Eq. (1.13) for a uniform wire of infinite length as is shown in fig. 3. For the non-uniform wire, however, axial heat transfer does occur at the junction because of dissimilar material properties. At large frequencies $\omega / \omega_n >> 1$, however, the amplitude ratio derived from Eq. (1.35) for the wire of infinite length asymptotically approaches the value predicted by Eq. (1.34) for a wire of finite length as shown in fig. 6. The latter result is similar to the features of fig. 3 at large frequencies for the case of a uniform thermocouple wire. These latter features reflect the fact that the time scales of the ambient gas temperature fluctuations at high frequency are too small for axial heat conduction to occur.

The phase angle Φ for both expressions Eqs. (1.34) and (1.35) is graphed in fig. 7. The phase angle varies over the range $0 \geq \Phi \geq -\pi/2$ and approaches the lower limit of $-\pi/2$ for large frequencies . It is apparent that the effect of axial heat conduction is to reduce the magnitude of the phase angle.

The amplitude ratio $|T_1(0)|$ derived from Eq. (1.34) for a type B thermocouple wire is computed in fig. 8. Since the material properties in this case are nearly equal on both sides of the junction, the indicated difference in the amplitude ratio is the result of different wire diameters across the junction. These results are strongly influenced by the magnitude of the factor Q_o defined by Eq. (1.37). If

the parameter $Q_0 \sim 1$ as is the case for the upper curve in fig. 8, both regions 1 and 2 in the schematic of fig. 2 are equally weighted in the expression for the frequency response given by Eq. (1.34). However, increasing the wire diameter D_2 in region 2 means Q_0 is reduced in magnitude such that $Q_0 < 1$. Now the amplitude ratio is more strongly influenced by the properties of the larger wire in region 2. The phase angle is plotted in fig. 9 for the same wire configuration.

The amplitude ratio $|T_1(x)|$ is also computed as a function of the axial distance down the type B thermocouple wire in fig. 10. This was accomplished by substituting the expression for the constant A_1 given by Eq. (1.32) into the general solution for the frequency response Eq. (1.22). As discussed above, if the ratio $Q_0 < 1$ because of an increase in D_2, a large increase in the rate of heat transfer occurs in region 2 down the larger wire. This additional axial heat conduction reduces the amplitude ratio at the thermocouple junction compared to the case of $Q_0 \sim 1$ for the wire geometry represented by the upper curve in fig. 10.

The amplitude ratio derived from Eq. (1.34) for a type T thermocouple wire is graphed in fig. 11. Since the thermoconductivity of copper in region 1 is more than an order of magnitude larger than the thermoconductivity of constant in region 2, the parameter $Q_0 > 1$ for $D_1 / D_2 = 1$. Increasing the diameter of region 2, however, has a small effect on the amplitude ratio since $Q_0 > 1$, which remains unchanged, and the properties of region 1 continue to dominate the rate of heat transfer. The phase angle for the same configuration is computed in fig. 12.

The amplitude ratio $|T_1(x)|$ is also computed as a function of the axial distance down the type T thermocouple wire in fig. 13. As discussed above, $Q_0 >$ 1 for both wire configurations. Thus, the large rate of axial heat transfer down the copper wire in region 1 gives nearly equal spacial temperature profiles for both wire configurations and this fixes the junction temperature.

1.4 NOMENCLATURE

A = constant of integration

B = constant of integration

c = material specific heat $\left(J-gm^{-1}-{}^{0}K^{-1}\right)$

c_j = term in infinite series S_1, S_2

d_j = term in infinite series S_1, S_2

D = thermocouple wire diameter (cm)

G = $1+i(\omega/\omega_n)$

h = heat transfer coefficient $\left(J-cm^{-2}-s^{-1}-{}^{0}K^{-1}\right)$

i = unit imaginary number $\left(=\sqrt{-1}\right)$

k = material thermoconductivity $\left(J-cm^{-1}-s^{-1}-{}^{0}K^{-1}\right)$

k_f = gas thermoconductivity $\left(J-cm^{-1}-s^{-1}-{}^{0}K^{-1}\right)$

l = length of thermocouple wire (cm)

m_{12} = $(Q_0-1)/(Q_0+1)$

Nu = Nusselt number (= hD/k_f)

Q = $\left(k_1D_1^2q_1\right)/\left(k_2D_2^2q_2\right)$

Q_0 = $(k_1/k_2)^{.5}(D_1/D_2)^{1.25}$

Q_∞ = $(k_1/k_2)^{.5}(D_1/D_2)^{2}$

q = $(G/\gamma)^{.5}$

Re = Reynolds number $(= vD/\upsilon_f)$

S_1 = infinite sum

S_2 = infinite sum

t = time(s)

T = frequency response

T_f = amplitude of periodic gas temperature $\left({}^0K\right)$

T_g = gas temperature $\left({}^0K\right)$

T_0 = steady-state gas temperature $\left({}^0K\right)$

$\vec{T_\omega}$ = complex amplitude of periodic wire temperature $\left({}^0K\right)$

T_w = local wire temperature $\left({}^0K\right)$

v = gas velocity $\left(cm-s^{-1}\right)$

x = axial distance from center of wire (cm)

Greek Symbols

α = thermal diffusivity $\left(cm^2-s^{-1}\right)$

γ = α / ω_n $\left(cm^2\right)$

γ^+ = $1/\sqrt{\gamma_1} + 1/\sqrt{\gamma_2}$ $\left(cm^{-1}\right)$

γ^- = $1/\sqrt{\gamma_1} - 1/\sqrt{\gamma_2}$ $\left(cm^{-1}\right)$

υ_f = kinematic viscosity of gas $\left(cm^2-s^{-1}\right)$

ω = angular frequency $\left(s^{-1}\right)$

ω_n = natural frequency of wire $(=4h/\rho cD)\left(s^{-1}\right)$

Φ = phase angle (degrees)

ψ = normalized temperature at junction

ρ = material density (gm - cm^{-3})

1.5 REFERENCES

1. Carslaw, H. S., Introduction to the Mathematical Theory of the Conduction of Heat in Solids, Dover Publications, 2nd edition (1945).

2. Dils, R. R. and Follansbee, P. S., Wide Bandwidth Gas Temperature Measurements in Combustor and Combustor Exhaust Gases, Instrumentation in the Aerospace Industry, 21 (B. Washburn, ed.), ISA 76245 (1976).

3. Elmore, D. L., Robinson, W. W. and Watkins, W. B., Dynamic Gas Temperature Measurement System: Final Report, NASA CR-168267 (1983).

4. Elmore, D.L., Robinson, W. W. and Watkins, W. B., Further Development of the Dynamic Gas Temperature Measurement System: Vol. I - Technical Efforts, NASA CR-179513 (1986).

5. Forney, L. J., Frequency Response of a Thermocouple Wire: Effects of Axial Conduction, NASA/ASEE Case-Lewis Summer Faculty Fellowship Program, 1988 Final Report, pp. 78-79.

6. Fralick, G. C., Correlation of Velocity and Velocity-Density Turbulence in the Exhaust of an Atmospheric Burner, Turbine Engine Hot Section Technology - 1985, NASA CP-2465, pp. 81-85.

7. Forney, L. J., and Fralick, G. C., Frequency Response of a Supported Thermocouple Wire: Effects of Axial Heat Conduction, Progress Report Georgia Tech E19-666-2, April (1991).

8. Hildebrand, F. B., Advanced Calculus for Applications, (2nd Ed), Prentice - Hall (1976).

9. Scadron, M.D. and Warshawsky, I., Experimental Determination of Time Constants and Nusselt Numbers for Bare-Wire Thermocouples in High-Velocity Air Streams and Analytic Approximation of Conduction and Radiation Errors, NACA TN-2599 (1952).

10. Touloukian, Powell, Ho and Clemens, (ed.), Thermal Physical Properties of Matter, Purdue Research Foundation, Plenum Pub. (1970).

1.6 TABLES AND FIGURES

Table 1 - Uniform Wire Conditions

Dimensions (cm)	Air Properties
D = .0076	T_0 = 300 °K
l = .1	P = 1 atm
	v = 50 m/sec

Properties of Type B

	$\rho c\left(\frac{J}{cm^3 - {}^\circ K}\right)$	$\alpha\left(\frac{cm^2}{\sec}\right)$
Pt - 6% Rh	2.73	.238
Pt - 30%Rh	2.86	.190
Average	2.8	.214

Table 2 - Properties of Non-Uniform Wire

Dimensions (cm)				Wire Location		
D_1(cm)	D_2(cm)	D_2/D_1	l(cm)	Region	Type B	Type T
.0076	.0076	1	.1	1	Pt-6%Rh	Copper
.0076	.0152	2	.1	2	Pt-30%Rh	Constantan

Properties of Type T

	$\rho c\left(\frac{J}{cm^3 - {}^\circ K}\right)$	$\alpha\left[\frac{cm^2}{\sec}\right]$
Copper	3.44	1.16
Constantan	3.48	.067

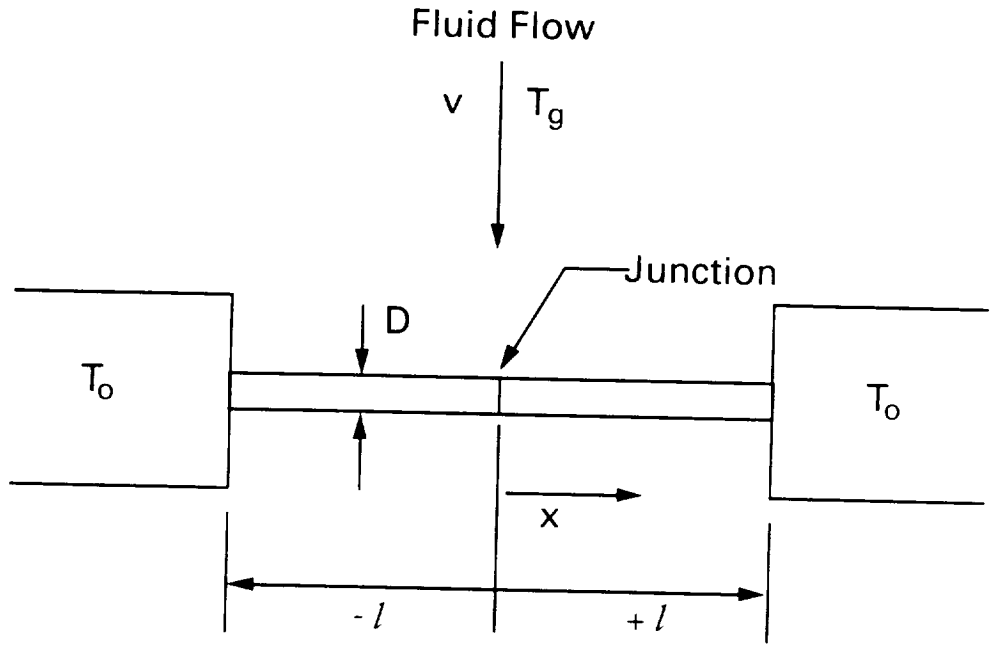

Fig. 1 Schematic of uniform wire

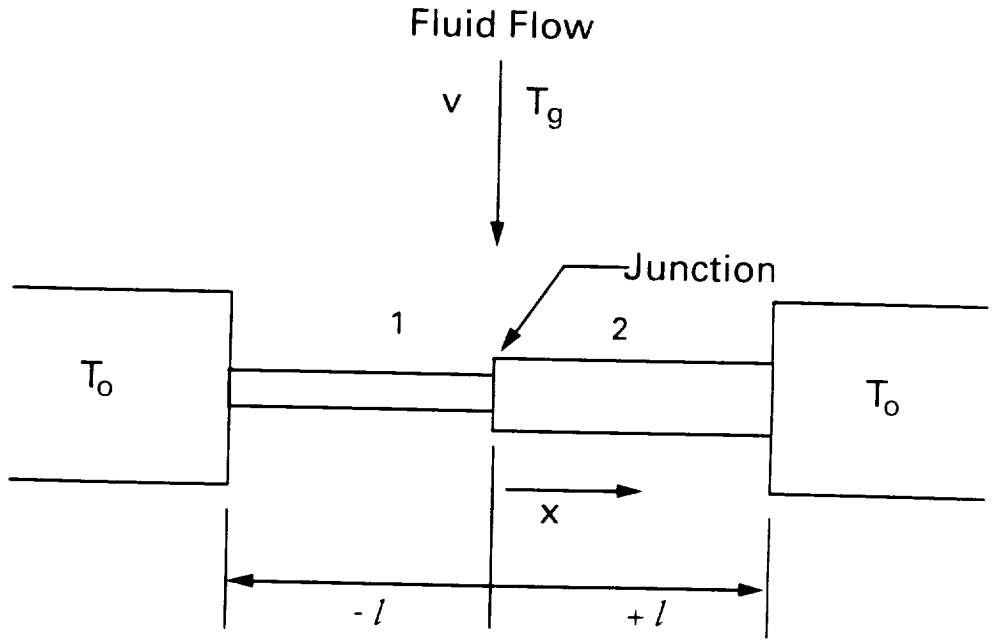

Fig. 2 Schematic of non-uniform wire

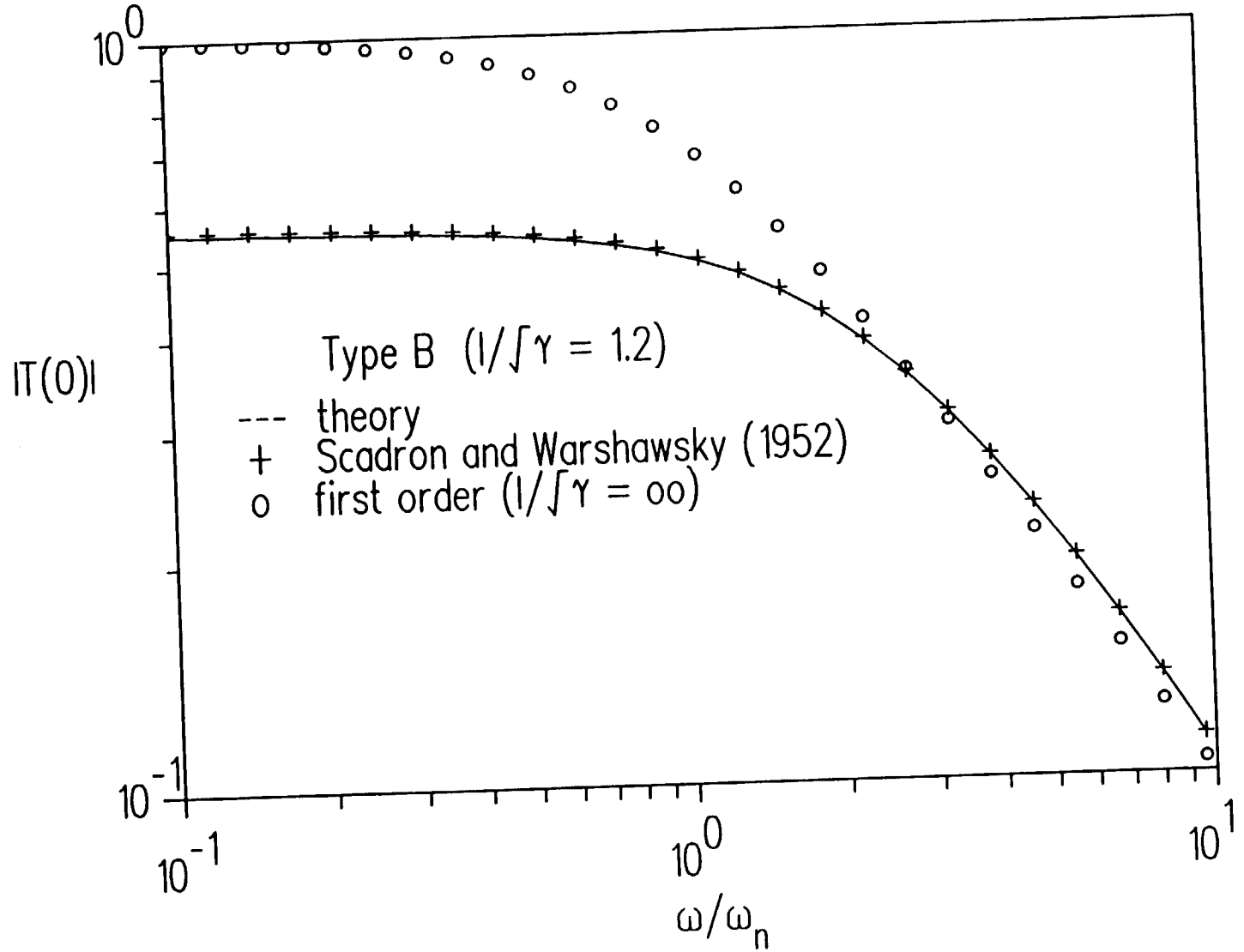

Fig. 3 Amplitude ratio vs angular frequency for uniform wire. Solid line, Eq. (12); Circles, Eq. (13).

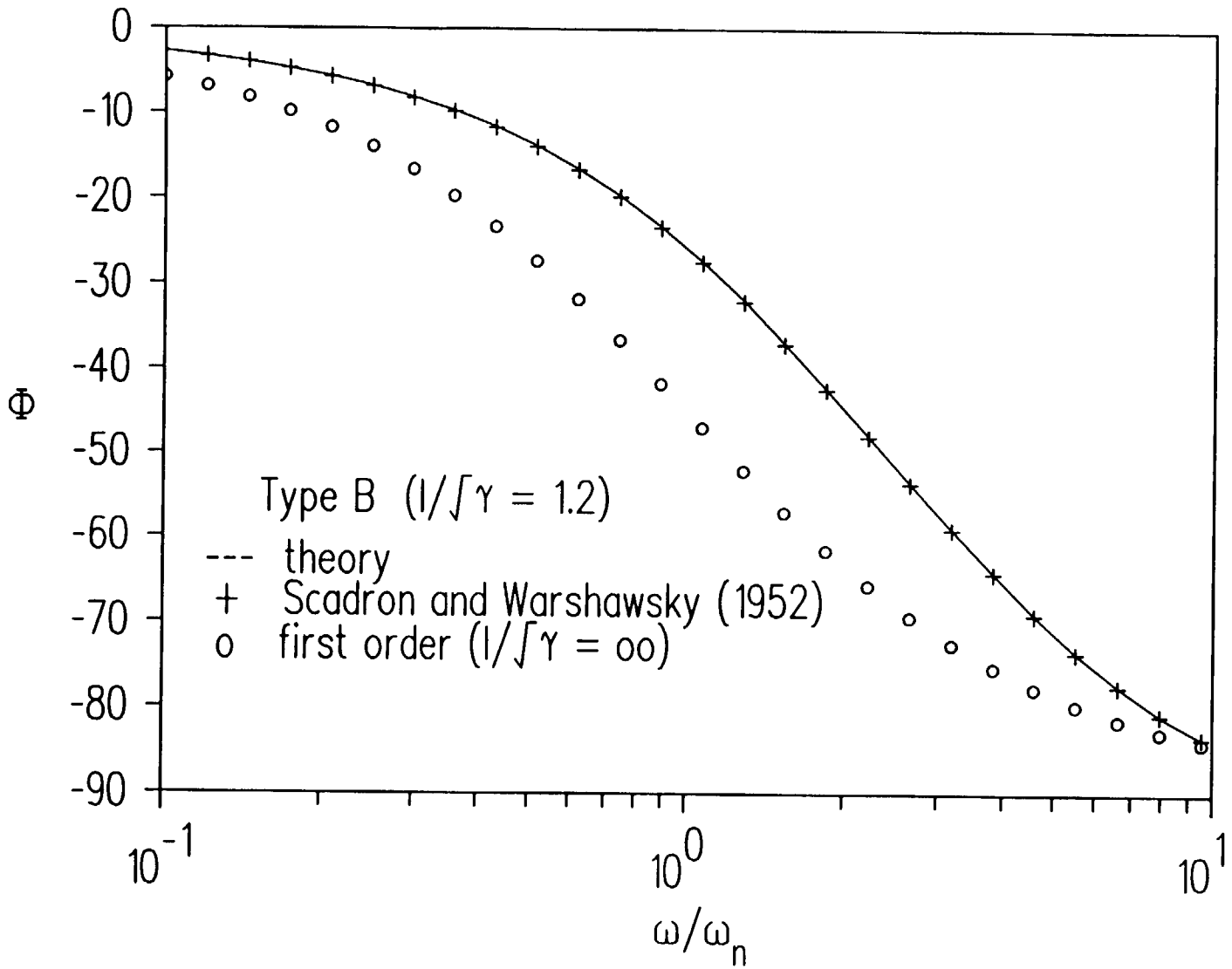

Fig. 4 Phase angle vs angular frequency for uniform wire. Solid line, Eq. (12); Circles, Eq. (13).

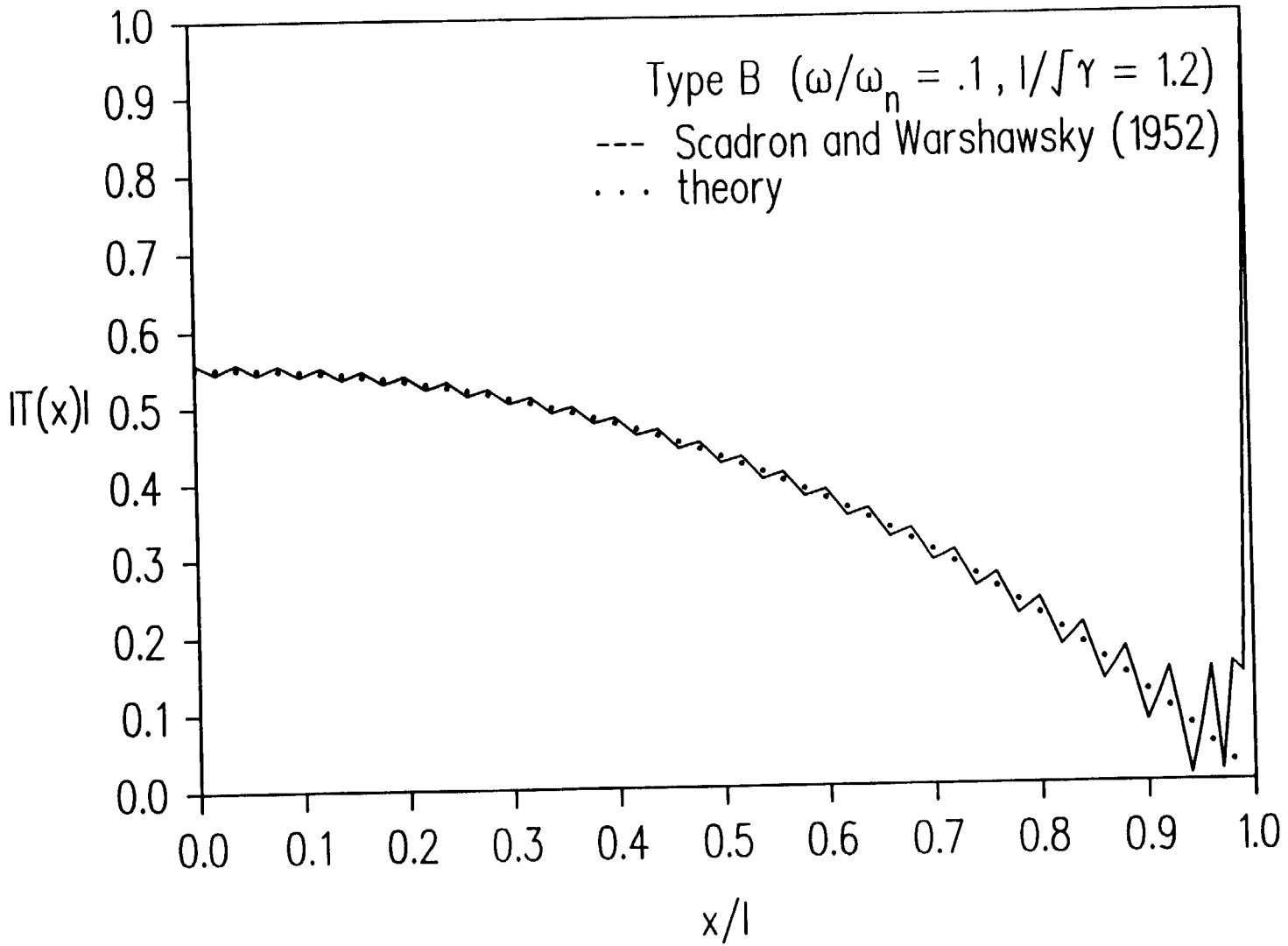

Fig. 5 Amplitude ratio vs axial distance for uniform wire. Dotted line, Eq. (11).

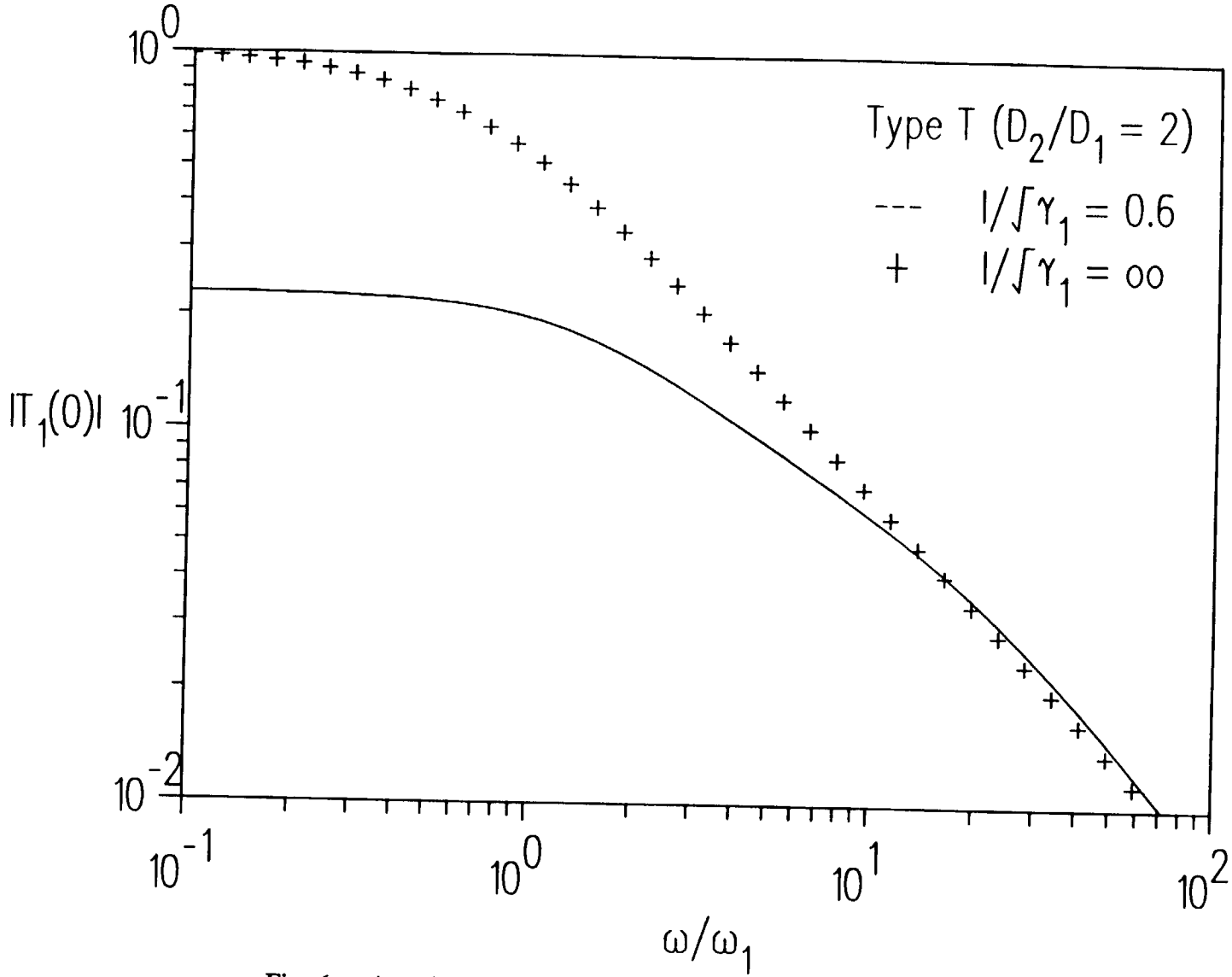

Fig. 6 Amplitude ratio vs angular frequency for non-uniform wire. Upper curve is Eq. (35). Lower curve is Eq. (34).

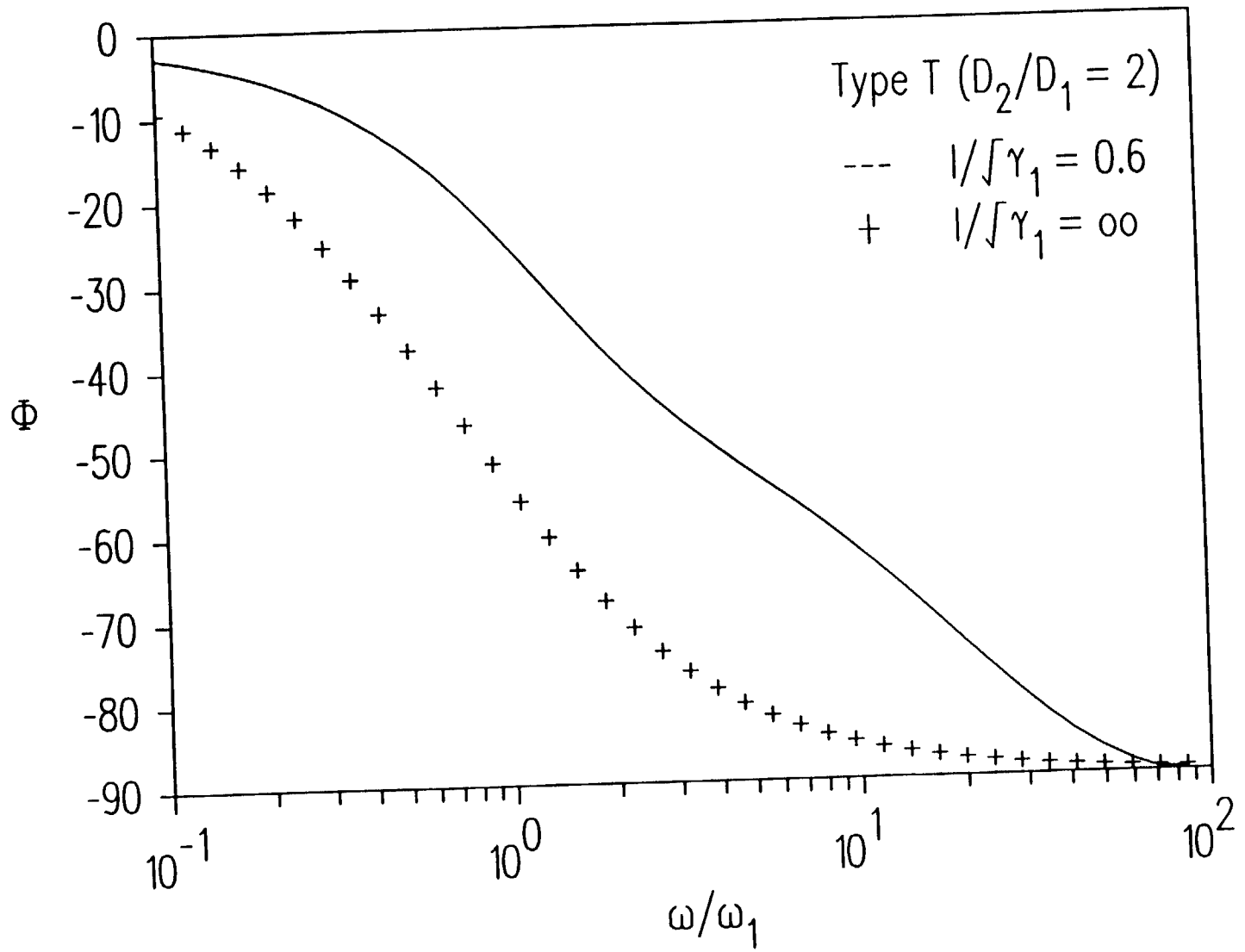

Fig. 7 Phase angle vs angular frequency for non-uniform wire. Upper curve is derived from Eq. (34). Lower curve from Eq. (35).

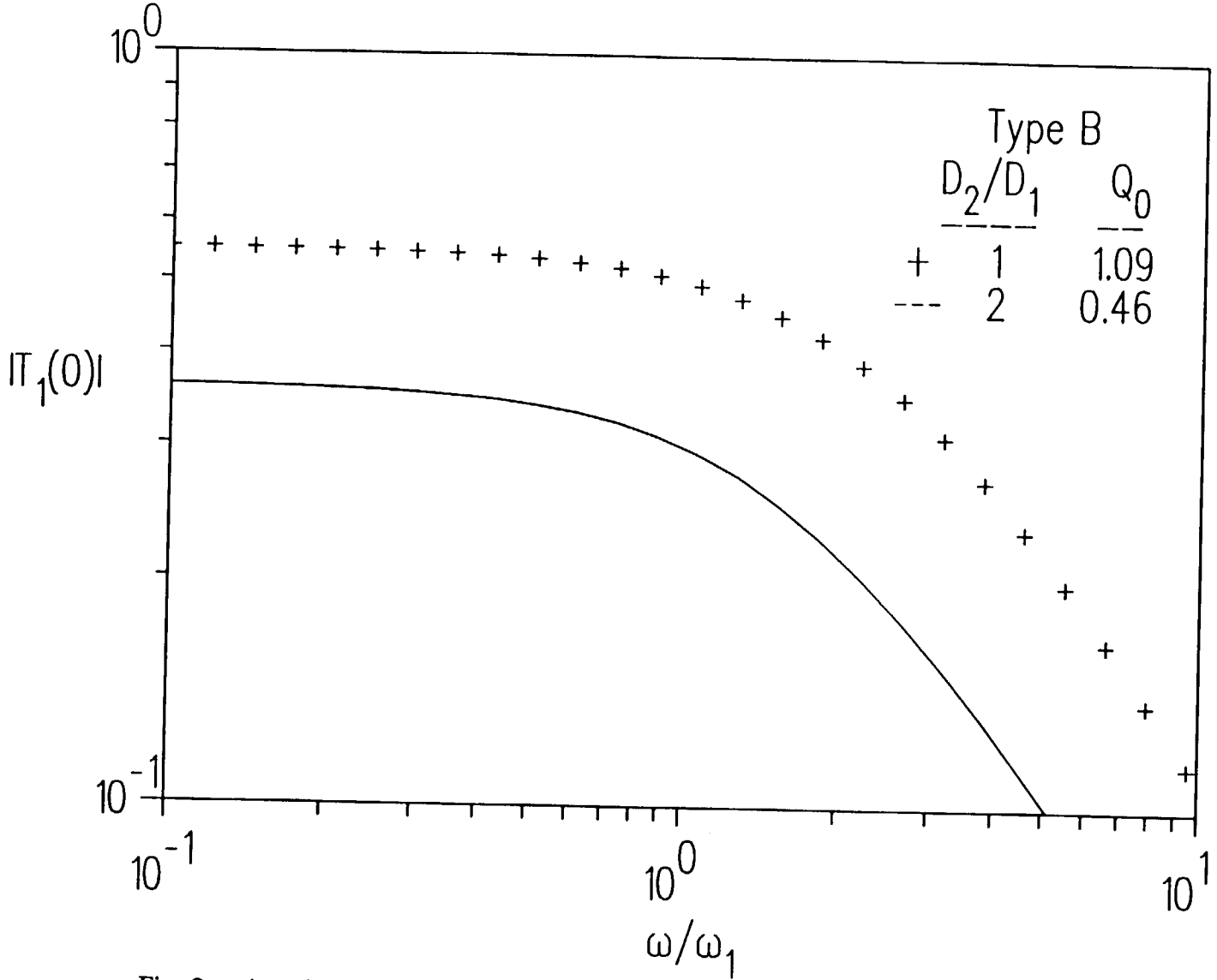

Fig. 8 Amplitude ratio vs angular frequency for non-uniform wire with similar material properties. Curves are Eq. (34).

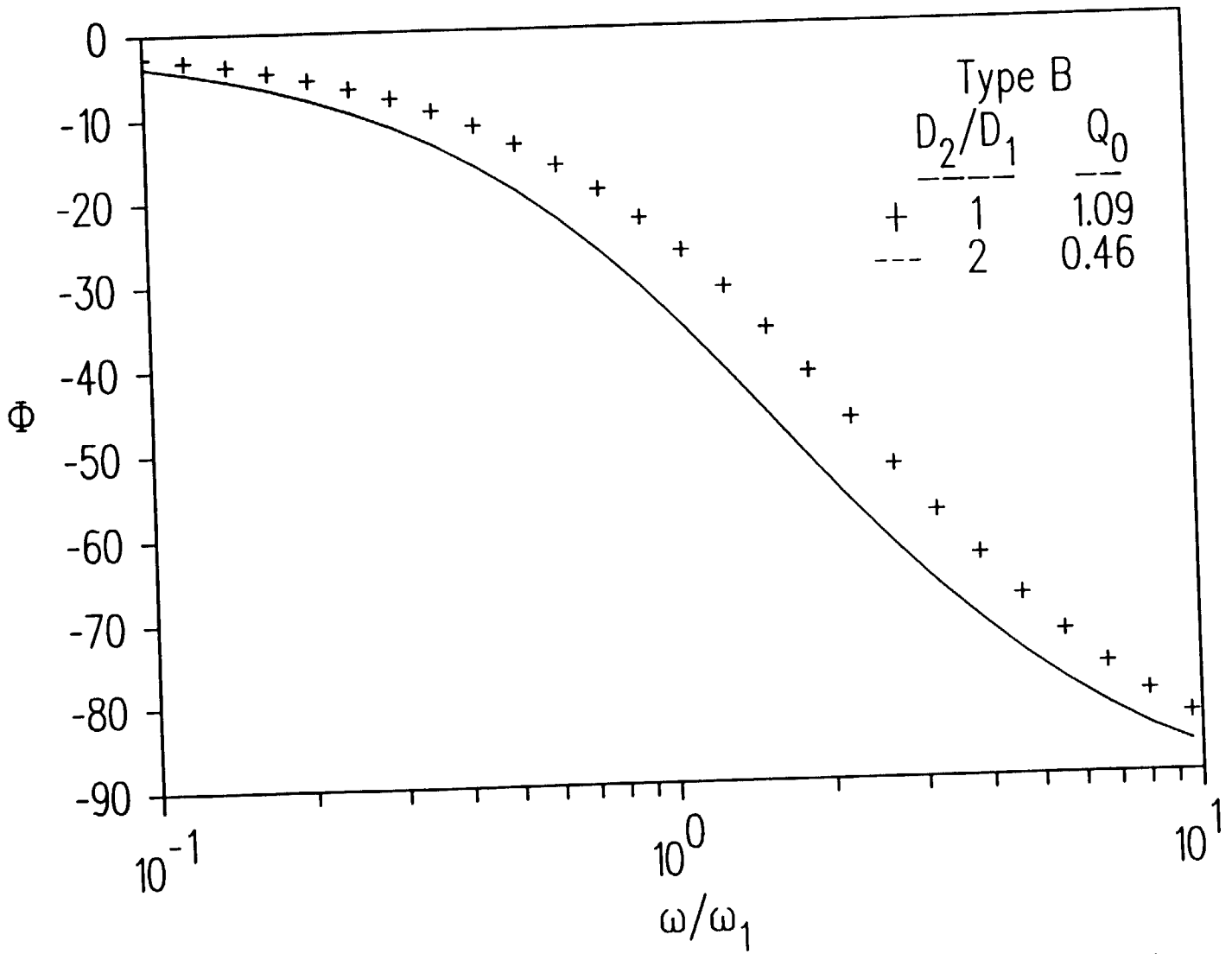

Fig. 9 Phase angle vs angular frequency for non-uniform wire with similar material properties. Curves derived from Eq. (34).

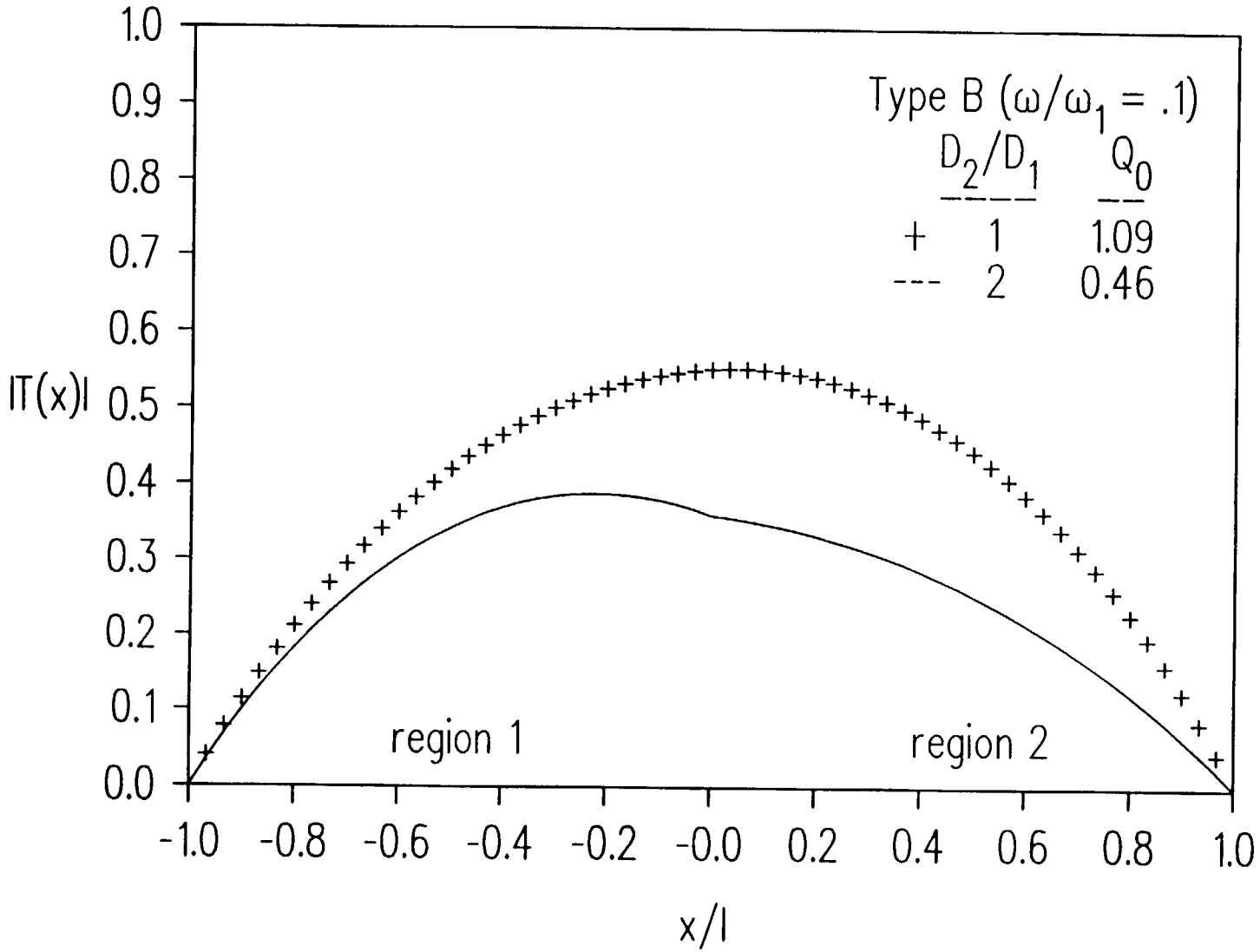

Fig. 10 Amplitude ratio vs axial distance for non-uniform wire with similar material properties. Each curve is derived from Eqs. (22) and (32).

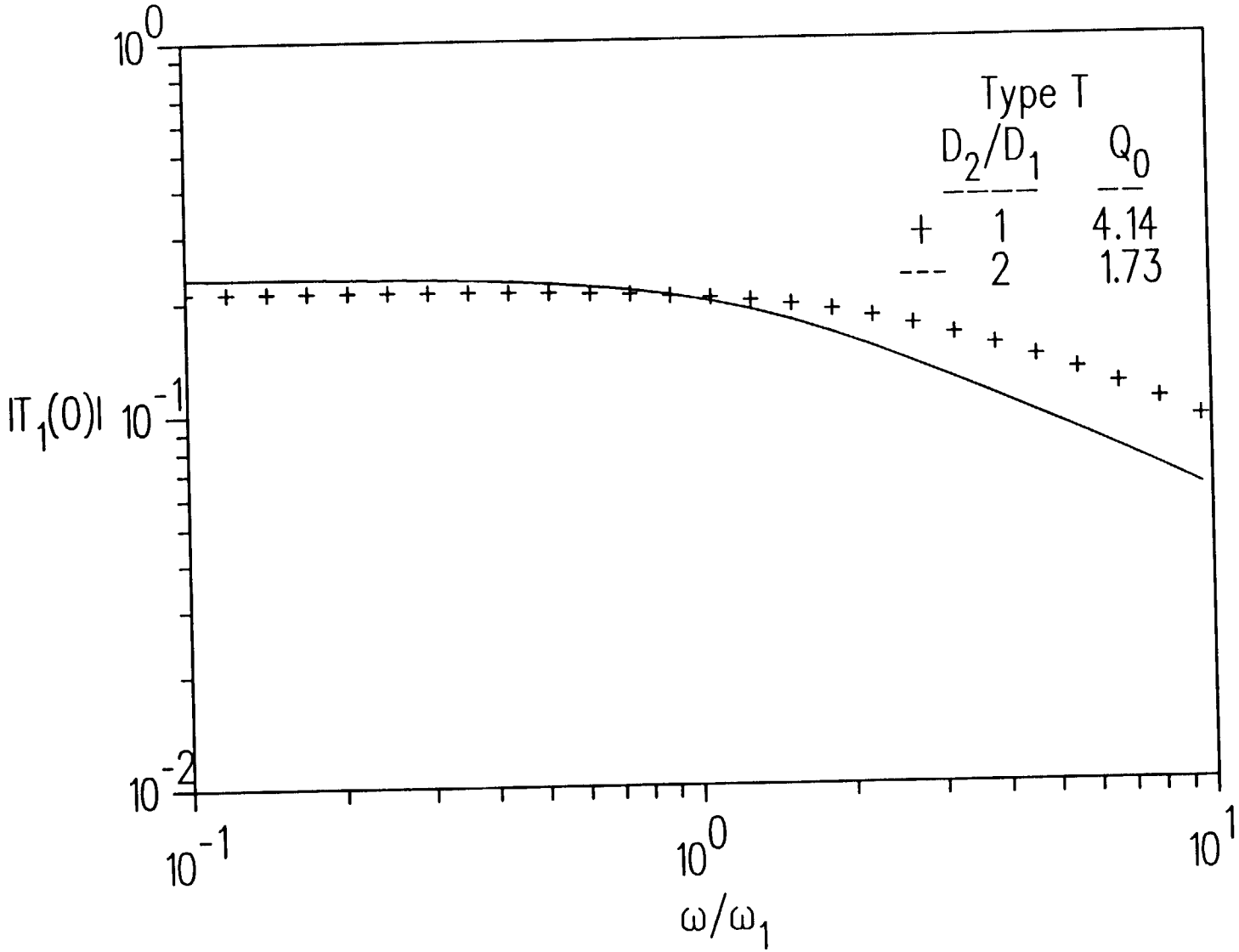

Fig. 11 Amplitude ratio vs angular frequency for wire with dissimilar material properties. Curves are Eq. (34).

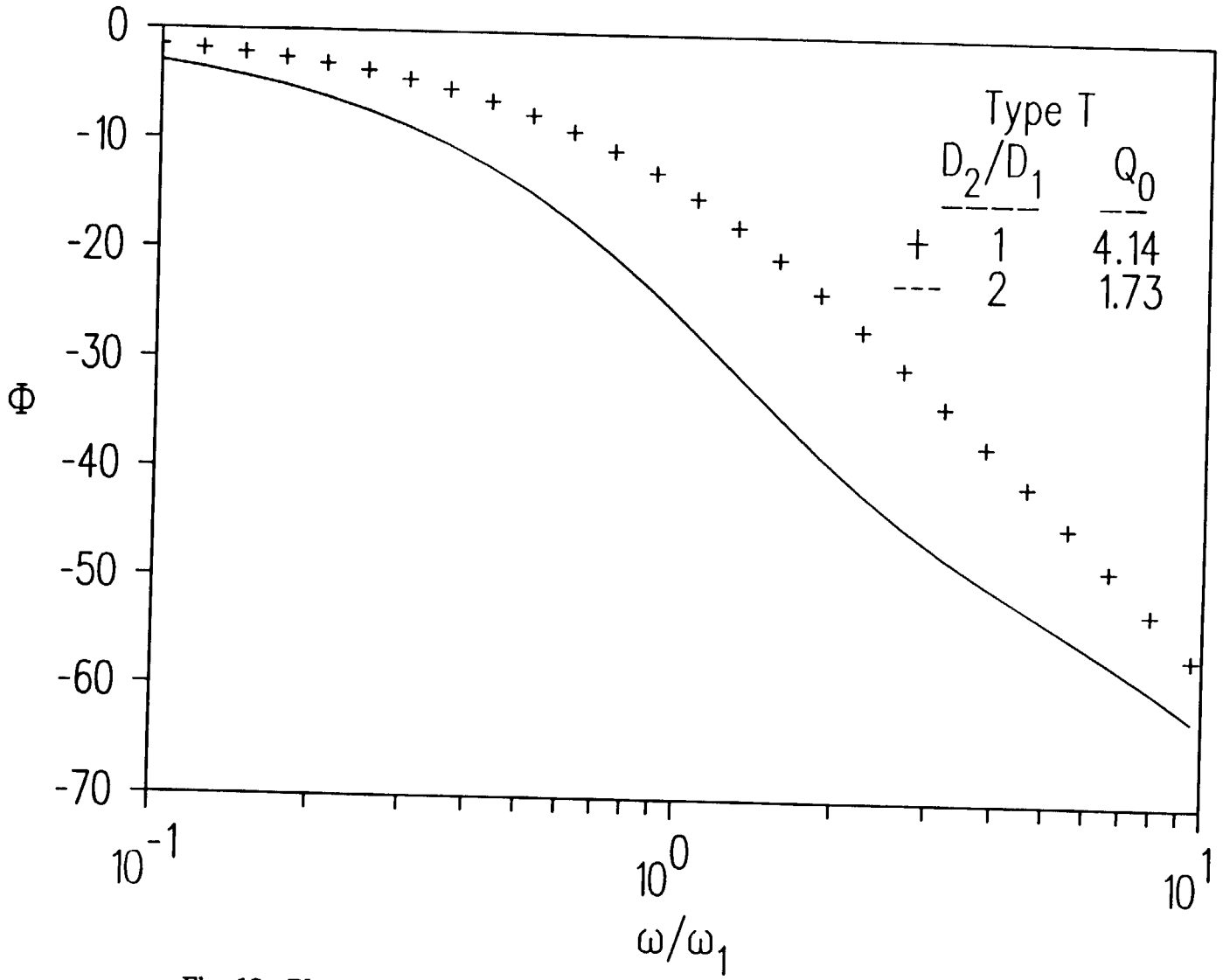

Fig. 12 Phase angle vs angular frequency for wire with dissimilar material properties. Curves derived from Eq. (34).

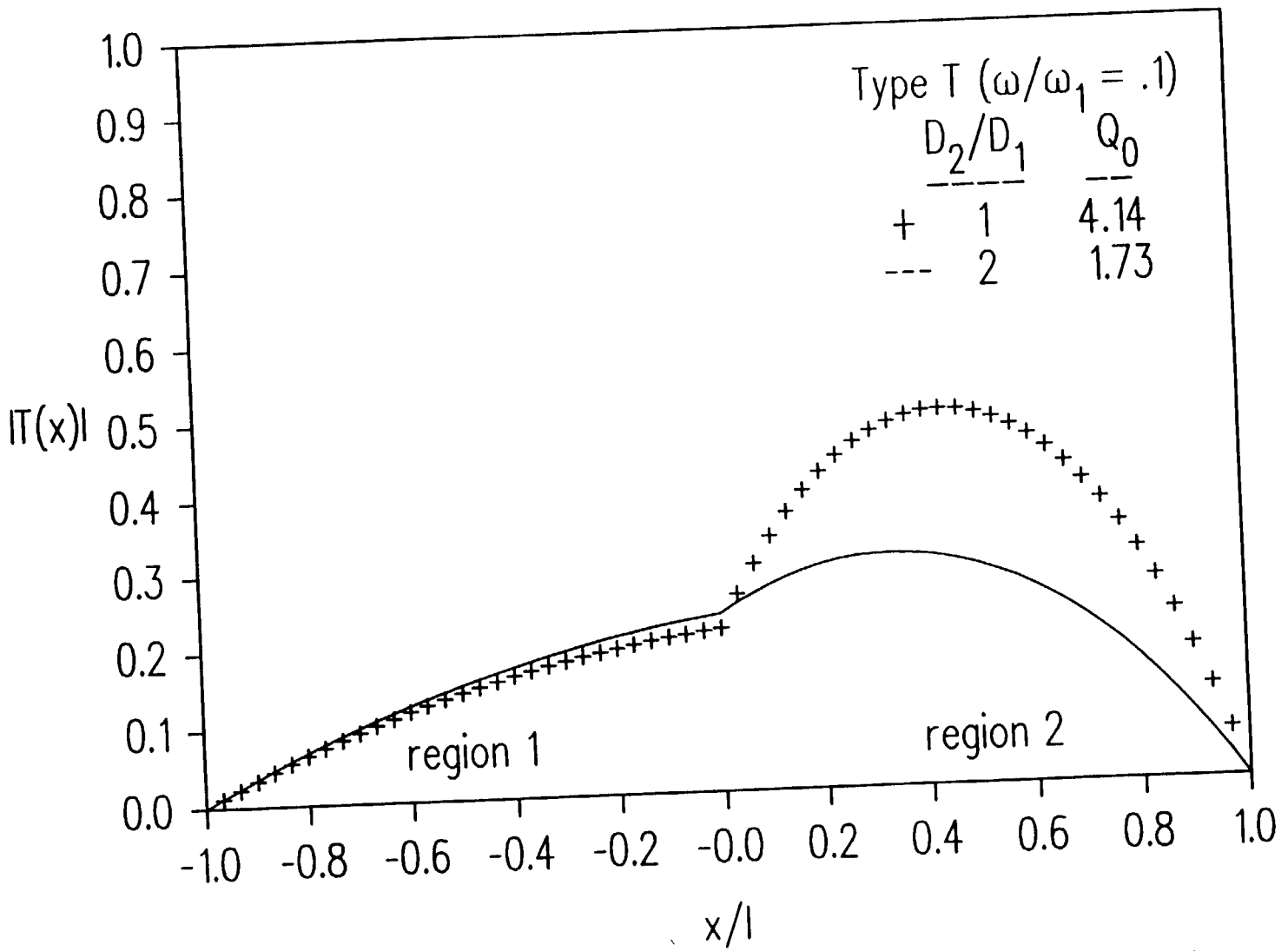

Fig. 13 Amplitude ratio vs axial distance for wire with dissimilar material properties. Each curve is derived from Eqs. (22) and (32).

2.0 SUPPORTED THERMOCOUPLE WIRE: THEORY AND EXPERIMENT

Theoretical expressions are derived for the steady-state frequency response of a supported thermocouple wire. In particular, the effects of axial heat conduction are demonstrated for both a supported one material wire and a two material wire with unequal material properties across the junction. For the case of a one material supported wire, an exact solution is derived which compares favorably with an approximate expression that only matches temperatures at the support junction. Moreover, for the case of a two material supported wire, an analytical expression is derived that closely correlates numerical results.

Experimental data were taken with a type K supported thermocouple. The test thermocouple was constructed with dimensions to demonstrate the effects of axial heat conduction assuming constant physical properties across the junction.

2.1 INTRODUCTION

In the present chapter, the theoretical steady-state frequency response of a supported thermocouple wire has been calculated to include the effects of axial heat conduction. These solutions, which represent an extension of earlier work (Forney and Fralick, 1991) are derived for both a supported thermocouple wire with equal physical properties across the junction (e.g., roughly the same thermoconductivity, etc.) and a supported wire with unequal properties across the junction. Solutions are presented in the form of the amplitude ratio and phase angle for both cases.

2.2 THEORY FOR ONE MATERIAL THERMOCOUPLE

The steady-state frequency response of a thermocouple wire will be developed with the following assumptions: (a) the amplitude of the fluctuating fluid temperature is small relative to the mean absolute temperature (b) the thermocouple dimensions are small relative to the size of the turbulent eddies or enclosure dimensions (c) radial temperature gradients in a wire cross section can be neglected and (d) radiative heat transfer can be neglected relative to conduction and convection.

In this section the geometry of Fig. 1 is considered where the material properties of thermal conductivity k, specific heat c and wire density ρ are assumed to be equal on both sides of the thermocouple junction. If the probe is immersed in a flowing fluid, the expression for the local conservation of energy in the thermocouple wire becomes (Scadron and Warshawsky, 1952)

$$\frac{\partial T_w}{\partial t} = \alpha \frac{\partial^2 T_w}{\partial x^2} + \frac{4h}{\rho c D}\left(T_g - T_w\right) \tag{2.1}$$

where $\alpha = k/\rho c$ is the thermal diffusivity of the wire, T_g is the ambient fluid temperature, h is the convective heat transfer coefficient, D is the wire diameter and T_w is the local wire temperature measured along the axis at a distance x from the centerline (Fig. 1.)

The wire and fluid temperatures are measured relative to the mean fluid temperature T_0. The ambient fluid temperature is taken to be a mean temperature together with a sinusoidal varying deviation from the mean,

$$T_g(t) = T_0 + T_f e^{i\omega t} \tag{2.2}$$

where ω is the angular frequency of the ambient temperature. Since Eq. (2.1) is

linear, we now seek a solution for the local wire temperature of the form (Hildebrand, 1976)

$$T_w = T_0 + \vec{T}_\omega(x)e^{i\omega t}. \tag{2.3}$$

Referencing all temperatures with respect to the mean gas temperature T_o and normalizing with respect to the amplitude of the fluctuating ambient fluid temperature T_f, one defines a local normalized steady-state frequency response $\vec{T}(x)$ for the thermocouple wire of the form

$$\frac{T_w - T_0}{T_f} = \frac{\vec{T}_\omega(x)e^{i\omega t}}{T_f} = \vec{T}(x)e^{i\omega t}. \tag{2.4}$$

Substituting Eqs. (2.2) and (2.3) into Eq. (2.1), one obtains an ordinary differential equation of the form

$$i\omega T = \alpha \frac{d^2T}{dx^2} + \omega_n(1-T) \tag{2.5}$$

where $T = \vec{T}(x)$ is the frequency response and the vector notation will be dropped for simplicity. Thus, for the geometry of fig. 1, one seeks a solution to the non-homogeneous linear second order differential equation for the dependent variable T of the form (Forney and Fralick, 1990)

$$\gamma T'' - G(\omega)T = -1. \tag{2.6}$$

The general solution to Eq.(2.6) can be written in the form (Hildebrand, 1976)

$$T(x) = A\sinh qx + B\cosh qx + \frac{1}{G(\omega)} \tag{2.7}$$

where the parameters in Eqs. (2.5) and (2.6) are defined as

$$\omega_n = \frac{4h}{\rho cD}, \quad \gamma = \frac{\alpha}{\omega_n}, \quad G(\omega) = 1 + i\left(\frac{\omega}{\omega_n}\right) \tag{2.8}$$

while in Eq. (2.7) the constants A and B are complex, $1/G(\omega)$ represents the particular solution and the parameter

$$q = \sqrt{\frac{G(\omega)}{\gamma}}.$$

2.2.1 Approximate Solution

Assuming that the material properties are constant across the junction and that the wire diameters are D_1 and D_2 in regions 1 and 2, respectively, Eq. (2.6) is subject to the boundary conditions

$$T_1(l) = T_2(l) = T_a \tag{2.9a}$$

$$T_2(l+L) = 0 \quad . \tag{2.9b}$$

In this case, we seek a simple approximate solution that neglects the heat transfer at the interface between regions 1 and 2 at $x = \pm l$ where the parameters in Eqs. (2.5) and (2.6) are defined in terms of the wire diameters in each region. A similar approach will be used in a later section to obtain an approximate solution for the case in which the material properties of the two elements of the thermocouple are distinctly different. Hence, in region 1

$$\omega_1 = \frac{4h_1}{\rho c D_1}, \qquad \gamma = \frac{\alpha}{\omega_1}, \qquad G_1(\omega) = 1 + i\left(\frac{\omega}{\omega_1}\right) \tag{2.0}$$

where ω_1 is the natural frequency of the wire in region 1 of fig. 1.

The solution to Eq. (2.6) for the one material wire on both sides of the junction in region 1 can be written in the form

$$T_1(x) = A_1 \sinh q_1 x + B_1 \cosh q_1 x + \frac{1}{G_1(\omega)} \; . \tag{2.11}$$

Substituting $x = \pm l$ in Eq. (2.11), the boundary conditions in Eq. (2.9) yield values for the constants

$$A_1 = 0, \qquad B_1 = \frac{1}{\cosh q_1 l}\left(T_a - \frac{1}{G_1}\right). \tag{2.12}$$

Thus, one obtains a steady-state temperature distribution for the wire in region 1 of Fig. 1 in the form

$$T_1(x) = \frac{1}{G_1}\left(1 - \frac{\cosh q_1 x}{\cosh q_1 l}\right) + T_a\left(\frac{\cosh q_1 x}{\cosh q_1 l}\right) \tag{2.13}$$

We now seek a solution in region 2 that satisfies the boundary conditions of Eq. (2.9). Since the temperature is symmetric about x = 0, it is convenient to define a continuous steady-state temperature distribution for the large wire of diameter D_2 over the entire region $-(l+L) \le x \le (l+L)$ or

$$T_2(x) = \frac{1}{G_2}\left(1 - \frac{\cosh q_2 x}{\cosh q_2 (l+L)}\right). \tag{2.14}$$

Since $T_a = T_2(l)$, one obtains the boundary value from Eq. (2.14)

$$T_a = \frac{1}{G_2}\left(1 - \frac{\cosh q_2 l}{\cosh q_2 (l+L)}\right). \tag{2.15}$$

Substituting the value for T_a at $x = l$ of Eq. (2.15) into Eq. (2.13), the approximate temperature distribution in region 1 becomes

$$T_1(x) = \frac{1}{G_1}\left(1 - \frac{\cosh q_1 x}{\cosh q_1 l}\right) + \frac{1}{G_2}\left(1 - \frac{\cosh q_2 l}{\cosh q_2 (l+L)}\right)\frac{\cosh q_1 x}{\cosh q_1 l} \tag{2.16}$$

Thus, the approximate frequency response at the thermocouple junction (x = 0) for the one material wire becomes

$$T_1(0) = \frac{1}{G_1}\left(1 - \frac{1}{\cosh q_1 l}\right) + \frac{1}{G_2}\left(1 - \frac{\cosh q_2 l}{\cosh q_2 (l+L)}\right)\frac{1}{\cosh q_1 l} \tag{2.17}$$

The steady-state frequency at the thermocouple junction x=0 is normally characterized graphically in the form

$$T(0) = |T(0)|e^{i\Phi} \tag{2.18}$$

where $|T(0)|$ is the amplitude ratio and Φ is the phase angle. In the latter case, the phase angle in degrees is

$$\Phi = 57.3 \tan^{-1}\left[\frac{\text{Im } T(0)}{\text{Re } T(0)}\right] \tag{2.19}$$

where Im[T(0)] and Re[T(0)] are the imaginary and real parts of T(0), respectively.

2.2.2 Exact Solution

If the boundary conditions listed in Eq.(2.9) include equal rates of conductive heat transfer at the interface between the thermocouple and support wires at $x = \pm\ l$, the exact solution is subject to

$$T_1(l) = T_2(l) \tag{2.20a}$$

$$kD_1^2 \frac{dT_1(l)}{dx} = kD_2^2 \frac{dT_2(l)}{dx} \tag{2.20b}$$

$$T_2(l+L) = 0\ . \tag{2.20c}$$

Since the solution to Eq. (2.6) in region 1 is of the form

$$T_1(x) = A_1 \sinh q_1 x + B_1 \cosh q_1 x + \frac{1}{G_1} \tag{2.21}$$

where by symmetry $T_1(l) = T_1(-l)$, one obtains $A_1 = 0$. Thus, the form of the

solution in region 1 becomes

$$T_1(x) = B_1 \cosh q_1 x + \frac{1}{G_1} . \tag{2.22}$$

For region 2, where the spatial coordinate is in the range $l \le x \le (l+L)$, it is convenient to write

$$T_2(x) = A_2 \sinh q_2 (l+L-x) + B_2 \cosh q_2 (l+L-x) + \frac{1}{G_2} . \tag{2.23}$$

From the boundary condition $T_2(l+L)=0$, one obtains $B_2 = -1/G_2$ or the form of the solution in region 2 becomes

$$T_2(x) = A_2 \sinh q_2 (l+L-x) + \frac{1}{G_2}\left[1 - \cosh q_2 (l+L-x)\right] . \tag{2.24}$$

Substituting Eqs. (2.22) and (2.23) into boundary condition (2.20a), one obtains a linear equation for the constants B_1, A_2 or

$$B_1 \cosh q_1 l - A_2 \sinh q_2 L = \frac{1}{G_2}\left[1 - \cosh q_2 L\right] - \frac{1}{G_1} . \tag{2.25}$$

Similarly, substituting Eqs. (2.22) and (2.23) into boundary condition (2.20b), one obtains

a second linear equation for B_1, A_2 or

$$B_1 Q \sinh q_1 l + A_2 \cosh q_2 L = \frac{1}{G_2} \sinh q_2 L \tag{2.26}$$

where the complex constant Q is defined as

$$Q = \frac{D_1^2 q_1}{D_2^2 q_2} . \tag{2.27}$$

Solving Eqs. (2.25) and (2.26) for B_1 and A_2, one obtains the determinate system

$$B_1 = \frac{\begin{vmatrix} \frac{1}{G_2}[1-\cosh q_2 L]-\frac{1}{G_1} & -\sinh q_2 L \\ \frac{1}{G_2}\sinh q_2 L & \cosh q_2 L \end{vmatrix}}{DET} \tag{2.28}$$

and

$$A_2 = \frac{\begin{vmatrix} \cosh q_1 l & \frac{1}{G_2}[1-\cosh q_2 L]-\frac{1}{G_1} \\ Q\sinh q_1 l & \frac{1}{G_2}\sinh q_2 L \end{vmatrix}}{\mathrm{DET}} \tag{2.29}$$

where the determinate in the denominator is equal to

$$DET = \cosh q_1 l \cosh q_2 L + Q\sinh q_1 l \sinh q_2 L. \tag{2.30}$$

Thus, solving for the constants B_1 and A_2 from Eqs. (2.28) and (2.29) and substituting B_1 into Eq. (2.22), one obtains an exact expression for the steady-state temperature distribution in the form

$$T_1(x) = \frac{\left[\frac{1}{G_2}(\cosh q_2 L-1) - \frac{1}{G_1}\cosh q_2 L\right]\cosh q_1 x}{\cosh q_1 l \cosh q_2 L + Q\sinh q_1 l \sinh q_2 L} + \frac{1}{G_1}. \tag{2.31}$$

Thus, the steady-state frequency response at the thermocouple junction x=0 becomes

$$T(0) = \frac{\frac{1}{G_2}(\cosh q_2 L-1) - \frac{1}{G_1}\cosh q_2 L}{\cosh q_1 l \cosh q_2 L + Q\sinh q_1 l \sinh q_2 L} + \frac{1}{G_1}. \tag{2.32}$$

2.3 THEORY FOR TWO MATERIAL THERMOCOUPLE

Certain types of thermocouples have distinctly different material properties across the junction. For example, a copper-constantan thermocouple has a thermal conductivity on the copper side that is more than an order of magnitude larger than constantan. In this case, the expressions developed in the previous section for the frequency response are in error since unequal material properties would provide an asymmetric temperature profile.

Referring to fig. 2, the thermocouple schematic now has four distinct regions that are distinguished by either different wire diameters or physical properties. For example, on the left side of the schematic of fig. 1 the thermal conductivity, density and specific heat have the values k_1, ρ_1 and c_1, respectively, while on the right side of the schematic the material properties are k_2, ρ_2 and c_2.

2.3.1 Temperature Distribution for Small Wire

Since the differential equation describing the steady-state frequency response Eq. (2.6) applies to all regions of the schematic of fig. 1, the steady-state frequency response in regions 1 and 2 are given, respectively, by the expressions

$$T_1(x) = A_1 \sinh q_1 x + B_1 \cosh q_1 x + \frac{1}{G_1} \tag{2.33}$$

$$T_2(x) = A_2 \sinh q_2 x + B_2 \cosh q_2 x + \frac{1}{G_2}. \tag{2.34}$$

Here, the four constants designated by A and B in Eqs. (2.33) and (2.34) are determined by the four boundary conditions

$$T_1(0) = T_2(0) \tag{2.35a}$$

$$k_1 D_1^2 \frac{dT_1(0)}{dx} = k_2 D_1^2 \frac{dT_2(0)}{dx} \tag{2.35b}$$

$$T_1(-l) = T_a \tag{2.35c}$$

$$T_2(l) = T_b \ . \tag{2.35d}$$

Solving for the four values of the constants designated by A and B in Eqs. (2.33) and (2.34), one obtains an expression for the steady-state temperature distribution in region 1 of the form

$$T_1(x) = \frac{1}{G_1} + \left\{\sinh q_1(x+l)\left[\left(\frac{1}{G_2} - \frac{1}{G_1}\right)\cosh q_2 l + \left(T_b - \frac{1}{G_2}\right)\right]\right.$$

$$\left. + \left(T_a - \frac{1}{G_1}\right)\left[Q_t \cosh q_1 x \sinh q_2 l \ - \ \sinh q_1 x \cosh q_2 l\right]\right\}\left(\frac{1}{\Delta_1}\right) \tag{2.36a}$$

and in region 2

$$T_2(x) = \frac{1}{G_2} + \left\{-Q_t \sinh q_2(l-x)\left[\left(\frac{1}{G_2} - \frac{1}{G_1}\right)\cosh q_1 l - \left(T_a - \frac{1}{G_1}\right)\right]\right.$$

$$\left. + \left(T_b - \frac{1}{G_2}\right)\left[\cosh q_2 x \sinh q_1 l \ + \ Q_t \cosh q_1 l \sinh q_2 x\right]\right\}\left(\frac{1}{\Delta_1}\right) . \tag{2.36b}$$

Here, it should be noted that the two functions above can be obtained from each other by interchanging the subscripts 1 and 2, the values a and b and by changing the sign of x. Also, in Eqs. (2.36a) and (2.36b) the parameters

$$\Delta_1 = Q_t \cosh q_1 l \sinh q_2 l + \cosh q_2 l \sinh q_1 l$$

and

$$Q_t = \frac{k_1 q_1}{k_2 q_2} .$$

2.3.2 Temperature Distribution for Large Wire

In this section a solution is sought for the large wire in regions 3 and 4 of the schematic of fig. 2. To simplify the analysis, a continuous solution is derived for the steady-state frequency response over the entire region $-(l+L) \le x \le (l+L)$. This solution must satisfy the boundary conditions

$$T_3(0) = T_4(0) \tag{2.37a}$$

$$k_1 D_3^2 \frac{dT_3(0)}{dx} = k_2 D_3^3 \frac{dT_4(0)}{dx} \tag{2.37b}$$

$$T_3(-l-L) = 0 \tag{2.37c}$$

$$T_4(l+L) = 0. \tag{2.37d}$$

In principle, it is now possible to derive a continuous solution for $T_3(x)$ over the range $-(l+L) \le x \le 0$ and for $T_4(x)$ over the range $0 \le x \le (l+L)$. These solutions are obtained from Eqs. (2.36a) and (2.36b) by replacing the subscripts $1 \rightarrow 3$ and $2 \rightarrow 4$ and by redefining the parameters $l \rightarrow l+L$ and setting the boundary conditions $T_a = T_b = 0$. Moreover, the boundary condition $T_a = T_3(-l)$ is obtained from the resulting expression for $T_3(x)$ by substituting $x = -l$ while the boundary condition $T_b = T_4(l)$. Thus, one obtains values for T_a, T_b that appear in Eqs. (2.36a) and (2.36b) in the form

$$T_a = \frac{1}{G_3} + \left\{\sinh q_3 L\left[\left(\frac{1}{G_4} - \frac{1}{G_3}\right)\cosh q_4(l+L) - \frac{1}{G_4}\right]\right.$$

$$\left. - \frac{1}{G_3}\left[Q_s \cosh q_3 l \sinh q_4(l+L) + \cosh q_4(l+L)\sinh q_3 l\right]\right\}\left(\frac{1}{\Delta_2}\right) \tag{2.38}$$

and

$$T_b = \frac{1}{G_4} + \left\{Q_s \sinh q_4 L\left[\left(\frac{1}{G_3} - \frac{1}{G_4}\right)\cosh q_3(l+L) - \frac{1}{G_3}\right]\right.$$

$$\left. - \frac{1}{G_4}\left[\cosh q_4 l \sinh q_3(l+L) + Q_s \cosh q_3(l+L)\sinh q_4 l\right]\right\}\left(\frac{1}{\Delta_2}\right). \qquad (2.39)$$

Here, the parameters are defined as

$$\Delta_2 = Q_s \cosh q_3(l+L)\sinh q_4(l+L) + \cosh q_4(l+L)\sinh q_3(l+L)$$

and

$$Q_s = \frac{k_1 q_3}{k_2 q_4} .$$

2.3.3 Frequency Response

The steady-state frequency response for the two material supported thermocouple is obtained from Eq. (2.36a) or (2.36b) by setting x = 0:

$$T(0) = \frac{1}{\Delta_1}\left\{Q_t \sinh q_2 l\left[T_a + \frac{1}{G_1}(\cosh q_1 l - 1)\right] + \sinh q_1 l\left[T_b + \frac{1}{G_2}(\cosh q_2 l - 1)\right]\right\} \qquad (2.40)$$

where T_a and T_b are given by Eqs. (2.38) and (2.39).

It should be noted that the steady-state frequency response Eq. (2.40) provides a wire temperature that is continuous everywhere and conserves the heat flux at the junction x = 0. This represents an approximate solution since the heat flux at the interface between the large and small wires $x = \pm l$ has been neglected.

2.4 RESULTS

The amplitude ratio and phase angle of the thermocouple frequency response were plotted graphically for the case of a one material wire as shown in the

schematic of fig. 1. In this case, average properties of a type B or $Pt/6\%\ Rh - Pt/30\%\ Rh$ were used since the material properties were nearly equal across the thermocouple junction. The wire dimensions, properties and gas conditions are listed in table 1(Touloukian et al., 1970).

The amplitude ratio and phase angle were also plotted for a two material thermocouple wire as shown in the schematic of fig. 2. In this case, a type B thermocouple described in table 1 was used in addition to a type T or copper - constantan described in table 2 (Touloukian et al., 1970).

The form of the convective heat transfer coefficient h that appears in the computation of the natural frequency ω_n defined in Eq. (2.8) was determined from the expression (Scadron and Warshawsky 1952)

$$Nu = .485\,\mathrm{Re}^{1/2}\,\mathrm{Pr}^{1/3} \tag{2.41}$$

where $Nu\,(= hD/k_f)$ is the Nusselt number, k_f is the thermal conductivity of the ambient fluid, $\mathrm{Pr}\left(= \upsilon_f/\alpha\right)$ is the Prandl number, and $\mathrm{Re}\,(= v\,D/\upsilon_f)$ is the Reynolds number of the thermocouple wire. Here, v and υ_f are the fluid velocity and kinematic viscosity, respectively. It should be noted that the convective heat transfer coefficient $h\ \alpha\ D^{1/2}$ and the natural frequency of a thermocouple wire for given material properties $\omega_n\ \alpha\ D^{-3/2}$.

2.4.1 One Material Thermocouple

The amplitude ratio $|T(0)|$ at the wire junction for the steady-state frequency response derived from Eqs. (2.17) and (2.32) is shown in fig. 3. This assumes a type

B thermocouple wire with the dimensions listed in table 1. In this case, the average material properties listed in table 1 were used since the one material theory assumes that the properties of the thermocouple wire are uniform across the junction. It is evident in fig. 3 that the amplitude ratio derived from the approximate expression Eq. (2.17) is nearly identical to the exact derivation Eq. (2.32). Thus, it appears that the conservation of heat flux at the interface between the small and large wires of the schematic of fig. 1 is of secondary importance.

Also included in fig. (3) are the numerical computations of Stocks (1986). These solutions represent explicit finite difference solutions to the one dimensional unsteady heat transfer equation as shown in Eq. (2.1). The small deviation of the numerical results from the exact solution at low frequency in fig. (3) is apparently due to the unsteady character of the numerical results. Similar computations of the phase angle Φ for the type B thermocouple are represented in fig. 4. As indicated, the phase angle varies over the range $0 \geq \Phi \geq -\pi/2$ and approaches the lower limit of $-\pi/2$ for large frequencies $\omega/\omega_n >> 1$.

The spacial variation of the amplitude ratio $|T(x)|$ derived from Eqs. (2.17) and (2.32) is graphed in fig. 5. These computations were made at an angular frequency of ω/ω_n = 0.1 for the type B thermocouple. As evident in fig. 5, the difference between the exact and approximate expression is somewhat exaggerated at a very low frequency. Nevertheless, the error represented by the approximate solution is less than 7% over the length of the thermocouple. As stated earlier, matching the heat flux at the interface between the small and large wire at $x = \pm l$ in the schematic of fig. 1 appears to be of secondary importance in relation to providing a

continuous temperature profile along the wire.

The amplitude ratio $|T(0)|$, phase angle Φ and spacial variation $|T(x)|$ are also plotted in figs. (6), (7) and (8), respectively, from the steady-state frequency response represented by Eqs. (2.17) and (2.32). These results represent a type B thermocouple with a smaller diameter ratio $D_2/D_1 = 2$ (see table 1 for dimensions). As indicated in figs. (6), (7) and (8), the approximate and exact solutions represent comparable results in all three cases. Thus, the diameter ratio of the large and small wire appears to have little effect in the favorable comparison between the approximate and exact solutions representing the one material steady-state frequency response.

2.4.2 Two Material Thermocouple

The amplitude ratio $|T(0)|$ at the wire junction for the steady-state frequency response derived from Eqs. (2.17) and (2.40) is shown in fig. 9. This assumes a type B thermocouple wire with the dimensions listed in table 2. In this case, the average material properties listed in Table 2 were used for the amplitude of the frequency response derived from the one material solution of Eq. (2.17). Also plotted in fig. 9 is the amplitude ratio derived from the two material solution of Eq. (2.40). In the latter case, the individual material properties listed in Table 2 were used.

As expected, the amplitude ratio for the steady-state frequency response of a type B thermocouple is nearly identical with either the one material or two material approximate solutions. This is a consequence of roughly equal material properties across the junction for type B thermocouples. This plot also validates

the two material approximate solution Eq. (2.40) and the values of the boundary conditions for T_a and T_b substituted from Eqs (2.38) and (2.39). The same conclusion can be drawn with respect to the phase angle Φ, shown in fig. 10.

The spacial variation of the amplitude ratio $|T(x)|$ derived from Eqs. (2.17) and (2.40) is plotted in fig. 11. These computations were made at an angular frequency of $\omega/\omega_n = 0.1$ for the type B thermocouple with the dimensions listed in table 2. It is interesting to note the small asymmetry in the amplitude ratio on the left and right side of the junction. This asymmetry is the result of the small differences in the physical properties across the junction as listed in table 2.

The steady state amplitude ratio $|T(0)|$ for a type T thermocouple is plotted in fig. 12 using equations (2.17) and (2.40). The dimensions and material properties are listed in table 2. The average material properties listed in Table 2 were used to compute the amplitude ratio of the frequency response with the one material solution, Eq. (2.17). Also plotted in fig. 12 is the amplitude ratio derived from the two material solution, Eq. (2.40). In the latter case, the individual material properties also listed in table 2 were used.

As indicated in fig. 12, the amplitude ratio for the approximate one material steady-state frequency response of a type T thermocouple is distinctly different from the two material approximate solution. This is a consequence of unequal material properties across the junction for the type T thermocouple. Also shown in fig. 12 is a numerical solution of the second order ordinary differential equation for the temperature, Eq. (2.6). The numerical finite difference solution of the boundary value problem of Eq. (2.6) matches both the temperature and heat flux at

$x = 0$ and $x = \pm l$ in the schematic of fig. 2. It is clear from fig. 12 that the approximate two material analytical solution, equation (2.40), is in good agreement with the numerical results despite some differences at low frequencies $\omega/\omega_1 < .04$. Similar results are indicated for the phase angle Φ in fig. 13.

The spacial variation of the amplitude ratio $|T(x)|$ derived from Eqs. (2.17) and (2.40) is graphed in fig. 14. These computations were made at an angular frequency of $\omega/\omega_1 = 0.1$ for the type T thermocouple. As evident in fig. 14, the two material solution derived from Eq. (2.40) accurately represents the features of the asymmetry associated with a type T thermocouple. In particular, the relatively large resistance to axial heat conduction in the constantan wire on the right of the junction is reflected in the larger values of the amplitude ratio $|T(x)|$. Also shown in fig. 14 is the approximate one material solution represented by Eq. (2.17). In the latter case, the average values for the material properties of a type T thermocouple were used as listed in Table 2. Therefore, one can conclude that for thermocouples whose material properties on either side of the junction are markedly different, the two material solution developed in this paper is a substantial improvement in accuracy both in frequency response and in temperature distribution along the wire.

2.5 EXPERIMENTAL PROCEDURE

In the experiment described below, thermocouple sensors were exposed to a constant velocity air stream of varying temperature. In particular, the dynamic response of the thermocouple sensors to a square wave temperature profile was

measured for a range of frequencies.

2.5.1 Rotating Wheel Experiment

A rotating wheel configuration was used to deliver the test airstream to the proposed sensors. A similar experimental apparatus is described in detail by Elmore et al. (1986). A schematic of the rotating wheel apparatus used in the present experiment is shown in figure 15. As the wheel rotates, the holes pass the two air supply tubes which allow slugs of hot and cold air to alternately enter a transition tube assembly mounted directly above the rotating wheel. In the transition tube the slugs of hot and cold air coalesce into a single air stream providing roughly a square wave temperature profile covering a range of frequencies from roughly 1 to 30 Hz.

The analog temperature signal was digitized with a Data Translation DT-2801 board mounted in an expansion slot of an IBM AT compatible computer as shown in figure 15. The ASYST software loaded on the hard disc of the personal computer provided a flexible system for data storage, manipulation and display.

The true temperature profile of the airstream was measured with a constant current anemometer (TSI 1054-A) and sensor (1226 PI 2.5).

2.5.2 Thermocouple Construction

Thermocouple wire of the desired length and type is threaded into the four hole ceramic with the thermocouple end last. Three or four kinks are made in each wire near the thermocouple end so the wire must be firmly pulled into the tube leaving enough wire sticking out to make the thermocouple. Drops of epoxy

are picked up with a piece of .010" diameter wire, added to the ceramic tube at A (see fig. 16) and pushed down around both wires. The kinks and epoxy firmly fasten the wires in the ceramic so they do not twist when the free ends are manipulated for electrical connections.

The junction at B in figure 16 is made by cutting the large wire about half way through with a razor blade, laying the small diameter wire in the cut, and welding the cut closed with a stored energy spot welder. After the weld, the excess wire ends that protrude through the weld area are bent and broken off to clean up the junction.

For the chromel alumel couples, the junction at C of figure 16 was made using a stored energy spot welder. The wires are crossed and welded and then trimmed with a razor blade and bent with tweezers under a microscope until collinear.

A stored energy spot welder will not work for the copper constantan couples. For these couples the junctions were made by silver soldering. The silver solder wire is coated with flux and the end heated with a torch until a drop forms. A twisted pair of thermocouple wires is pushed briefly into the flux coated solder drop. The solder will wet the pair up to where the twist stops. Again using a razor blade and tweezers under a microscope, the thermocouple is bent and trimmed until collinear.

2.5.3 ASYST Software

ASYST software was developed to acquire temperature data simultaneously from the thermocouple and constant current anemometer. Data were digitized for

two channels at a sampling rate of 512 Hz per channel for a total sample time of two seconds. The ASYST software code is listed in figure 17.

The ASYST code first plotted the temperature profiles versus time from the thermocouple and anemometer and an example of the plot is shown in figure 18. The ASYST software next took the Fast Fourier Transform of the temperature data in each channel and recorded the amplitude ratio and phase angle between both channels at the first harmonic for the square wave. These data are discussed in the next section.

2.6 EXPERIMENTAL RESULTS

Initial tests with a signal generator and the output from an RC circuit indicated that the ASYST code and data acquisition hardware were operating properly. Several test sensors were constructed and tested with the dimensions listed in table 3. In each case measurements of the amplitude and phase angle were compared with the appropriate theory. A discussion of the results is given below.

2.6.1 First Order Response

The amplitude ratio and phase angle were measured with the type K thermocouple listed first in table 3. The lengths of the thermocouple and support wires in this case were chosen to eliminate the effects of axial heat conduction. The experimental data representing the amplitude ratio are plotted in figure 19 along with the theory representing a first order frequency response. The experimental data were correlated with a natural frequency $\omega_1 = 5.5\,\mathrm{sec}^{-1}$ and a

thermal diffusivity of $\alpha = .059\ cm^2 / \text{sec}$.

As indicated in figure 19 the data has been correlated with the theory to within 10%. Although the experimental data is reproducible, there is a noticeable drift of the data relative to the theory with increasing wheel frequency ω. The drift is probably due to a small increase in the natural frequency ω_1 of the thermocouple wire with increasing wheel frequency ω.

The natural frequency ω_1 of Equation (2.10) depends on accurate predictions of the convective heat transfer coefficient h from Equation (2.41). However, there may be a small change in either the mean air velocity or unsteadiness in the mean velocity which would lead to small changes in the heat transfer coefficient h and the natural frequency ω_1.

Also plotted in figure 20 are experimental data representing the phase angle Φ for the first order frequency response of the type K thermocouple. In this case the data is correlated to within 7% of the theory. The experimental data for the phase angle also indicate a small drift in the natural frequency ω_1 as was apparent in figure 19.

2.6.2 Frequency Response (one material)

The amplitude ratio and phase angle were measured with the second type K thermocouple listed in table 3. The lengths of the thermocouple and support wires in this case were chosen (i.e., shortened) to demonstrate the effects of axial heat conduction. The experimental data representing the amplitude ratio are plotted in figure 21 along with the theoretical prediction given by Eq. (2.32). Both

the data and theory were correlated by assuming that the material properties are uniform across the thermocouple junction. In this case the data were correlated with a natural frequency $\omega_1 = 5.0\ \text{sec}^{-1}$ and a thermal diffusivity of $\alpha = .059\ cm^2 / \text{sec}.$

As indicated in figure 21 the data has been correlated with the theory to within 10% over most of the range of wheel frequencies. The data is reproducible but again a noticeable drift of the experimental data exists relative to the theory as was discussed in the previous section.

Also plotted in figure 22 are experimental data representing the phase angle Φ for the frequency response of the shortened type K thermocouple. The data is correlated to within 7% of the theory. The experimental data for the phase angle also indicate a small drift in the natural frequency ω_1.

2.7 NOMENCLATURE

A	=	constant of integration
B	=	constant of integration
c	=	material specific heat $\left(J-gm^{-1}-{}^{0}K^{-1}\right)$
D	=	thermocouple wire diameter (cm)
G	=	$1+i(\omega/\omega_n)$
h	=	heat transfer coefficient $\left(J-cm^{-2}-s^{-1}-{}^{0}K^{-1}\right)$
i	=	unit imaginary number $\left(=\sqrt{-1}\right)$
k	=	material thermoconductivity $\left(J-cm^{-1}-s^{-1}-{}^{0}K^{-1}\right)$
k_f	=	gas thermoconductivity $\left(J-cm^{-1}-s^{-1}-{}^{0}K^{-1}\right)$
l	=	length of small thermocouple wire (cm)
L	=	length of large thermocouple wire (cm)
Nu	=	Nusselt number (= hD/k_f)
Pr	=	Prandl number (= υ_f/α)
Q	=	$\frac{D_1^2 q_1}{D_2^2 q_2}$
Q_t	=	$\frac{k_1 q_1}{k_2 q_2}$
Q_s	=	$\frac{k_1 q_3}{k_2 q_4}$
q	=	$(G/\gamma)^{.5}$
Re	=	Reynolds number (= vD/υ_f)
t	=	time (s)

T	=	steady-state frequency response
T_f	=	amplitude of periodic gas temperature $\left({}^0K\right)$
T_g	=	gas temperature $\left({}^0K\right)$
T_0	=	mean gas temperature $\left({}^0K\right)$
$\vec{T}_\omega$	=	complex amplitude of periodic wire temperature$\left({}^0K\right)$
T_w	=	local wire temperature $\left({}^0K\right)$
v	=	gas velocity $\left(cm-s^{-1}\right)$
x	=	axial distance from center of wire (cm)

Greek Symbols

α	=	thermal diffusivity $\left(cm^2-s^{-1}\right)$
γ	=	$\alpha / \omega_n \ \left(cm^2\right)$
υ_f	=	kinematic viscosity of gas $\left(cm^2-s^{-1}\right)$
ω	=	angular frequency $\left(s^{-1}\right)$
ω_n	=	natural frequency of wire $(=4h/\rho cD)\left(s^{-1}\right)$
Φ	=	phase angle
ρ	=	material density (gm - cm^{-3})
Δ_1	=	dimensionless function
Δ_2	=	dimensionless function

2.8 REFERENCES

1. Carslaw, H. S., Introduction to the Mathematical Theory of the Conduction of Heat in Solids, Dover Publications, 2nd edition (1945).

2. Dils, R. R. and Follansbee, P. S., Wide Bandwidth Gas Temperature Measurements in Combustor and Combustor Exhaust Gases, Instrumentation in the Aerospace Industry, 21 (B. Washburn, ed.), ISA 76245 (1976).

3. Elmore, D. L., Robinson, W. W. and Watkins, W. B., Dynamic Gas Temperature Measurement System: Final Report, NASA CR-168267 (1983).

4. Elmore, D.L., Robinson, W. W. and Watkins, W. B., Further Development of the Dynamic Gas Temperature Measurement System: Vol. I - Technical Efforts, NASA CR-179513 (1986).

5. Stocks, D. R., Further Development of the Dynamic Gas Temperature Measurement System: Vol. II - Computer Program User's Manual, NASA CR-179604 (1986).

6. Forney, L. J. and Fralick, G. C., Frequency Response of a Uniform Thermocouple Wire: Effects of Axial Conduction, Proceedings of the 6th Miami International Symposium on Heat and Mass Transfer (1990).

7. Fralick, G. C., Correlation of Velocity and Velocity-Density Turbulence in the Exhaust of an Atmospheric Burner, Turbine Engine Hot Section Technology - 1985, NASA CP-2465, pp. 81-85.

8. Forney, L. J. and Fralick, G. C., Frequency Response of a Thermocouple Wire: Effects of Axial Heat Conduction, Progress Report Georgia Tech E19-666-1, Sept. (1990).

9. Hildebrand, F. B., Advanced Calculus for Applications, (2nd Ed), Prentice - Hall (1976).

10. Scadron, M.D. and Warshawsky, I., Experimental Determination of Time Constants and Nusselt Numbers for Bare-Wire Thermocouples in High-Velocity Air Streams and Analytic Approximation of Conduction and Radiation Errors, NACA TN-2599 (1952).

11. Touloukian, Powell, Ho and Clemens, (ed.), Thermal Physical Properties of Matter, Purdue Research Foundation, Plenum Pub. (1970).

2.9 TABLES AND FIGURES

Table 1 - Properties of One Material Wire (Type B)

Dimensions (cm)

D_1	D_2	D_2/D_1	l	L
.025	.05	2	.2	.35
.0076*	.038	5	.1	.2

Average Properties of Type B

$\rho c\left(\frac{J}{cm^3 - {}^\circ K}\right)$	$\alpha\left(\frac{cm^2}{\sec}\right)$
3.8	.22

Gas Properties

$T_0 = 900\,{}^\circ K$

$M = .26$

$P = 1\ atm$

*$\omega_1 = 32.9\ \sec^{-1}$

Table 2 - Properties of Two Material Wire

Dimensions (cm)

D_1	D_2	D_2/D_1	l	L
.0076	.038	5	.1	.2

Air Properties

$T_0 = 300\ °K$

$P = 1\ atm$

$V = 50\ m/\sec$

Properties of Type B

	$\rho c\left[\frac{J}{cm^3 - ok}\right]$	$\alpha\left[\frac{cm^2}{\sec}\right]$
Pt - 6% Rh	2.73	.238
Pt - 30% Rh	2.86	.190
Average	2.8	.214

Properties of Type T

	$\rho c\left[\frac{J}{cm^3 - °K}\right]$	$\alpha\left[\frac{cm^2}{\sec}\right]$
Copper	3.44	1.16
Constantan	3.48	.067
Average	3.46	.614

Wire Location

Region	Type B	Type T
1	Pt - 6% Rh	Copper
2	Pt - 30% Rh	Constantan

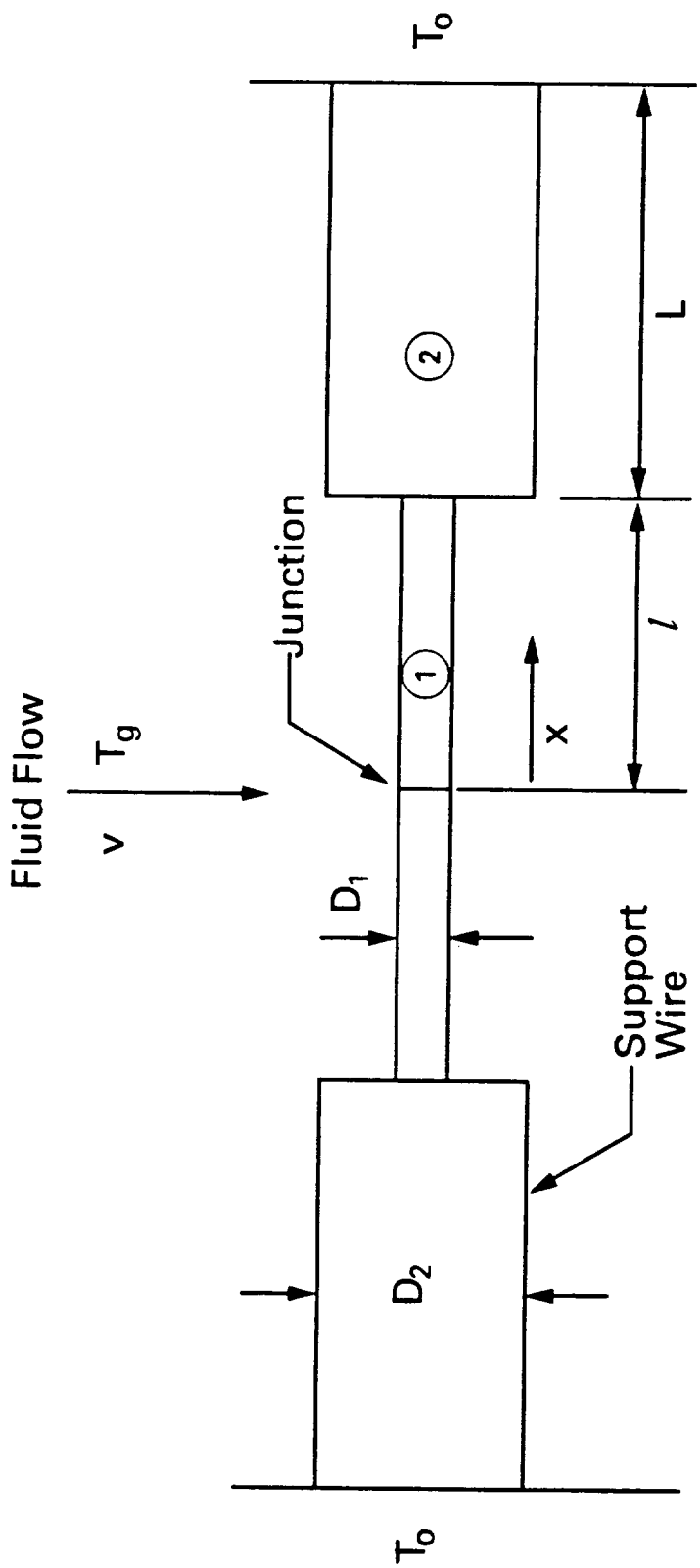

1. Schematic of one material supported wire.

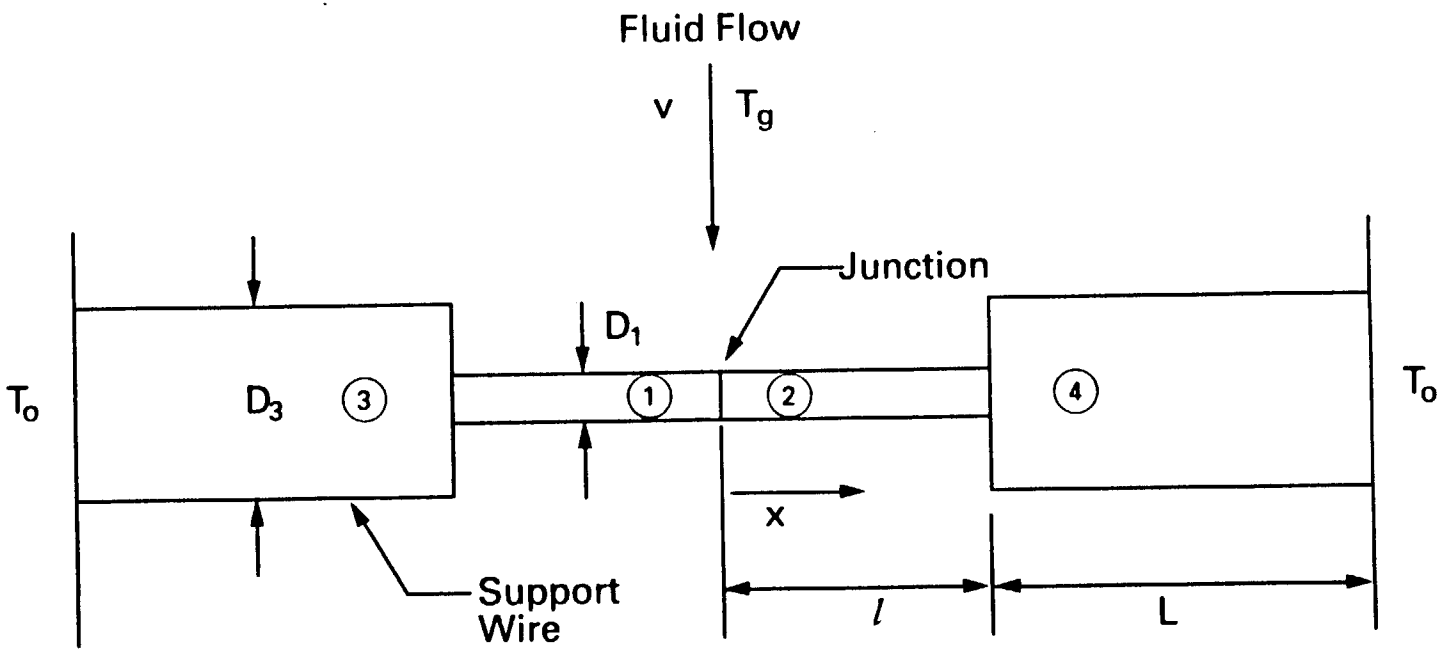

2. Schematic of two material supported wire.

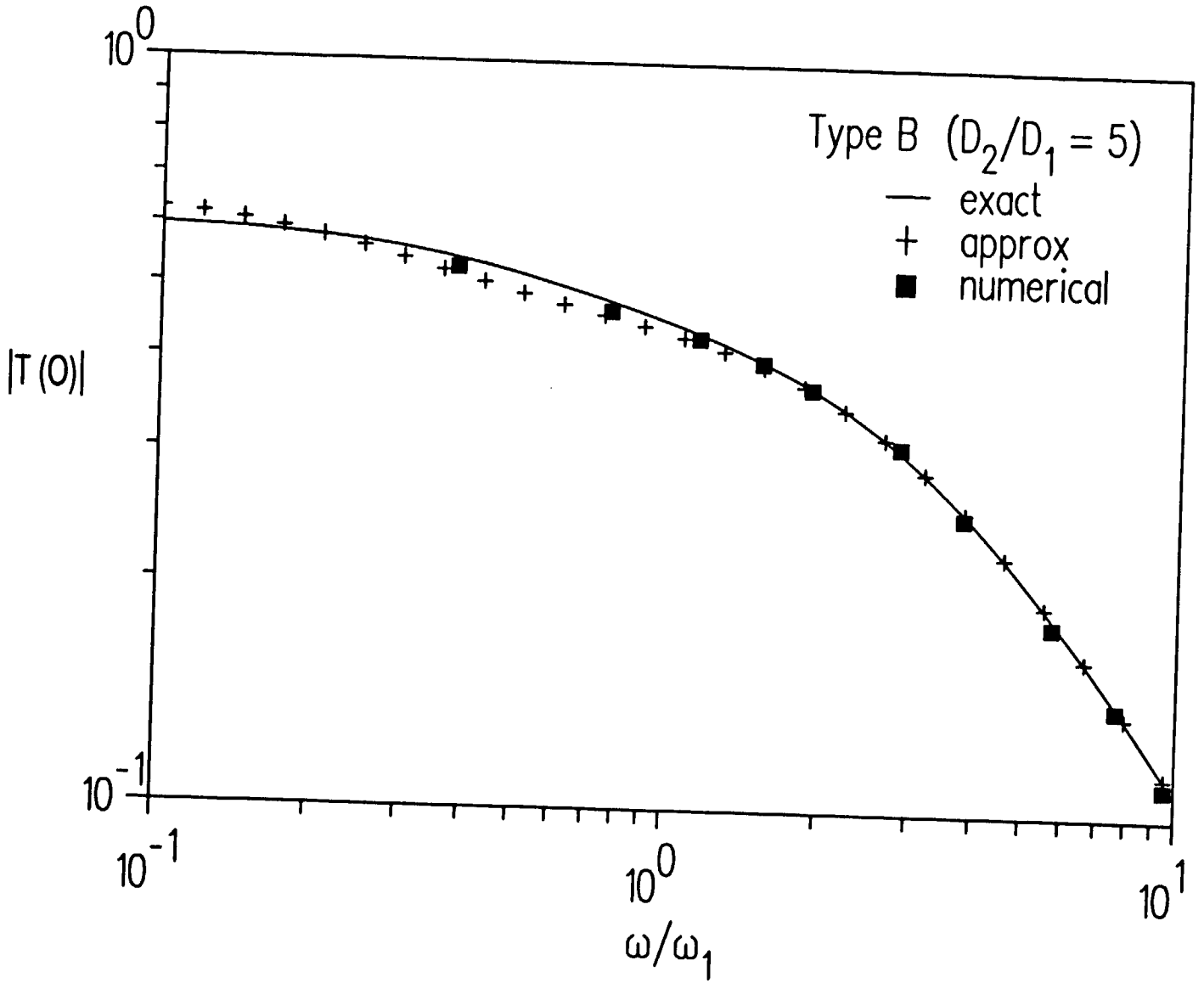

3. Amplitude ratio vs. angular frequency for one material wire. Solid line is exact solution Eq. (32); Crosses are approximate solution Eq. (17).

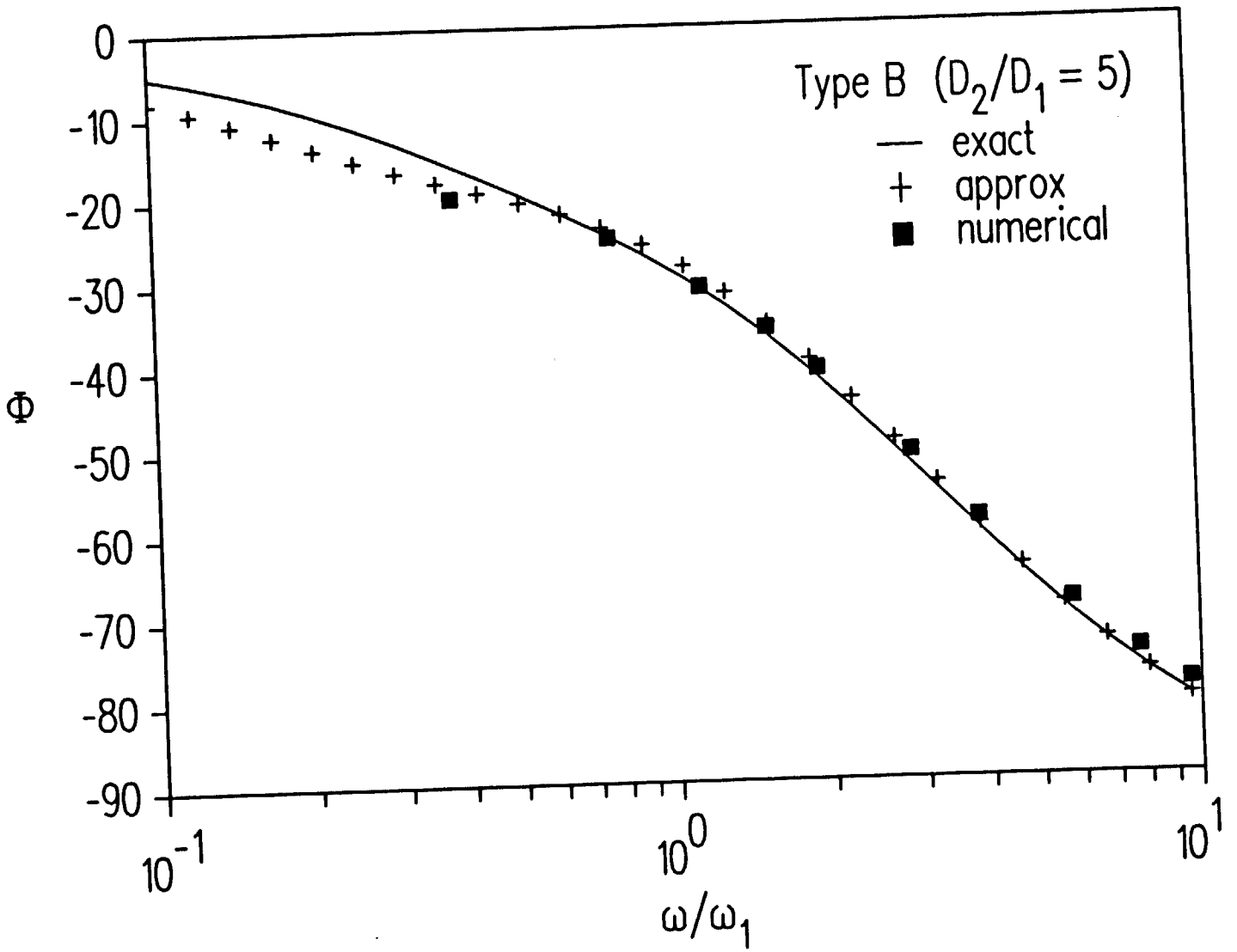

4. Phase angle vs. angular frequency for one material wire. Solid line is exact solution Eq. (32); Crosses are approximate solution Eq. (17).

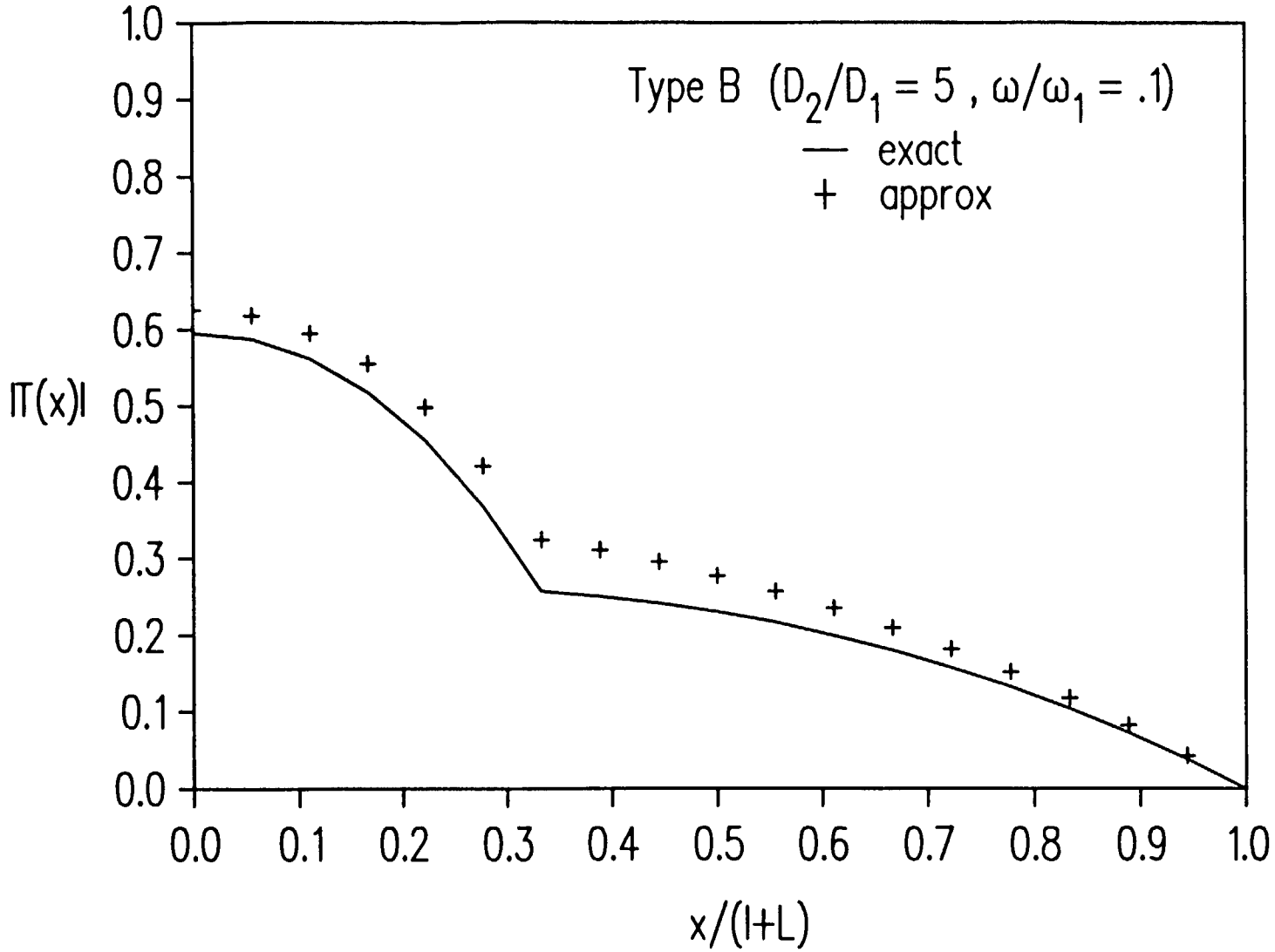

5. Amplitude ratio vs. distance for one material wire. Solid line is derived from Eqs. (24) and (31). Crosses are derived from Eqs. (14) and (16).

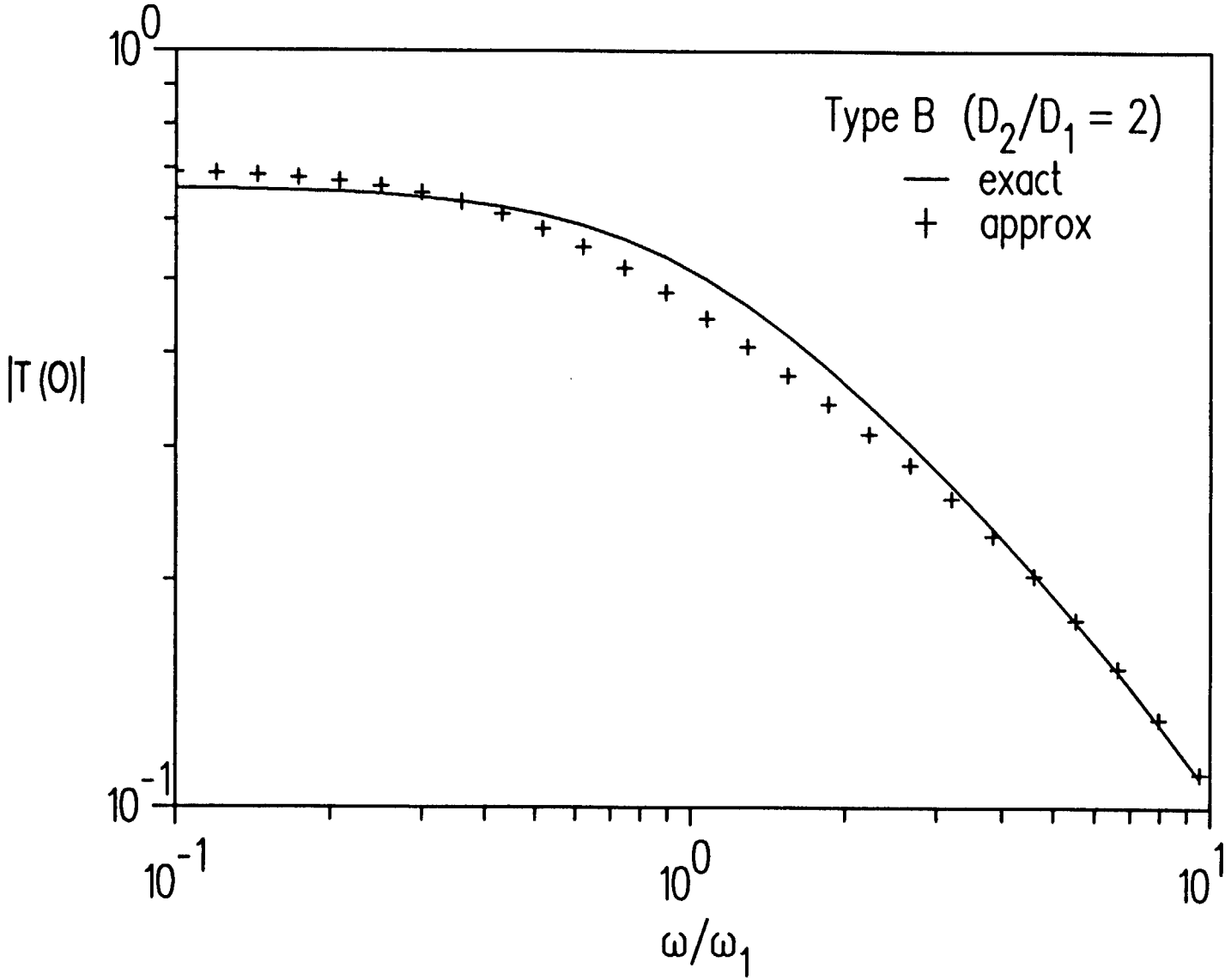

6. Amplitude ratio vs. angular frequency for one material wire. Solid line is Eq. (32). Crosses are Eq. (17).

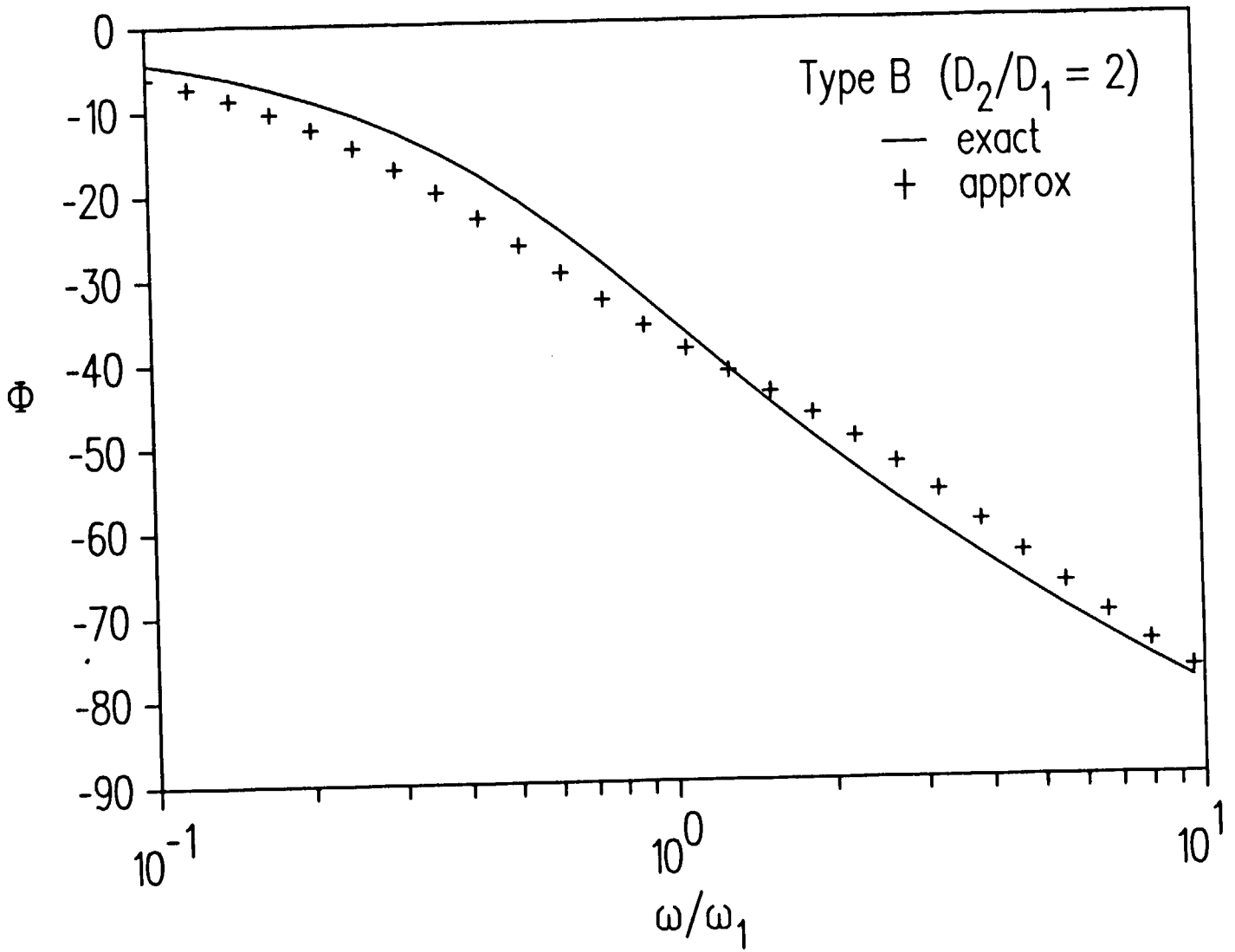

7. Phase angle vs. angular frequency for one material wire. Solid line is Eq. (32). Crosses are Eq. (17).

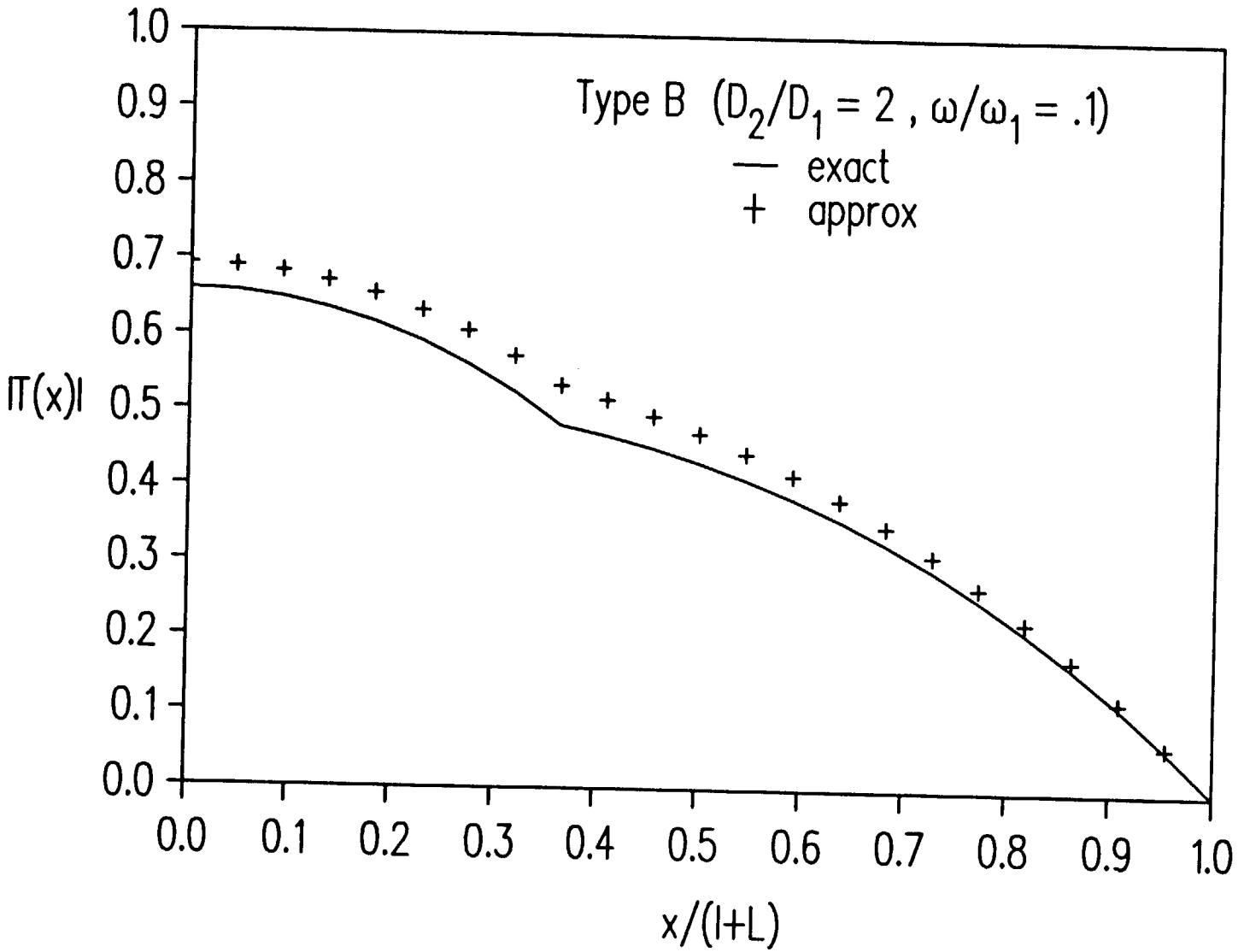

8. Amplitude ratio vs. distance for one material wire. Solid line derived from Eqs. (24) and (31). Crosses are derived from Eqs. (14) and (16).

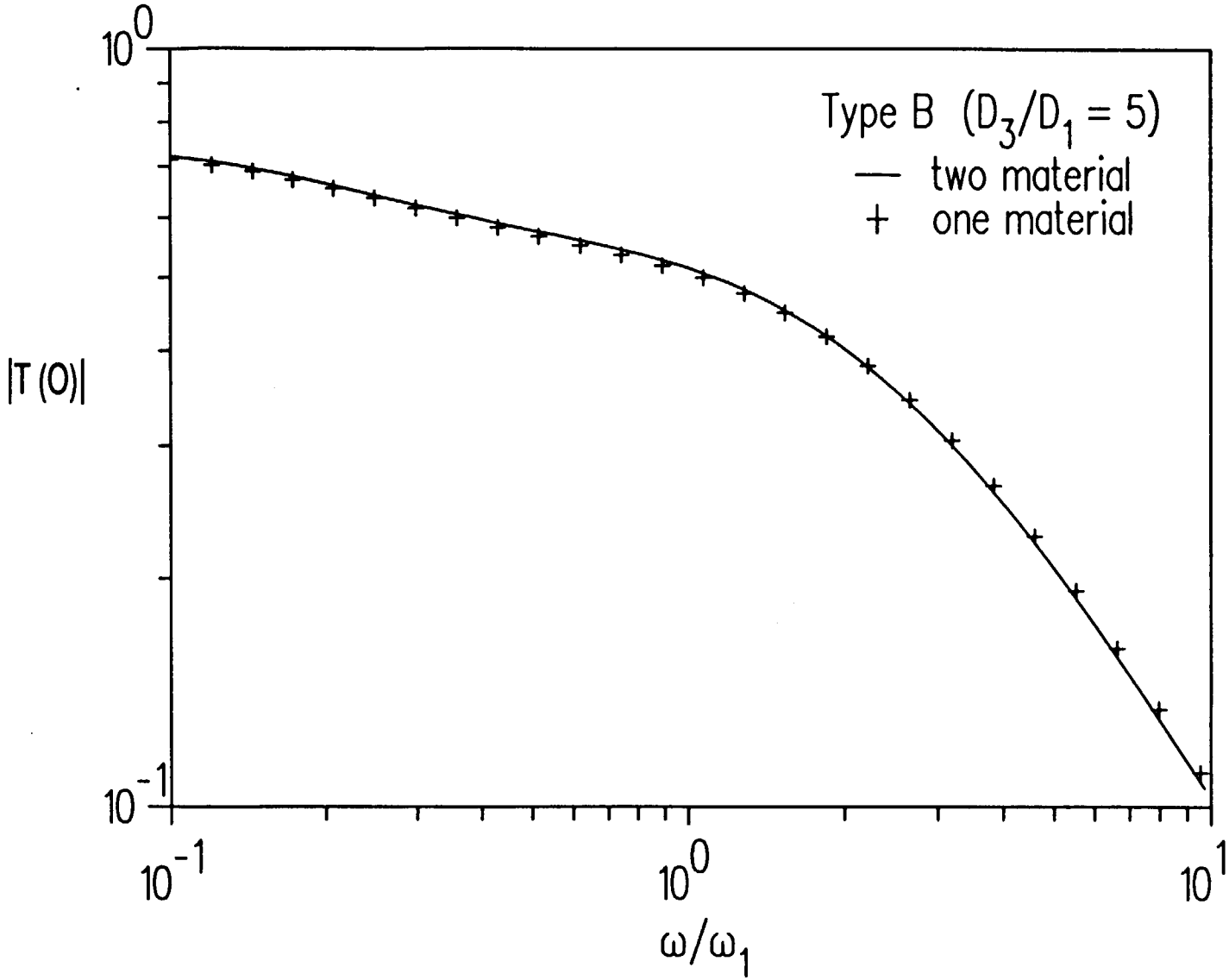

9. Amplitude ratio vs. angular frequency for two material wire. Solid line is Eq.. (40). Crosses are approximate one material solution Eq. (17).

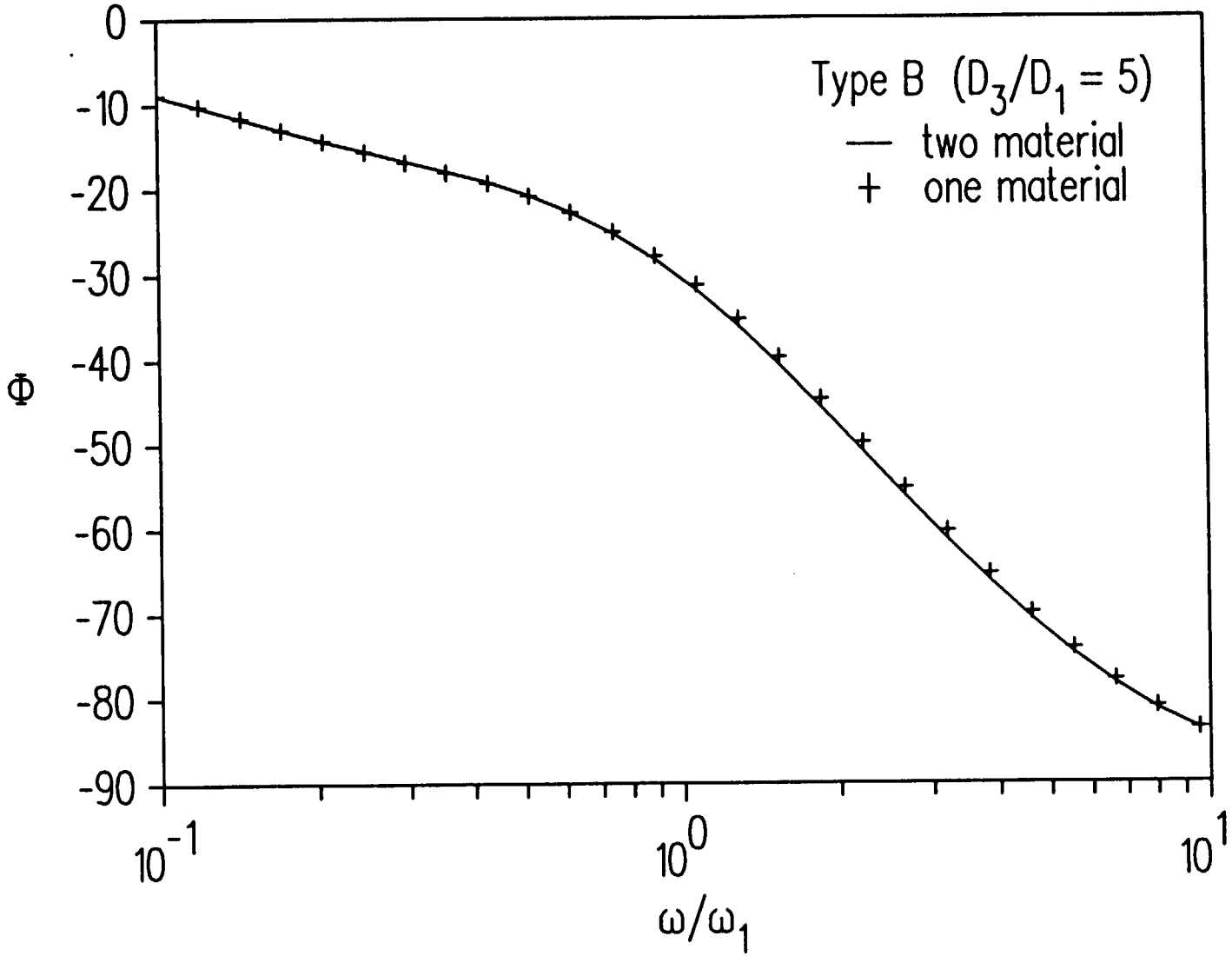

10. Phase angle vs. angular frequency for two material wire. Solid line is Eq. (40). Crosses are approximate one material solution Eq. (17).

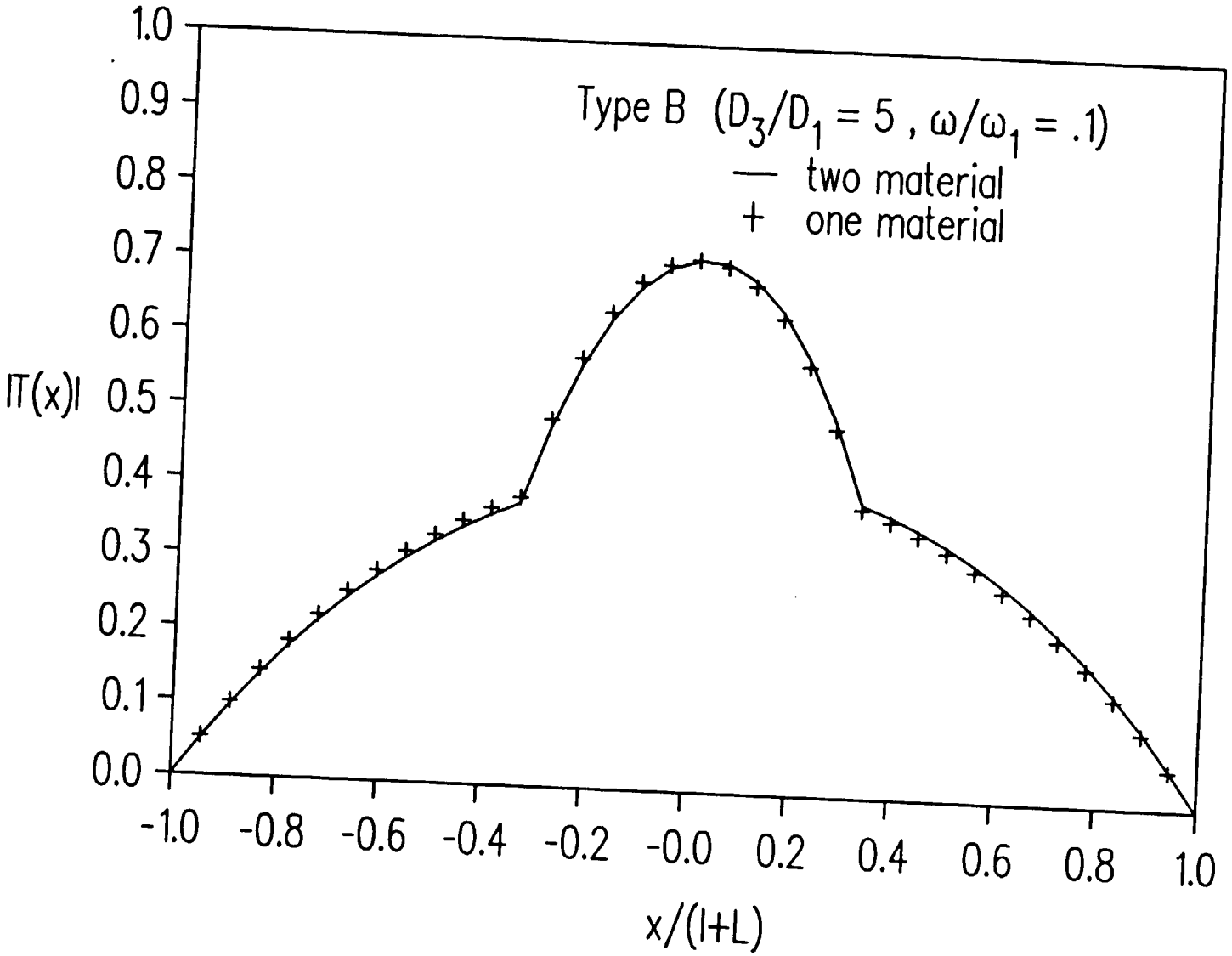

11. Amplitude ratio vs. distance for two material wire. Solid line derived from Eqs. (36a) and (36b). Crosses are approximate one material solution Eqs. (14) and (16).

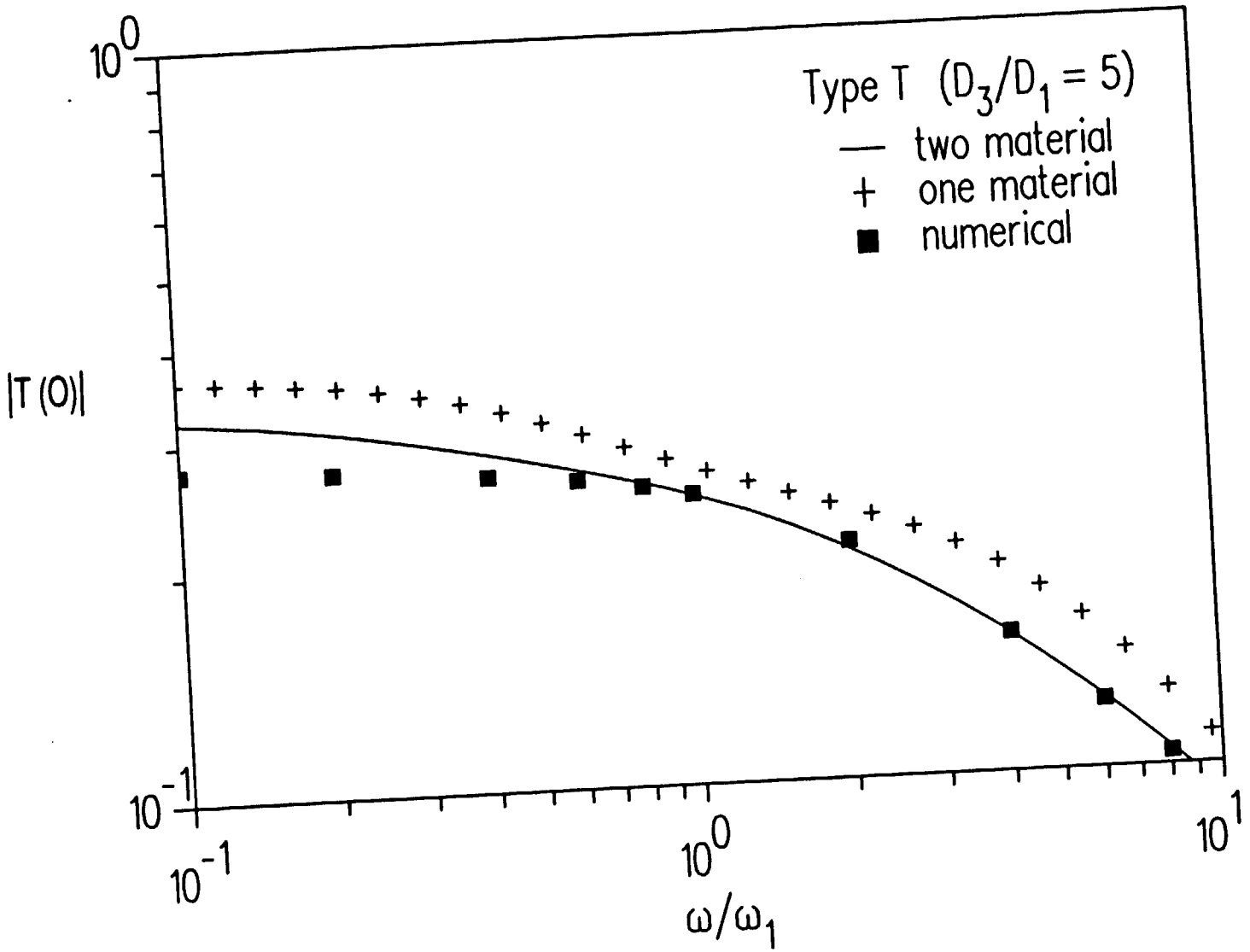

12. Amplitude ratio vs. angular frequency for two material wire. Solid line is Eq. (40). Crosses are approximate one material solution Eq. (17).

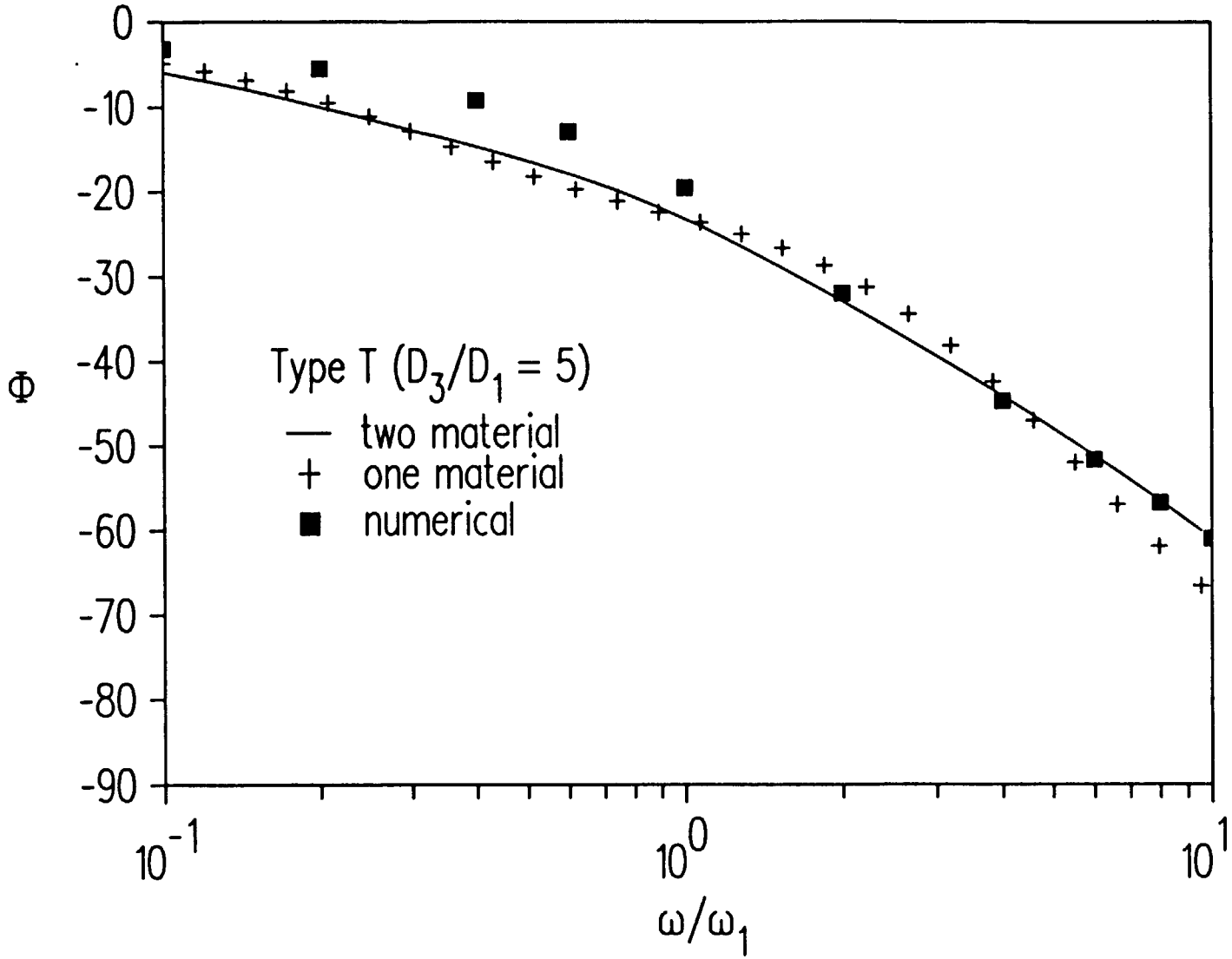

13. Phase angle vs.angular frequency for two material wire. Solid line is Eq. (40). Crosses are approximate on material solution Eq. (17).

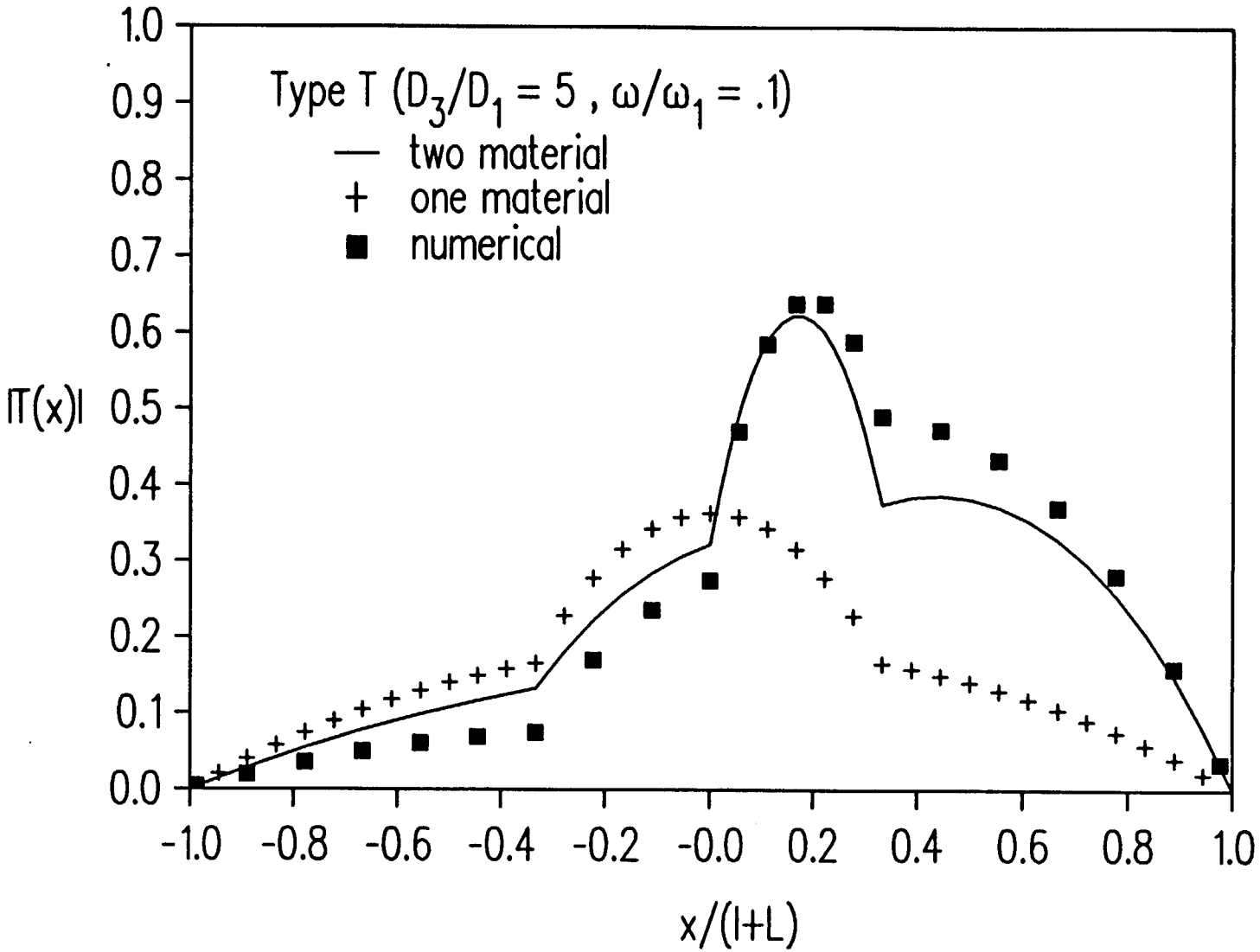

14. Amplitude ratio vs. distance for two material wire. Solid line derived from Eqs. (36a) and (36b). Crosses are approximate one material solution Eqs. (14) and (16).

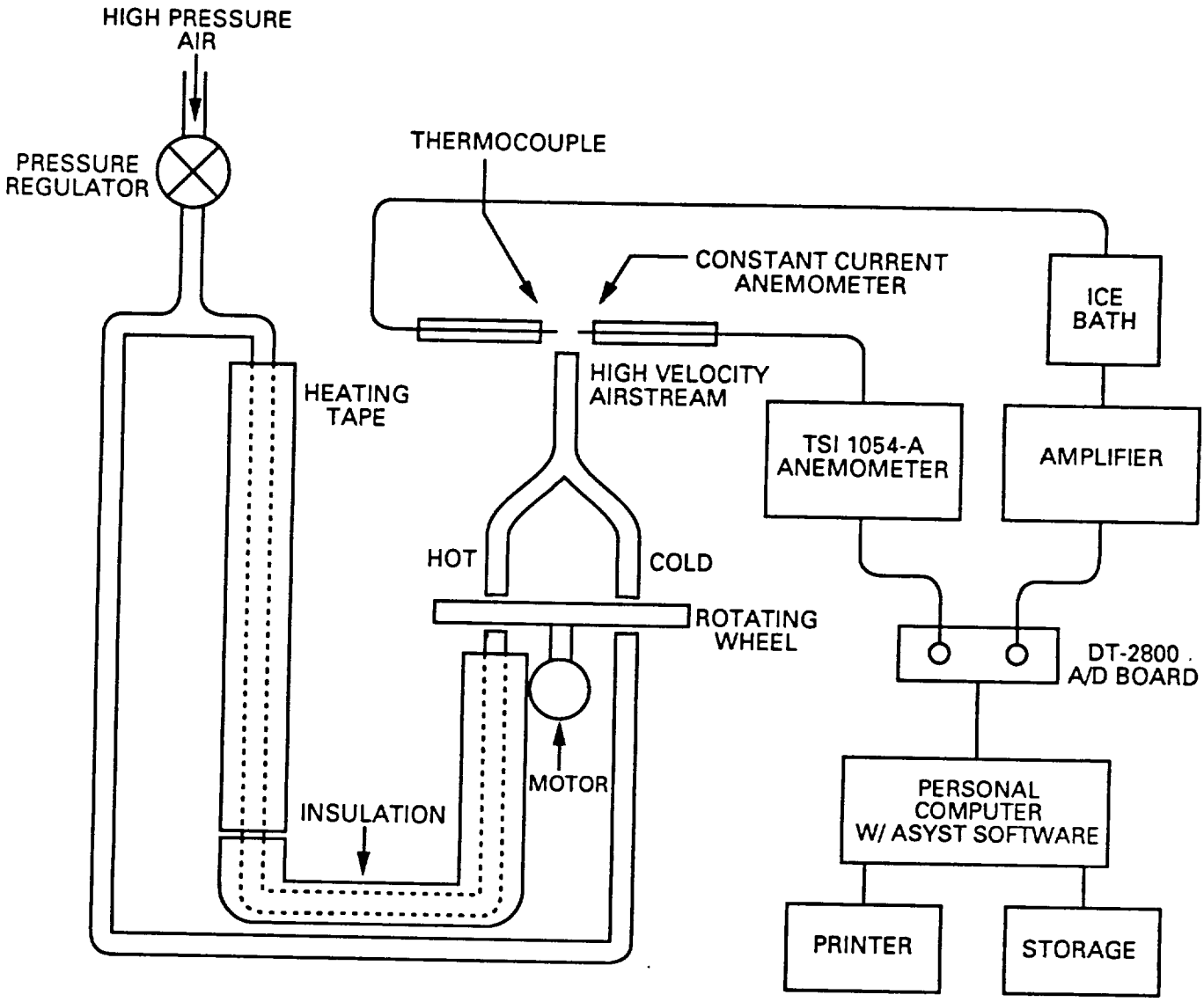

15. Rotating wheel experiment.

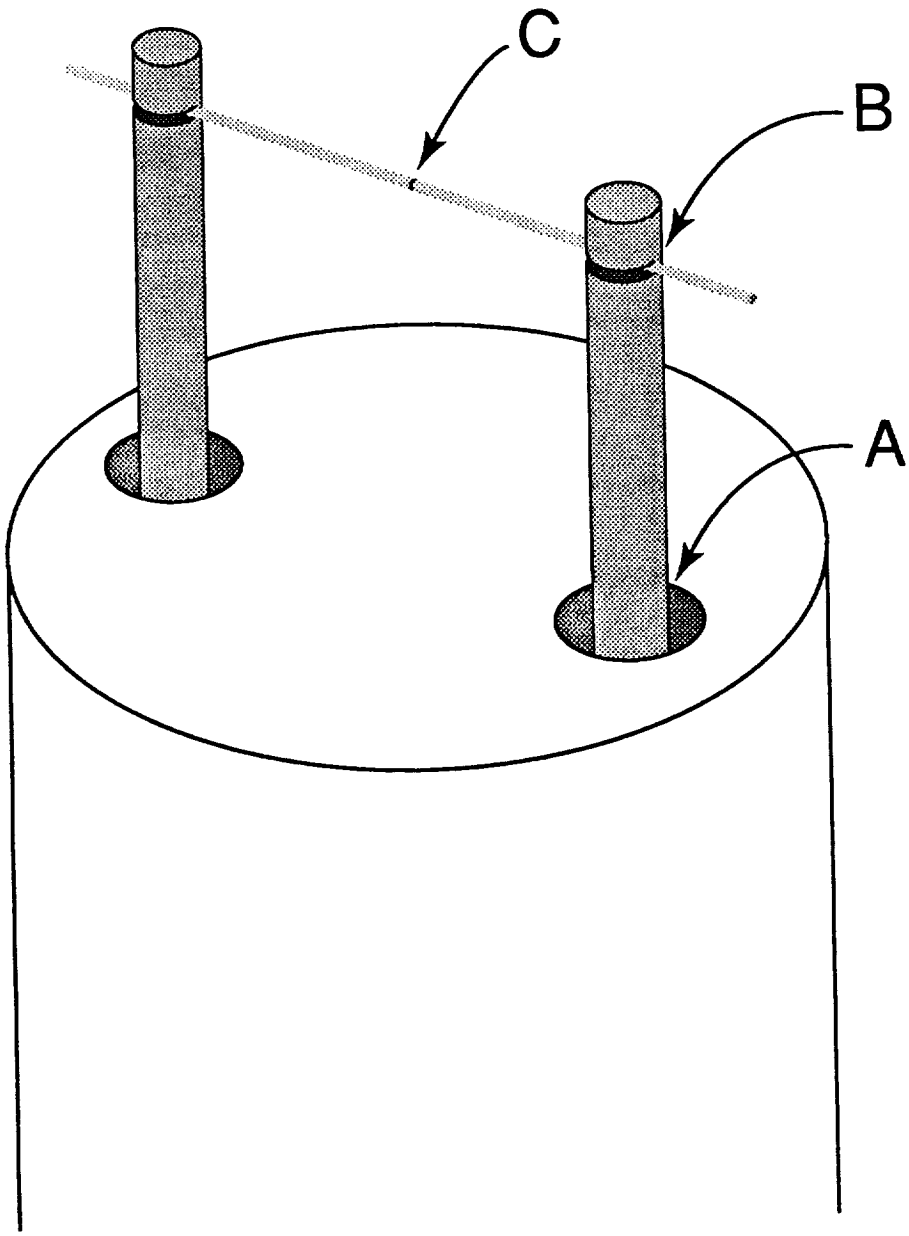

16. Schematic of test thermocouple

```
FORGET.ALL
REAL DIM[ 1024 ] ARRAY TIME
COMPLEX DIM[ 1024 ] ARRAY TRANS
REAL DIM[ 6 ] ARRAY ANS
REAL DIM[ 1024 ] ARRAY ZMAGO
REAL DIM[ 1024 ] ARRAY ZARGO
INTEGER SCALAR NUM
REAL SCALAR MEN
REAL SCALAR CD
REAL DIM[ 1024 ] ARRAY FREQS
REAL DIM[ 1024 ] ARRAY SIGNAL
INTEGER      dim[  1024 , 2  ]  array DATA.BUFFER


1. CD :=
.0000  DATA.BUFFER :=
LOAD.OVERLAY ACQUIS.SOV
.0000  1.0000  A/D.TEMPLATE DEMO.TEMPLATE  \ DEFINE AN A/D TEMPLATE
DATA.BUFFER TEMPLATE.BUFFER          \ DECLARE ARRAY AS A TEMPLATE BUFFER
CYCLIC                               \ SET TEMPLATE BUFFER TO CYCLIC MODE
 2048.0000  TEMPLATE.REPEAT          \ SET REPETITIONS FOR I/O INSTRUCTION
 CD  CONVERSION.DELAY                \ CONVERSION RATE (MSECS/SAMPLE)
DEMO.TEMPLATE A/D.INIT               \ INITIALIZE CURRENT A/D TEMPLATE
A/D.IN>ARRAY                         \ A/D INPUT TO TEMPLATES BUFFER
LOAD.OVERLAY WAVEOPS.SOV
1024 REAL RAMP 1 - 2 * CD * 1000 /  TIME :=  \ SET TIME AXIS

DATA.BUFFER  XSECT[ 1 ] 2048 -       \ CHANNEL 1 ON STACK (ANEMOMETER)
SIGNAL := SIGNAL
-2048 / 10 * -55.274 * 353. +        \ CALIBRATE (DEGREES C)
SIGNAL := SIGNAL
0.5 SET.CUTOFF.FREQ                  \ SMOOTH DATA (CYCLES/POINT)
SMOOTH  SIGNAL := SIGNAL
MEAN MEN := SIGNAL
MEN - SIGNAL :=                      \ CENTER ON ORIGIN
TIME SUB[ 1 , 500 , 1 ]  SIGNAL SUB[ 1 , 500 , 1 ]
XY.AUTO.PLOT SIGNAL                  \ PLOT CHANNEL 1
FFT                                  \ TAKE FFT
TRANS := TRANS ZMAG ZMAGO :=         \ MAGNITUDE OF FFT
5 SET.#.POINTS
1 SET.#.OPTIMA
ZMAGO SUB[ 1 , 120 , 1 ] LOCAL.MAXIMA  \ FIND INDEX AND MAX OF MAGNITUDE
SWAP NUM := NUM                      \ INDEX OF MAX MAGNITUDE
1 - CD / 1024. / 1000 * PI *         \ FREQUENCY AT MAX MAGNITUDE
ANS [ 1 ] := ANS [ 1 ] DROP ANS [ 2 ] :=
TRANS [ NUM ] DEG ZARG  ANS [ 3 ] :=    \ ARGUMENT AT MAX MAGNITUDE


DATA.BUFFER XSECT[ 2 ] 2048 -        \ CHANNEL 2 ON STACK (THERMOCOUPLE)
SIGNAL := SIGNAL
.124 * SIGNAL := SIGNAL              \ CALIBRATE (DEGREES F)
0.5 SET.CUTOFF.FREQ                  \ SMOOTH DATA (CYCLES/POINT)
SMOOTH  SIGNAL := SIGNAL
MEAN MEN := SIGNAL


ASYST Version 3.00
Page 1    TEMP3.FOR   03/13/91   11:42:33.77
```

```
MEN - SIGNAL :=                          \ CENTER ON ORIGIN
TIME SUB[ 1 , 500 , 1  ]
SIGNAL SUB[ 1 , 500 , 1 ]
XY.DATA.PLOT SIGNAL                      \ PLOT CHANNEL 2
FFT                                      \ TAKE FFT
TRANS := TRANS ZMAG ZMAGO :=             \ MAGNITUDE OF FFT
5 SET.#.POINTS
1 SET.#.OPTIMA
ZMAGO SUB[ 1 , 120 , 1 ] LOCAL.MAXIMA \ FIND INDEX AND MAX OF MAGNITUDE
SWAP NUM := NUM                          \ INDEX OF MAX MAGNITUDE
1 - CD / 1024. / 1000 * PI *             \ FREQUENCY AT MAX MAGNITUDE
ANS [ 4 ] := ANS [ 4 ] DROP ANS [ 5 ] :=
TRANS [ NUM ] DEG ZARG ANS [ 6 ] :=      \ ARGUMENT AT MAX MAGNITUDE

CR
."    FREQ       MAG       PHI   " CR
ANS [ 1 ]  ?  CR
ANS [ 5 ]  ANS [ 2 ] /  ? CR
ANS [ 3 ] -1 * ANS [ 6 ] + 180 PI / CD * 1000 / ANS [ 1 ] * - ? CR
FORGET.ALL
```

```
ASYST Version 3.00
Page 2     TEMP3.FOR    03/13/91    11:42:34.65
```

17. ASYST software

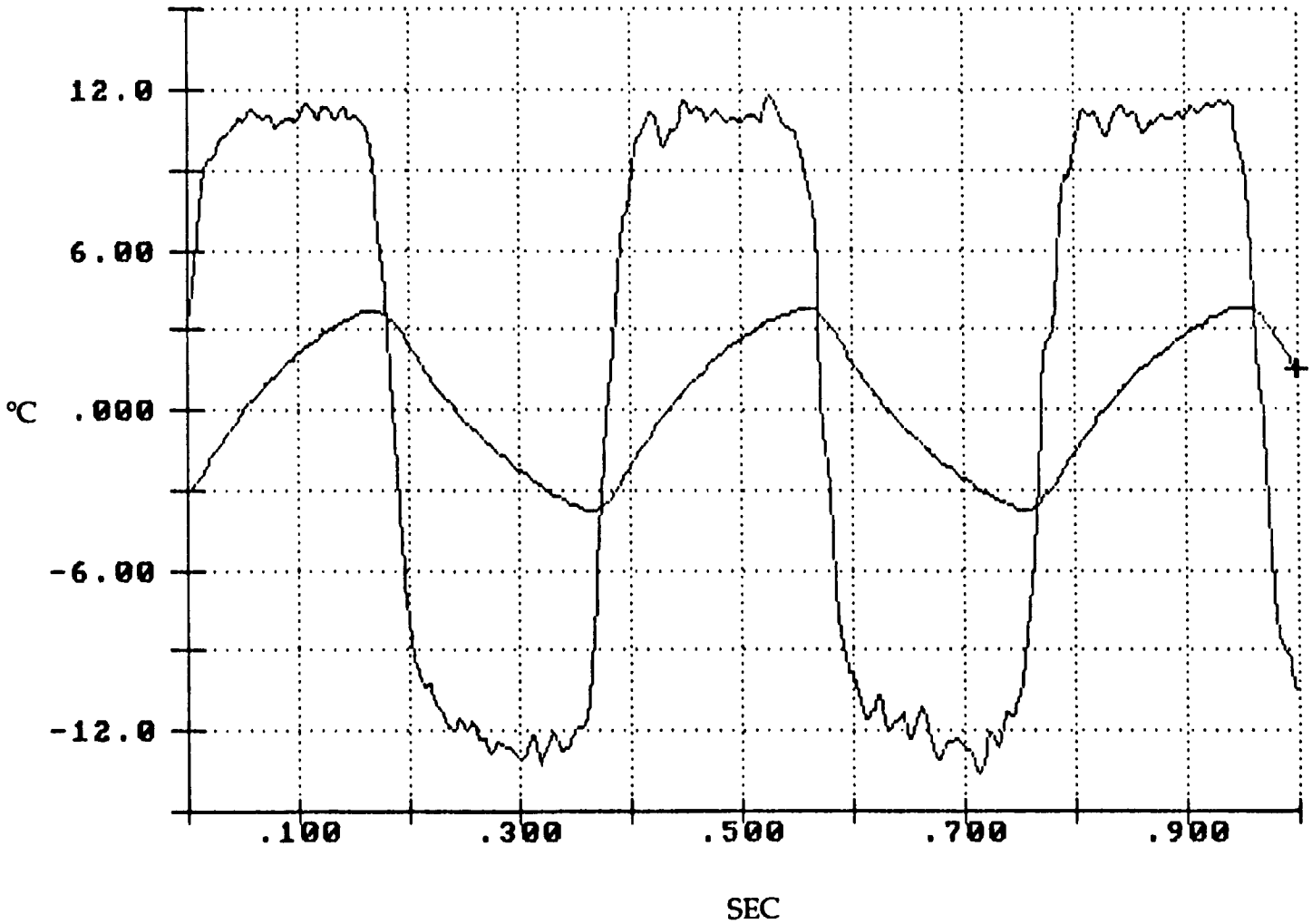

18. Gas Temperature Profile

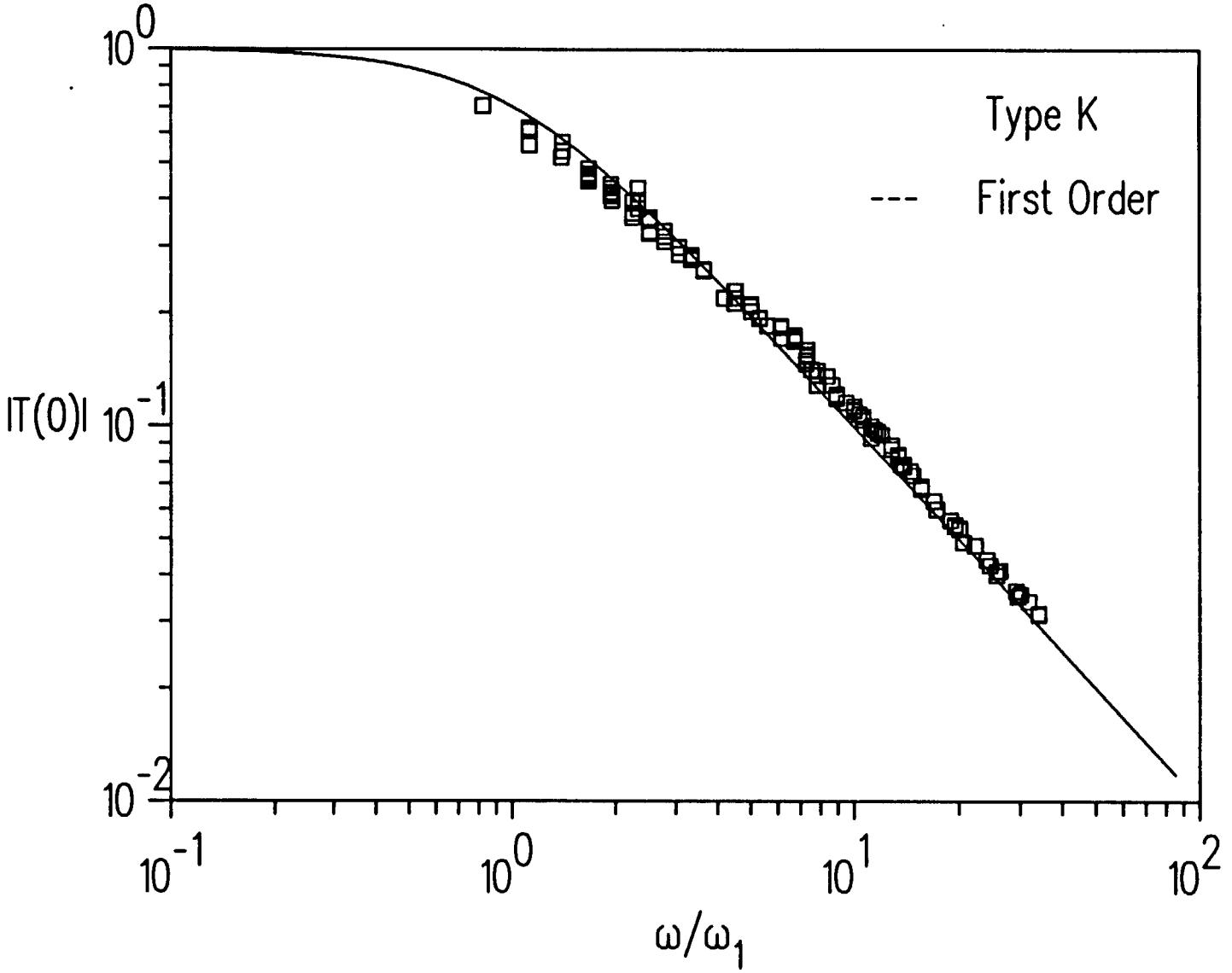

19. Amplitude ratio vs. angular frequency. $\omega_1 = 5.5\ \text{sec}^{-1}$, $\alpha = .059\ \text{cm}^2 / \text{sec}$.

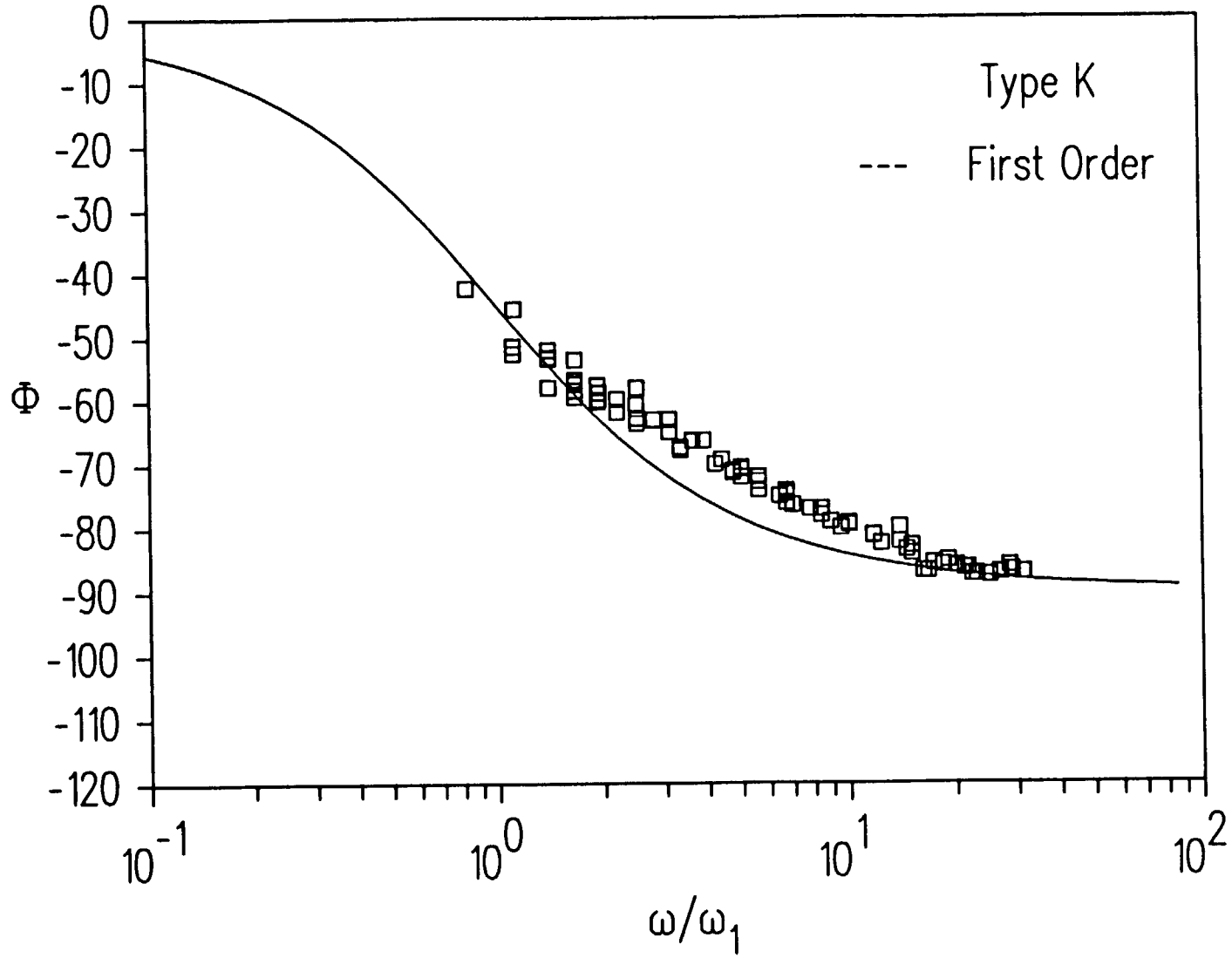

20. Phase angle vs. angular frequency. $\omega_1 = 5.5\ \text{sec}^{-1}$, $\alpha = .059\ \text{cm}^2 / \text{sec}$.

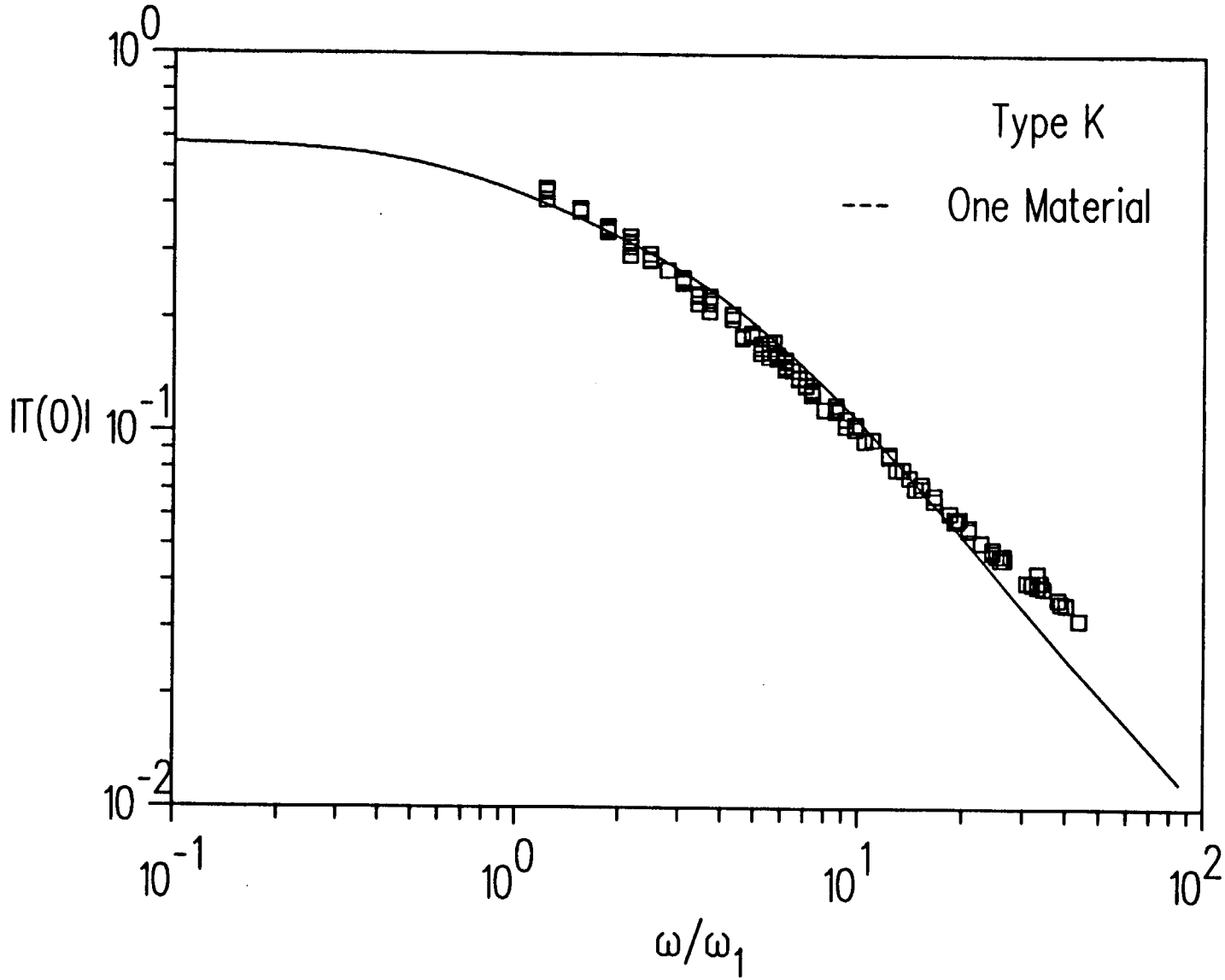

21. Amplitude ratio vs. angular frequency. Solid line is Eq. (32). $\omega_1 = 5.0\ \text{sec}^{-1}$, $\alpha = .059\ \text{cm}^2/\text{sec}$.

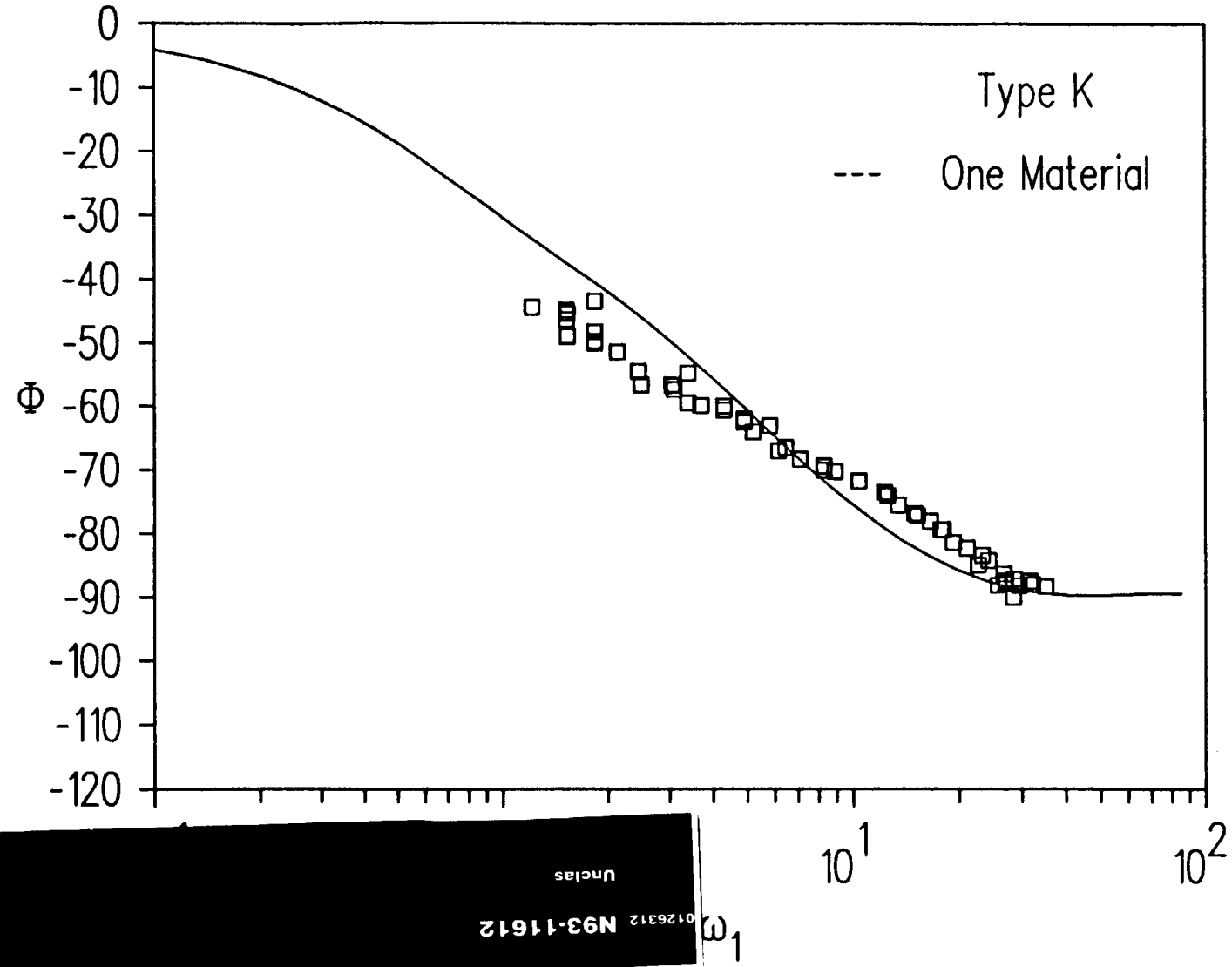

Solid line is derived from Eq. (32).

3.0 MEASUREMENT OF FREQUENCY RESPONSE

Experimental measurements are made for the steady-state frequency response of a supported thermocouple wire. In particular, the effects of axial heat conduction are demonstrated for both a supported one material wire (type K) and a two material wire (type T) with unequal material properties across the junction. The data for the amplitude ratio and phase angle are correlated to within 10% with the theoretical predictions of Forney and Fralick (1991). This is accomplished by choosing a natural frequency ω_n for the wire data to correlate the first order response at large gas temperature frequencies. It is found that a large bead size, however, will increase the amplitude ratio at low frequencies but decrease the natural frequency of the wire. The phase angle data are also distorted for imperfect junctions.

3.1 INTRODUCTION

The evaluation of jet engine performance and fundamental studies of combustion phenomena depend on the measurement of turbulent fluctuating temperatures of the gas within the engine (Dils and Follansbee, 1976). Historically, these temperatures have been measured with thermocouples. The advantages of thermocouples are their low cost, reliability and simplicity since they do not require optical access or elaborate support electronics. However, the design of a thermocouple represents a compromise between accuracy, ruggedness and rapidity of response.

For example, the measurement of fluctuating temperatures in the high speed exhaust of a gas turbine engine combustor is required to characterized the local gas density gradients or convective heat transfer (Fralick, 1985). Although thermocouples are suitable for the measurement of high frequency temperature fluctuations (<1 KHz) in a flowing gas or liquid, the measured signal must be compensated since the frequency of the time dependent fluid temperature is normally much higher than the corner frequency of the thermocouple probe (Scadron and Warshawsky, 1952). Moreover, the amplitude and phase angle of the thermocouple response may be attenuated by axial heat conduction for rugged thermocouples of finite length (Elmore, et al.; 1983, 1986).

In the present study, measurements are made of the steady-state frequency response of supported thermocouple wires. In particular, the effects of axial heat conduction are demonstrated for both a supported one material wire and a two material wire with unequal material properties across the junction. The measurements are presented in the form of the amplitude ratio and phase angle and these data are compared with the recent analytical results of Forney and Fralick, (1991).

3.2 THERMOCOUPLE FABRICATION

A supported thermocouple wire shown in figure 1 consists of a small diameter thermocouple element (horizontal wire) mounted on two large diameter supported wires (vertical wires). The large diameter support wires are mounted in a ceramic stick that assumes the mean gas temperature T_o. Since a supported

thermocouple is normally constructed manually, there are a number of physical imperfections that can affect the response. For example, three joints must be fabricated consisting of the thermocouple junction and joints at both ends of the thermocouple element. These three joints (welded or soldered) and the epoxy used to secure the support legs in the ceramic stick are darkened in the schematic at the bottom of figure 1. As indicated in figure 1, the supported thermocouple may not be symmetrical and there may be additional material or beads at the joint locations.

3.2.1. Physical Dimensions

The thermocouple support wires and the smaller thermocouple elements were analyzed by Elmore et al. (1983) for stresses at the maximum flow conditions for the F100 gas turbine engines of T = 1680°K, P = 2.01×10^6 Newton/meter^2 (202 psia) and a gas Mach number M = 0.36. The sensor location for these calculations corresponded to a wall position between the vanes downstream of the combustor exit. Elmore et al. (1983) also assumed an allowable stress in the thermocouple wire of 4.39×10^7 Newton/meter^2 (6360 psi). The maximum allowable length-to-diameter ratio L/D for the support wire was thus calculated to be 6.5 while the maximum value for the thermocouple element was found to be 15.5.

Elmore et al. (1986) also limited the smallest diameter of the thermocouple wire to 76 μm (.003 in) because of limitations to junction fabrication. These constraints limit the length of the thermocouple element on each side of the junction to roughly 1 mm or to a total length of 2 mm for the thermocouple wire

suspended between the support legs. Moreover, if the diameter of the supports is 380 μm(.015 in), the length of the support legs are limited to roughly 2 mm.

3.2.2. Materials

In the present study thermocouples are constructed of either type K (chromel-alumel) or type T (copper-constantan) materials. The properties of these materials including the product of specific heat and wire density ρc and the thermal diffusivity $\alpha = k/\rho c$ are listed in table 1. The type K thermocouple was chosen since one normally assumes that the material properties are equal across the junction. In contrast, the type T thermocouple has a distinctly different thermoconductivity across the junction. As a result, the temperature profile is asymmetric for the type T thermocouple and theoretical expressions derived to predict the frequency response must reflect these features.

The theoretical analysis of a supported thermocouple assumes that the radial temperature gradients in a wire cross section are negligable. In this case the heat conduction is one - dimensional down the axis of the wire. Schematics of both a one and two material supported wire are represented in figure 2. Here, wire diameters and lengths are illustrated and their values are listed in table 1.

The positive lead for both the type K and T thermocouples is positioned on the left of the junction in fig. 2 as indicated at the bottom of table 1. If the material properties are nearly equal across the junction, as is the case for a type K thermocouple, one can define two natural frequencies for wire regions 1 and 2 in fig. 2 where $\omega_1 = 4h_1/\rho c D_1$ and $\omega_2 = 4h_2/\rho c D_2$. For the type T thermocouple,

however, there are four natural frequencies. For example, two of these frequencies are $\omega_1 = 4h_1/\rho_1 c_1 D_1$ and $\omega_2 = 4h_1/\rho_2 c_2 D_1$ on both sides of the junction.

3.2.3 Construction

Thermocouple wire of the desired length and type was threaded into the ceramic with the thermocouple end last. Three or four kinks were made in each wire near the thermocouple end so the wire must be firmly pulled into the tube leaving enough wire sticking out to make the thermocouple. Drops of epoxy were picked up with a piece of .010 in. diameter wire, added to the ceramic tube at A (see fig. 3) and pushed down around both wires. The kinks and epoxy firmly fasten the wires in the ceramic so they do not twist when the free ends are manipulated for electrical connections.

The junction at B in fig. 3 was made by cutting the large wire about half way through with a razor blade, laying the small diameter wire in the cut, and silver soldering the cut closed. After the solder, the excess wire ends that protrude through the soldered area were bent and broken off to clean up the junction.

The type T thermocouple junctions at C in fig. 3 were constructed successfully by one of two procedures. In the first procedure, the silver solder wire was coated with flux and the end heated with a torch until a drop formed. A twisted pair of thermocouple wires was pushed briefly into the flux coated solder drop. The solder wetted the pair up to where the twist stops. Using a razor blade and tweezers under a microscope, the thermocouple was bent and trimmed until collinear. The silver solder technique was also used to fabricate the chromel alumel (type K)

thermocouples.

In the second procedure, the thermocouple junctions were fabricated by the Research Instrumentation Branch at the NASA Lewis Research Center. In this case, the wires were cut with a razor blade to produce a flat edge perpendicular to the wire axis. The wires segments were then mounted in a fixture such that the two faces of the junction were held together by springs. The junction was then formed by laser heating. The laser used was a KORAD model KWD Nd: YAG laser, operating at a wave length of 1060 namometers. The power settings depend on the wire size and material, but for the thermocouples described in this report, a pulse duration of 4 ms was used delivering a total energy of approximately 2 joules. One example of a type T junction (D = 76 μm) formed by laser heating are shown in fig. 4.

For the chromel alumel couples (type K), the junction at C in fig. 3 could also be fabricated using a stored energy spot welder. In this case, the wires were crossed and welded and then trimmed with a razor blade and bent with tweezers under a microscope until collinear. This method proved to be unsuccessful, however, since an apparent contact resistance was created by the procedure and the dynamic response of the thermocouple was inadequate.

3.3 EXPERIMENTAL APPARATUS

In the present experiment, thermocouple sensors are exposed to a constant velocity air stream (<19 m/sec) of varying temperature. In particular, the dynamic response of the thermocouple is measured for a square wave temperature profile

of varying frequency. A rotating wheel configuration is used to deliver the test air stream to the proposed sensors. A similar experimental apparatus was described in detail by Elmore et al. (1986).

A schematic of the rotating wheel apparatus used in the present experiment is shown in fig. 5. As the wheel rotates, holes pass the two air supply tubes (3/4 in. ID copper) that allow slugs of hot $(\leq 55^{\circ}C)$ and cold (~30°C) air to alternately enter a transition tube assembly mounted directly above the rotating wheel. In the transition tube the slugs of hot and cold air coalesce into a single air stream providing roughly a square wave temperature profile covering a range of gas temperature frequencies from roughly 1 to 30 Hz. A 3/4 in. to 1/2 in. smooth copper adaptor was inserted at the end of the coalescing tube (location of thermocouple) in fig. 5 to increase the air velocity to 18 m/sec.

The analog temperature signal is digitized with a Data Translation DT-2801 A/D board mounted in an expansion slot of an IBM AT compatible computer as shown in fig. 5. ASYST software was loaded onto the hard disc of the personal computer and this provided a flexible system for data storage, manipulation and display. The true temperature profile of the airstream is measured with a constant current anemometer (TSI 1054-A) and sensor (1226 PI2.5).

3.4 EXPERIMENTAL PROCEDURE

3.4.1 Calibration

The air velocity at the exit of the coalescing tube in fig. 5 (location of thermocouple) was maintained at roughly 17.5 to 18 m/sec. The voltage regulator

was adjusted such that the temperature of the hot line was maintained at an elevated temperature of $\leq 55°C$. One hole of the rotating wheel was positioned in a stationary position over the unheated line. The voltage output from both the thermocouple and constant current anemometer were recorded at the input terminals to the A/D board. The true temperature was also recorded with a thermometer suspended in the high velocity air stream. This procedure was repeated for several temperatures with the hole positioned over the hot line covering an air temperature range from 30°C to 55°C. It was found that both type K and T thermocouples had a constant calibration factor (°C/volt) over the small temperature range. The constant current anemometer, however, provided a non-linear response with the calibration factor varying with air temperature. Thus, a least square curve fit was determined to provide the gas temperature with the anemometer output. The calibration factors described above were then installed on the ASYST data acquisition software.

The thermocouple and constant current anemometer are mounted in the constant velocity air stream with both sensing elements parallel and separated by approximately 1 mm. The period or frequency of the square wave temperature profile is controlled over the range from 1.5 to 30 Hz with adjustment of the motor connected to the rotating wheel shaft.

3.4.2 Data Acquisition

ASYST software was developed to acquire temperature data sequentially from the thermocouple and constant current anemometer. The data are digitized for

two channels at a sampling rate of 512 Hz per channel for a total sample time of two seconds. An example of the gas temperature profile for a square wave frequency of 2.5 Hz is illustrated in fig. 6 where the smooth profile is the thermocouple response. After data acquisition, the Fast Fourier Transform (FFT) is taken for each channel. The largest peak (first harmonic) in the amplitude of the FFT is located for each channel which provides the frequency of the temperature profile. The ASYST software also records the amplitude ratio and phase angle between both channels at the first harmonic. In the latter case, the software corrects the phase angle for the conversion delay between channels. The amplitude ratio and phase angle are recorded for each frequency setting of the rotating wheel.

3.4.3 Data Correlation

Once the amplitude ratio and phase angle are recorded for a large number of gas temperature frequencies ω for a given thermocouple, the amplitude ratio and phase angle are plotted on separate graphs. Both quantities are plotted as a function of the ratio of the angular frequency of the square wave temperature profile ω to the natural frequency ω_1 of the positive thermocouple element. The natural frequency $\omega_1 = 4h_1/\rho_1 C_1 D_1$ is chosen to fit the amplitude ratio at large frequencies since the amplitude ratio should coincide with the first order response (independent of axial heat conduction) at large ω.

The lengths of the thermocouple element l and support wire L are then chosen such that theoretical predictions of the amplitude ratio are correlated with the

data at low gas temperature frequency ω. The remaining parameters representing wire diameters and material properties were recorded from the literature and the manufacture's specifications. These values were also introduced into the analytical expressions used to predict both the amplitude ratio and phase angle.

Theoretical predictions of the amplitude ratio and phase angle are plotted along with the data. For the type K thermocouples the material properties are assumed to be equal across the junction with the average values of the thermal diffusivity α and the product of the density and heat capacity ρc listed in table 1. Predictions of the amplitude and phase angle for the type K thermocouple were derived from the expression representing the frequency response (Forney and Fralick, 1991)

$$T(0) = \frac{\frac{1}{G_2}(\cosh q_2 L - 1) - \frac{1}{G_1}\cosh q_2 L}{\cosh q_1 l \cosh q_2 L + Q \sinh q_1 l \sinh q_2 L} + \frac{1}{G_1}. \tag{3.1}$$

where

$$Q = \frac{D_1^2 q_1}{D_2^2 q_2}$$

and

$$q_n = \sqrt{\frac{G_n}{\gamma_n}}, \quad \gamma_n = \frac{\alpha}{\omega_n}, \quad G_n = 1 + i(\omega/\omega_n), \quad \omega_n = \frac{4h_n}{\rho c D_n}.$$

Here, the subscripts 1 and 2 refer to the wire elements in the one-material schematic of figure 2 and $T(0) = |T(0)| \exp(i\Phi)$ where $|T(0)|$ is the amplitude ratio and Φ is the phase angle.

Theoretical predictions of the amplitude ratio and phase angle for the type T thermocouple were derived from the expression

$$T(0) = \frac{1}{\Delta_1}\left\{ Q_t \sinh q_2 l\left[T_a + \frac{1}{G_1}(\cosh q_1 l - 1)\right] + \sinh q_1 l\left[T_b + \frac{1}{G_2}(\cosh q_2 l - 1)\right]\right\} \quad (3.2)$$

where

$$Q_t = \frac{k_1 q_1}{k_2 q_2}$$

and

$$\Delta_1 = Q_t \cosh q_1 l \sinh q_2 l + \cosh q_2 l \sinh q_1 l \ .$$

The boundary temperatures T_a, T_b in Eq. (3.2) are given by the expressions

$$T_a = \frac{1}{G_3} + \left\{ \sinh q_3 L\left[\left(\frac{1}{G_4} - \frac{1}{G_3}\right)\cosh q_4(l+L) - \frac{1}{G_4}\right]\right.$$

$$\left. - \frac{1}{G_3}\left[Q_s \cosh q_3 l \sinh q_4(l+L) + \cosh q_4(l+L)\sinh q_3 l\right]\right\}\left(\frac{1}{\Delta_2}\right) \quad (3.3)$$

and

$$T_b = \frac{1}{G_4} + \left\{ Q_s \sinh q_4 L\left[\left(\frac{1}{G_3} - \frac{1}{G_4}\right)\cosh q_3(l+L) - \frac{1}{G_3}\right]\right.$$

$$\left. - \frac{1}{G_4}\left[\cosh q_4 l \sinh q_3(l+L) + Q_s \cosh q_3(l+L)\sinh q_4 l\right]\right\}\left(\frac{1}{\Delta_2}\right) \quad (3.4)$$

where

$$Q_s = \frac{k_1 q_3}{k_2 q_4}$$

$$\Delta_2 = Q_s \cosh q_3(l+L)\sinh q_4(l+L) + \cosh q_4(l+L)\sinh q_3(l+L)$$

Here, the wire elements 1 to 4 are shown in the schematic of a two-material thermocouple wire shown in figure 2.

3.5 RESULTS AND DISCUSSION

A type K thermocouple was silver soldered with a thermocouple element length of l = 0.9mm and a support wire length of L = 2.2mm. The thermocouple and support wires had diameters of $D_1 = 76\mu m$ and $D_2 = 380\mu m$, respectively. The amplitude ratio and phase angle were measured over a range of temperature square wave frequencies of 1.3 to 35 Hz and these data are plotted in figure 7. The data are also compared with the theoretical predictions derived from Equation (1).

A value of the natural frequency ω_1 was chosen to correlate the data when $\omega/\omega_1 > 1$. The value of ω_1 chosen was within 10% of the predicted value based on the air velocity and thermocouple wire diameter. As indicated in figure 7, all of the data are correlated with the theory to within 10%. It should also be noted that a small bead did exist at the junction with a diameter less than twice the diameter of the thermocouple element wire. Moreover, the attenuation of the signal because of axial heat conduction is properly accounted for with the theory provided the wire length l is increased in Eq. (3.1) by 20% to account for the bead at the junction.

A type T thermocouple junction was purchased from Omega Engineering and the thermocouple wire was silver soldered at the support legs. This thermocouple had an element length of l = 1.25mm and a support wire length of 2.2mm. The thermocouple and support wires had diameters of $D_1 = 76\mu m$ and $D_2 = 380\mu m$, respectively. The amplitude ratio and phase angle were measured over a range of temperature square wave frequencies of 1.3 to 30 Hz and these data are plotted in figure 8. The data are also compared with the theoretical predictions derived from

Equation (3.2).

A value of the natural frequency $\omega_1 = 20\,\mathrm{sec}^{-1}$ was chosen to correlate the data for the amplitude ratio at large frequencies $\omega/\omega_1 > 1$. As indicated in figure 8, the data for the amplitude ratio drift below the theoretical prediction by 10% for increasing gas temperature angular frequencies ω. Although the effect of axial heat conduction is properly accounted for in figure 8, the phase angle data also appear to be distorted and to lie significantly below the predictions. These effects are apparently due to the large bead diameter at the junction (greater than twice the diameter of the thermocouple wire). Here, as before, it was necessary to increase the wire length in Eq. (3.2) by 20% to correlate the data.

A type T thermocouple junction without a bead was constructed by laser heating with the support legs silver soldered, as before. The thermocouple had an element length of l = 1.25 mm and a support wire length of 2.5 mm. The thermocouple and support wires had diameters of D_1 = 76 μm and D_2 = 380 μm, respectively. The amplitude ratio and phase angle were measured and the results were compared with theory.

A value of the natural frequency $\omega_1 = 28\,\mathrm{sec}^{1}$ was necessary to correlate the amplitude data at large frequencies. This represents a larger air velocity compared to the data in figure 8. As shown in figure 9, there appears to be less drift in the amplitude ratio below the theory compared to the previous results taken with a beaded junction. An improved correlation is also observed for the phase angle data plotted in figure 9. The predicted phase angle from Equation (3.2) correlates the data well and there appears to be less distortion of the phase angle data

compared to the previous results with a bead at the juction. Moreover, no adjustments were necessary in the theory to correlate the data.

Finally, a type T thermocouple junction was constructed with silver solder on a twisted pair of thermocouple wires. The junction consisted of a twisted pair of soldered thermocouple wires 1.0 mm in length that was bent perpendicular to the axis of the wire elements suspended between the support legs. The wire element length was l = 1.3 mm and the length of the support leg was L = 2.2 mm, as before. This thermocouple configuration was constructed to determine the effect of an extremely large beas size on the frequency response.

The amplitude ratio and phase angle for the beaded type T thermocouple are plotted in figure 10. As indicated in figure 10, the amplitude is larger than predicted at low frequencies since the extended exterior surface of the bead (fin) enhances the rate of heat transfer to the junction. At large frequencies, $\omega/\omega_1 > 1$ however, the smaller area - to - volume ratio decreases the natural frequency of the bead configuration relative to a beadless cylinder and the amplitude data fall below the theory. More difficult to describe is the distortion in the phase angle data. As indicated in figure 10, the phase angle is shifted to larger values relative to the theory.

3.6 CONCLUSIONS

Supported type K and type T thermocouple wires were constructed. The thermocouple element $(D = 76\mu m)$ and wire support $(D = 380\ \mu m)$ lengths were approximately 1.0 and 2.0 mm, respectively. Measurements of the amplitude ratio

and phase angle that reflect the effects of axial heat conduction are correlated to within 10% with the theoretical predictions of Forney and Fralick, (1991). To correlate the experimental data, it is necessary to choose a natural frequency ω_n (depends on gas properties and velocity) for the amplitude data at large gas temperature frequencies. If there is a bead at the junction (typically twice the wire diameter), it is necesary to increase the wire length l by 20% in the theory to correlate the data.

The use of silver solder for the junction and wire supports is adequate for both the type K and type T thermocouples but will leave a small bead. A spot welding procedure for the type K thermocouple, however, appears to introduce a large contact resistance since the measured amplitude ratio in this case was only a fraction of its predicted value. The use of laser heating to form the junction, however, left no bead and required no adjustments to the wire length in the theory to correlate the data. Moreover, the use of laser heating for the purpose of fabricating thermocouple junctions without beads appears to improve the correlation of both the amplitude ratio and phase angle data with theory. In particular, the phase angle data from a beadless junction exhibited far less distortion compared to theoretical predictions. Also, the wire lengths used in the theory to correlate the data were realistic for the laser heated junctions.

It is found that a large bead at the thermocouple junction increases the amplitude ratio at low frequencies but decreases the natural frequency of the wire. The phase angle data are also distorted for imperfect junctions.

3.7 NOMENCLATURE

c	=	material specific heat $\left(J-gm^{-1}-{}^{0}K^{-1}\right)$
D	=	thermocouple wire diameter (cm)
G	=	$1+i(\omega/\omega_n)$
h	=	heat transfer coefficient $\left(J-cm^{-2}-s^{-1}-{}^{0}K^{-1}\right)$
i	=	unit imaginary number $\left(=\sqrt{-1}\right)$
k	=	material thermoconductivity $\left(J-cm^{-1}-s^{-1}-{}^{0}K^{-1}\right)$
l	=	length of small thermocouple element wire (cm)
L	=	length of large thermocouple support wire (cm)
Q	=	$\frac{D_1^2 q_1}{D_2^2 q_2}$
Q_t	=	$\frac{k_1 q_1}{k_2 q_2}$
Q_s	=	$\frac{k_1 q_3}{k_2 q_4}$
q	=	$(G/\gamma)^{.5}$
T	=	steady-state frequency response
x	=	axial distance from junction of wire (cm)

Greek Symbols

α	=	thermal diffusivity $\left(cm^2-s^{-1}\right)$
γ	=	$\alpha/\omega_n(cm^2)$
ω	=	angular frequency $\left(s^{-1}\right)$

ω_n = natural frequency of wire $(= 4h / \rho cD)(s^{-1})$

Φ = phase angle

ρ = material density (gm/cm^3)

Δ_1 = dimensionless function

Δ_2 = dimensionless function

3.8 REFERENCES

1. Dils, R. R. and Follansbee, P. S., Wide Bandwidth Gas Temperature Measurements in Combustor and Combustor Exhaust Gases, Instrumentation in the Aerospace Industry, 21 (B. Washburn, ed.), ISA 76245 (1976).

2. Elmore, D. L., Robinson, W. W. and Watkins, W. B., Dynamic Gas Temperature Measurement System: Final Report, NASA CR-168267 (1983).

3. Elmore, D. L., Robinson, W. W. and Watkins, W. B., Further Development of the Dynamic Gas Temperature Measurement System: Vol. I - Technical Efforts, NASA CR-179513 (1986).

4. Forney, L. J. and Fralick, G. C., Frequency Response of a Thermocouple Wire: Effects of Axial Heat Conduction, Int. Comm. Heat Mass Transfer, 18, 531(1991).

5. Fralick, G. C., Correlation of Velocity and Velocity-Density Turbulence in the Exhaust of an Atmospheric Burner, Turbine Engine Hot Section Technology - 1985, NASA CP-2465, pp. 81-85.

6. Forney, L. J. and Fralick, G. C., and Frequency Response of a Supported Thermocouple Wire: Effects of Axial Heat Conduction, Progress Report Georgia Tech E-19-666-2, April (1991).

7. Scadron, M.D. and Warshawsky, I., Experimental Determination of Time Constants and Nusselt Numbers for Bare-Wire Thermocouples in High Velocity Air Streams and Analytic Approximation of Conduction and Radiation Errors, NACA TN-2599 (1952).

8. Touloukian, Powell, Ho and Clements, (ed.), Thermal Physical Properties of Matter, Purdue Research Foundation, Plenum Pub. (1970).

3.9 TABLES AND FIGURES

Table 1 Properties of Thermocouples

Dimensions (cm)

D_1	D_2	D_2/D_1	1	L
.0076	.038	5	.1-.15	.17-.22

Properties of Type K

	$\rho c\left[\frac{J}{cm^3-^\circ K}\right]$	$\alpha\left[\frac{cm^2}{\sec}\right]$
Chromel	3.80	.048
Alumel	4.10	.070
Average	3.95	.059

Properties of Type T

	$\rho c\left[\frac{J}{cm^3-^\circ K}\right]$	$\alpha\left[\frac{cm^2}{\sec}\right]$
Copper	3.44	1.16
Constantan	3.48	.067
Average	3.46	.614

Wire Location

Region	Type K	Type T
left	Chromel	Copper
right	Alumel	Constantan

SUPPORTED THERMOCOUPLE

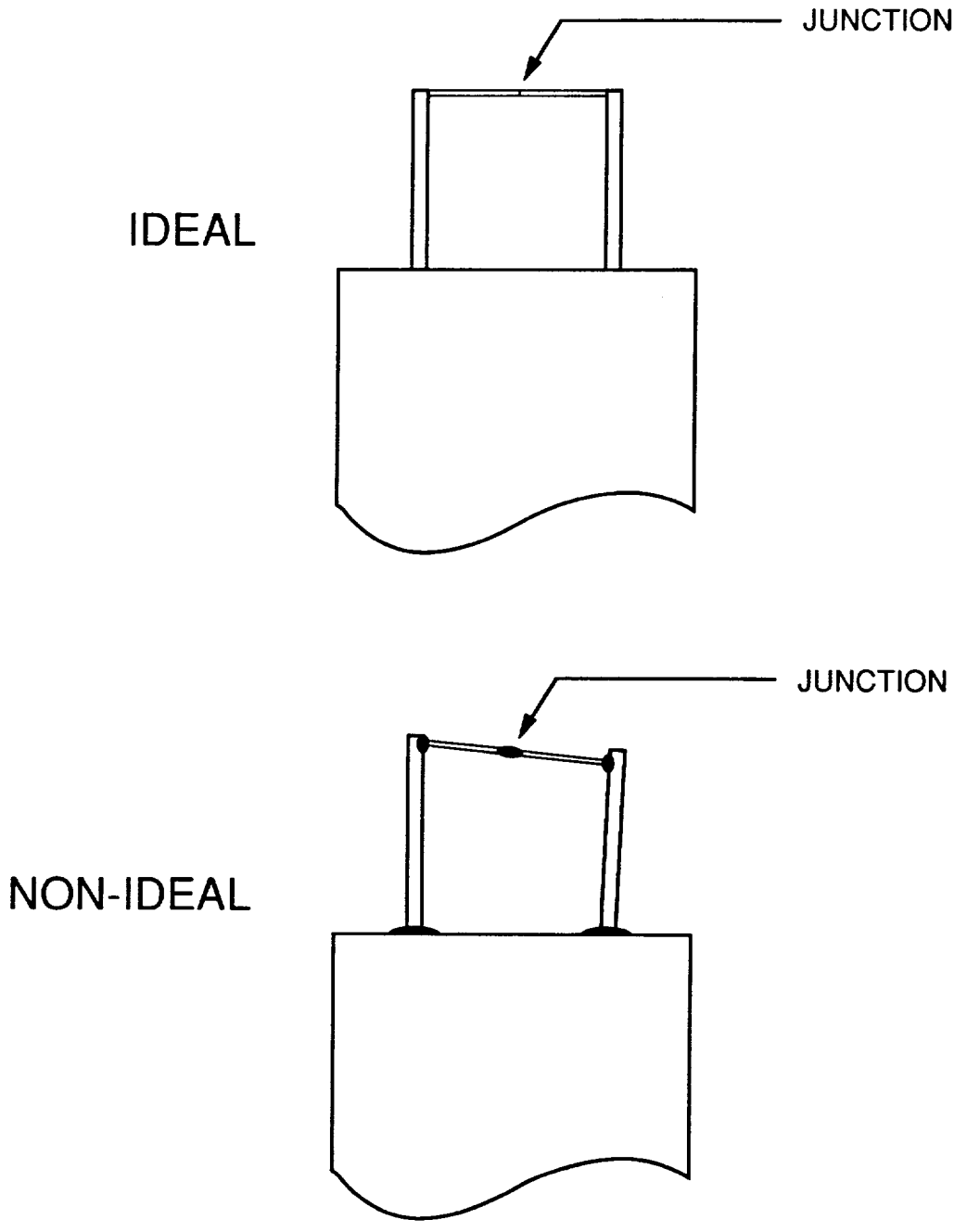

1. Schematic of Supported Thermocouple

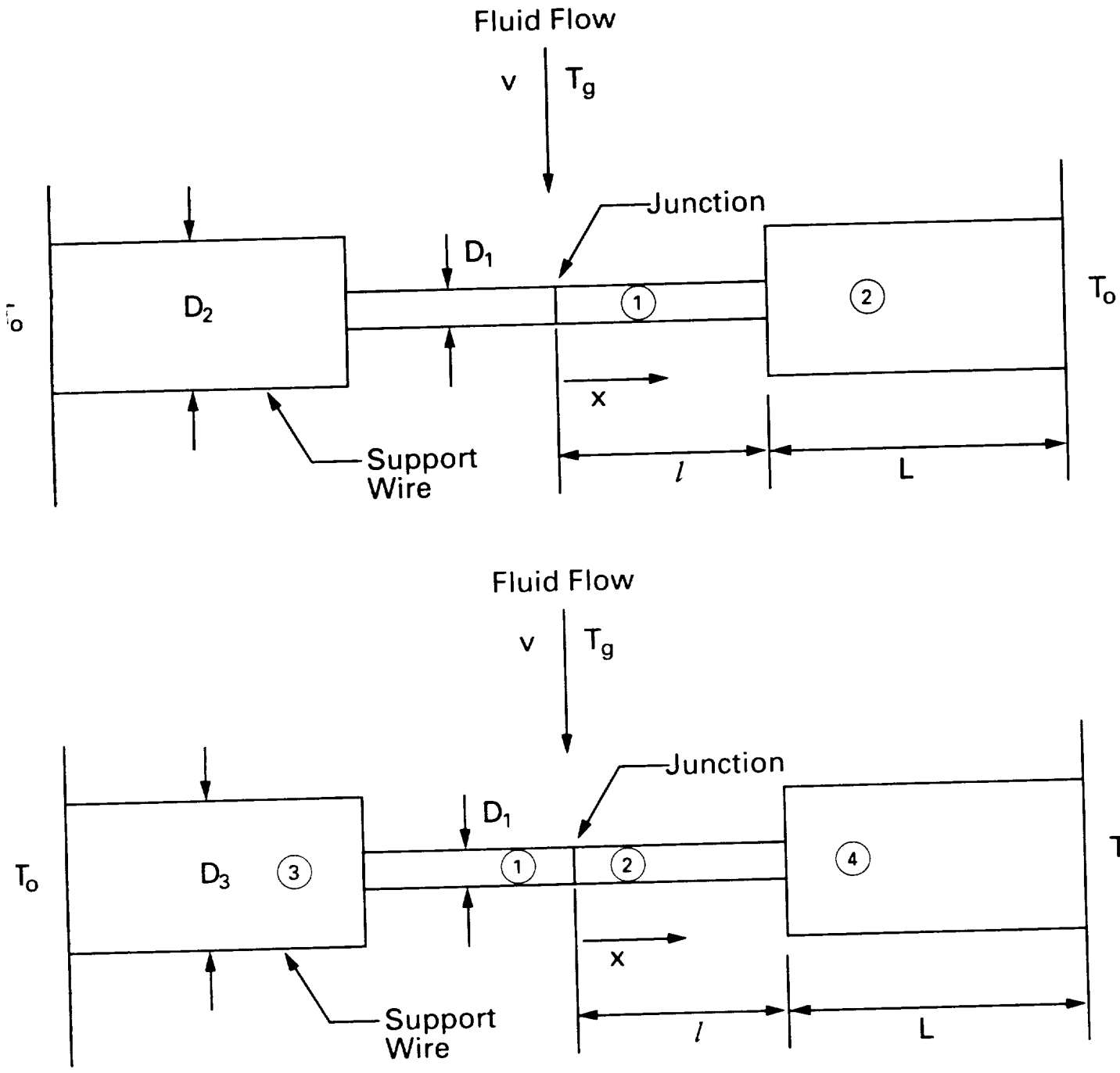

2. Schematic of One or Two Material Supported Wires

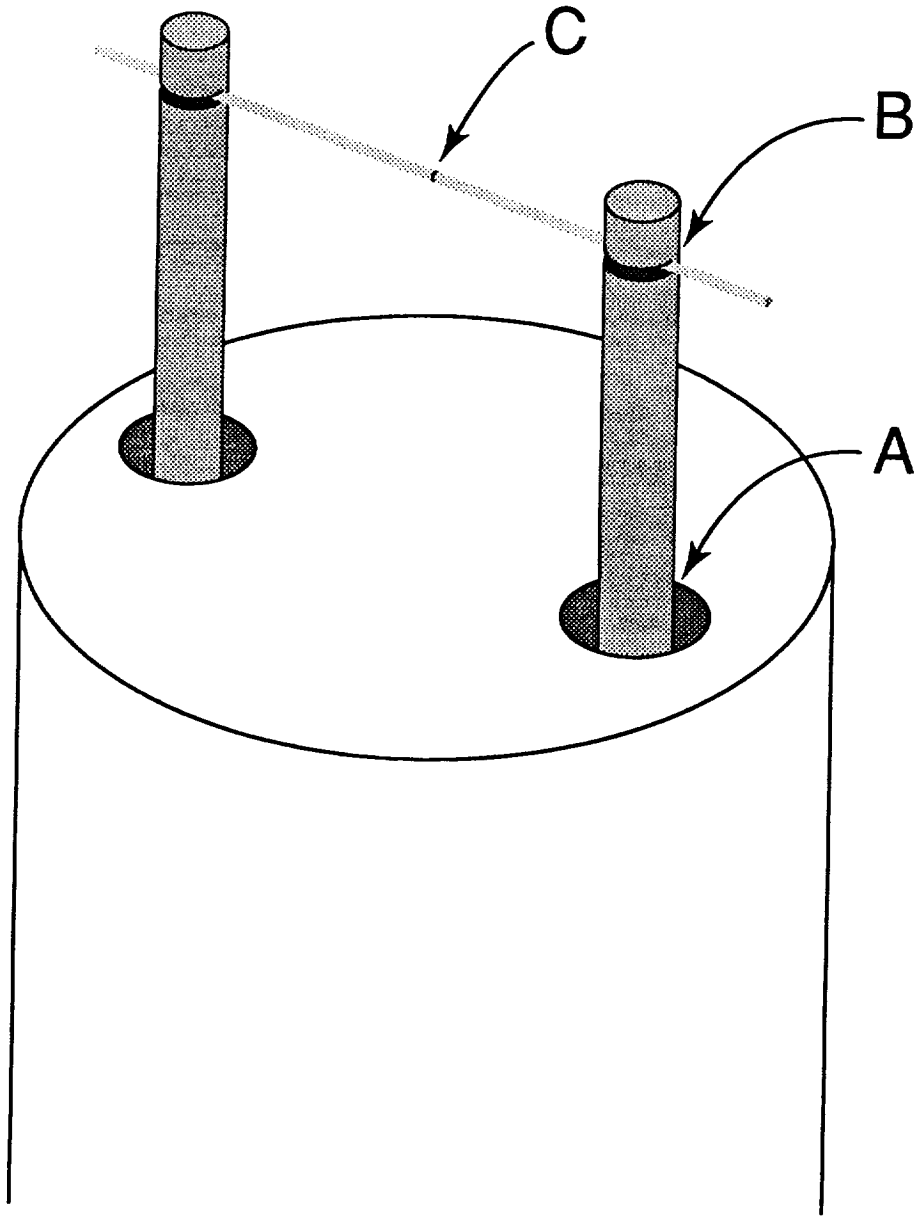

3. Configuration of Test Thermocouple

4. Photograph of a type T junction formed by laser heating. Diameter of wire is 76μm.

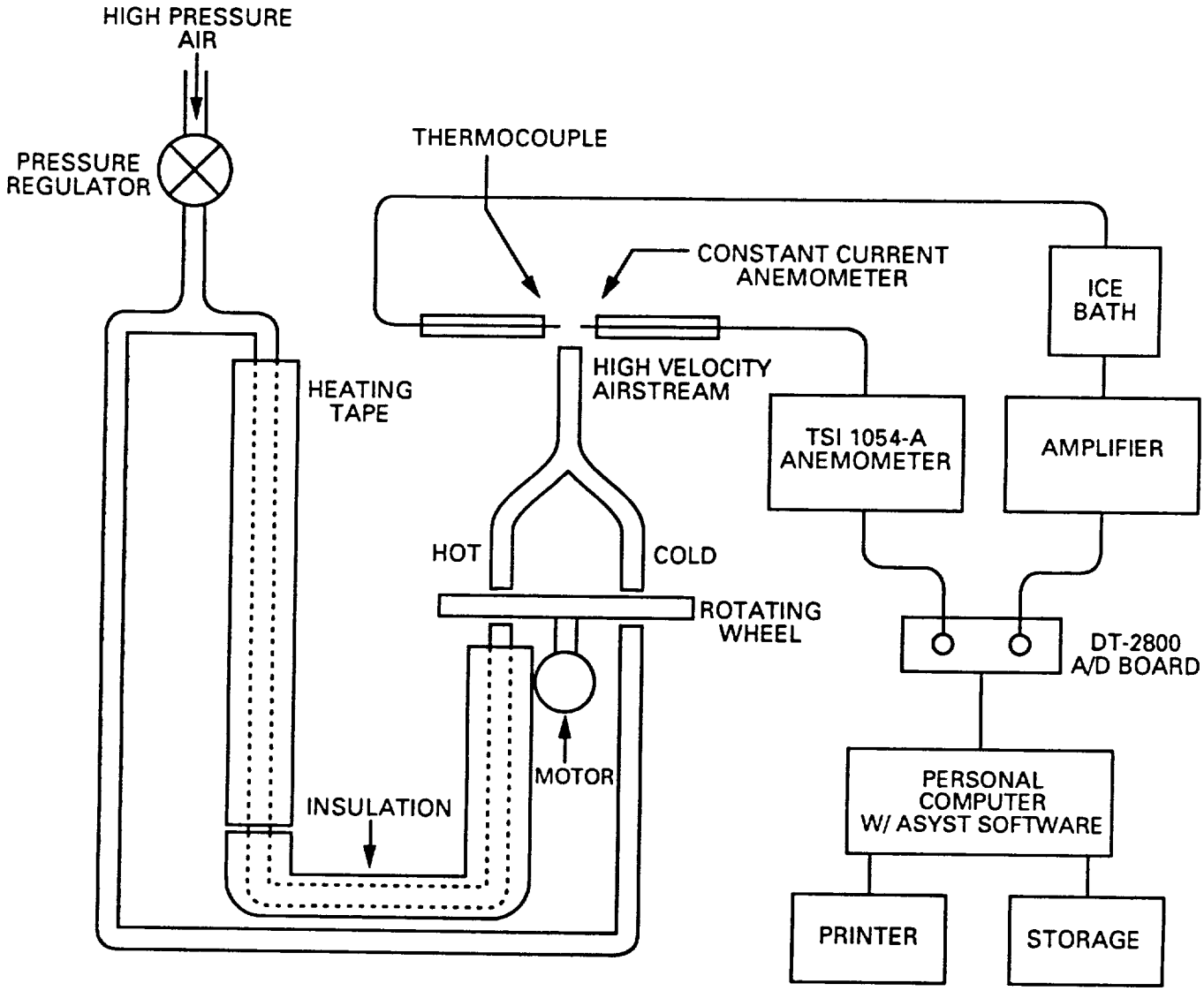

5. Schematic of Rotating Wheel Apparatus

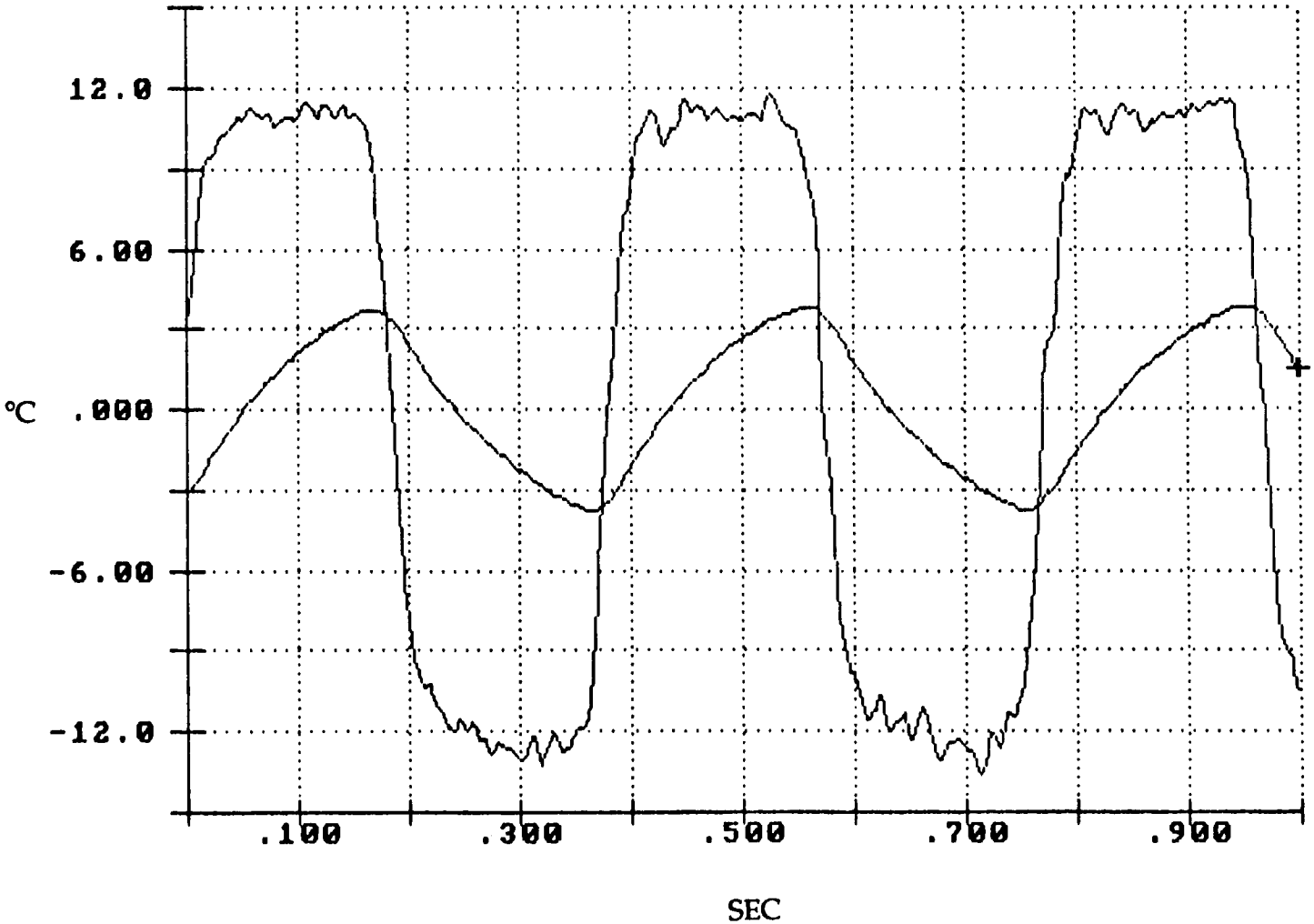

6. Gas Temperature Profile

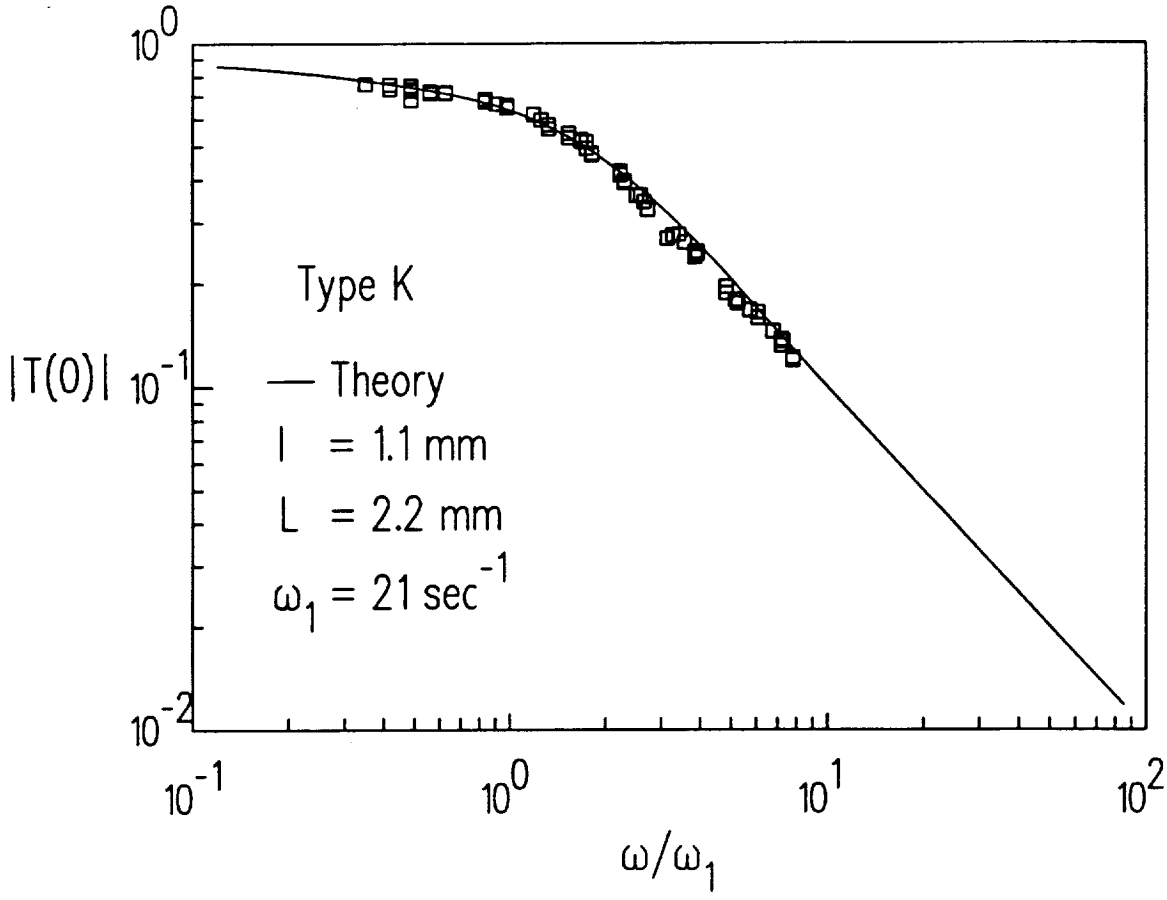

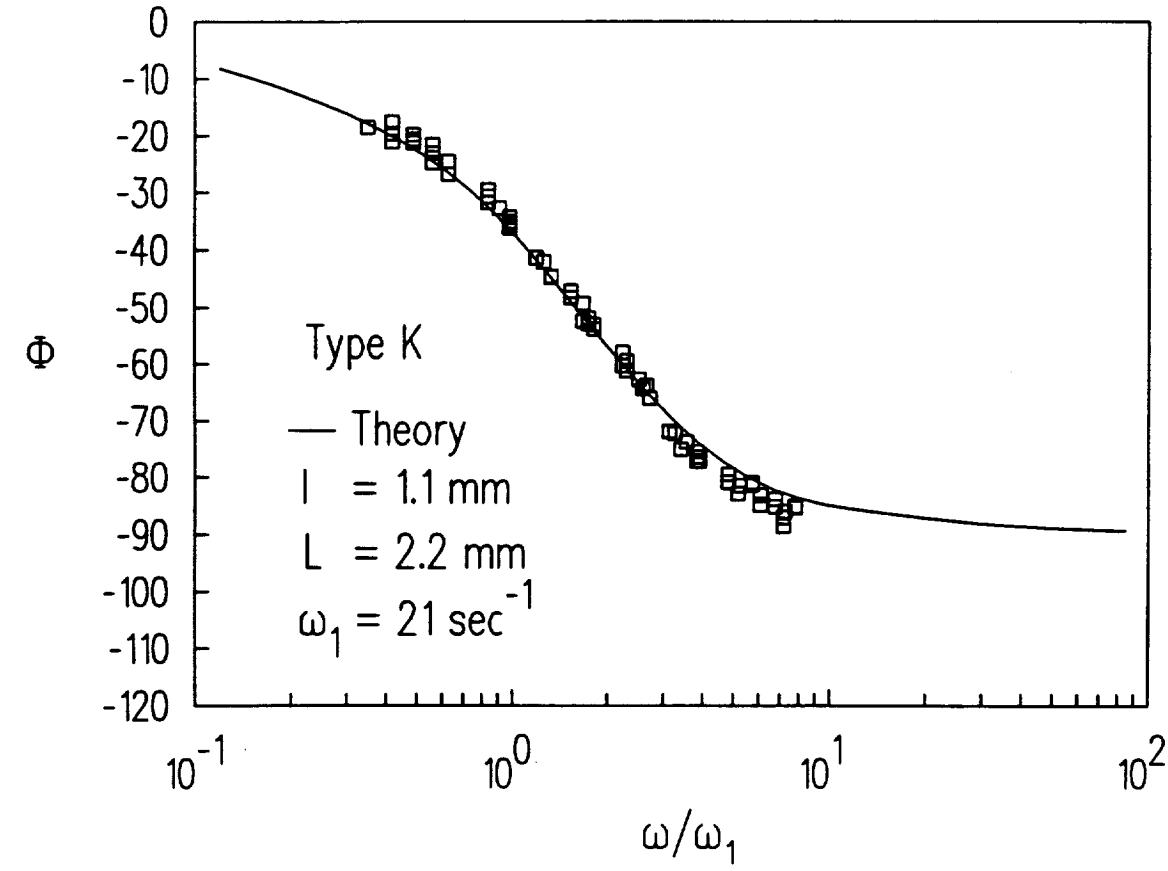

7. Amplitude Ratio and Phase Angle vs. Gas Temperature Frequency. Junction formed by silver soldering. Actual wire length: l = 0.9 mm.

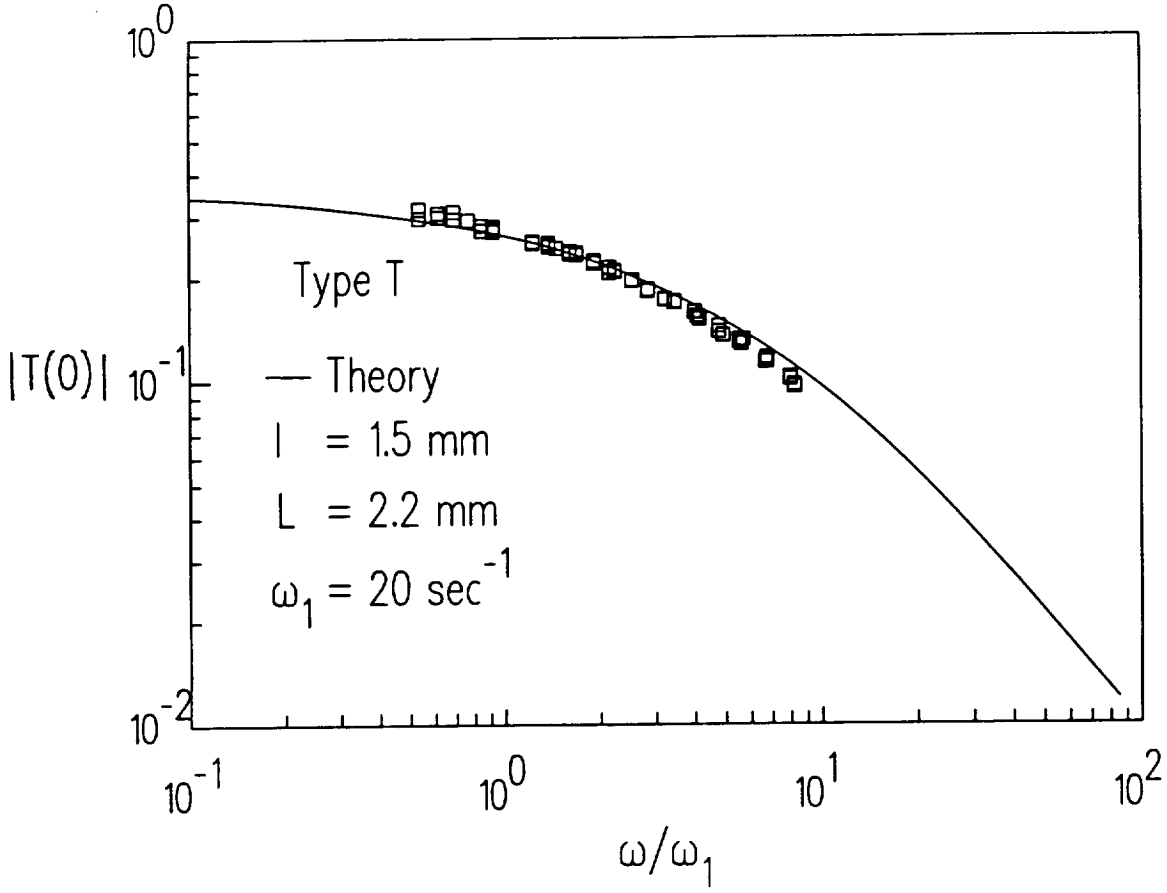

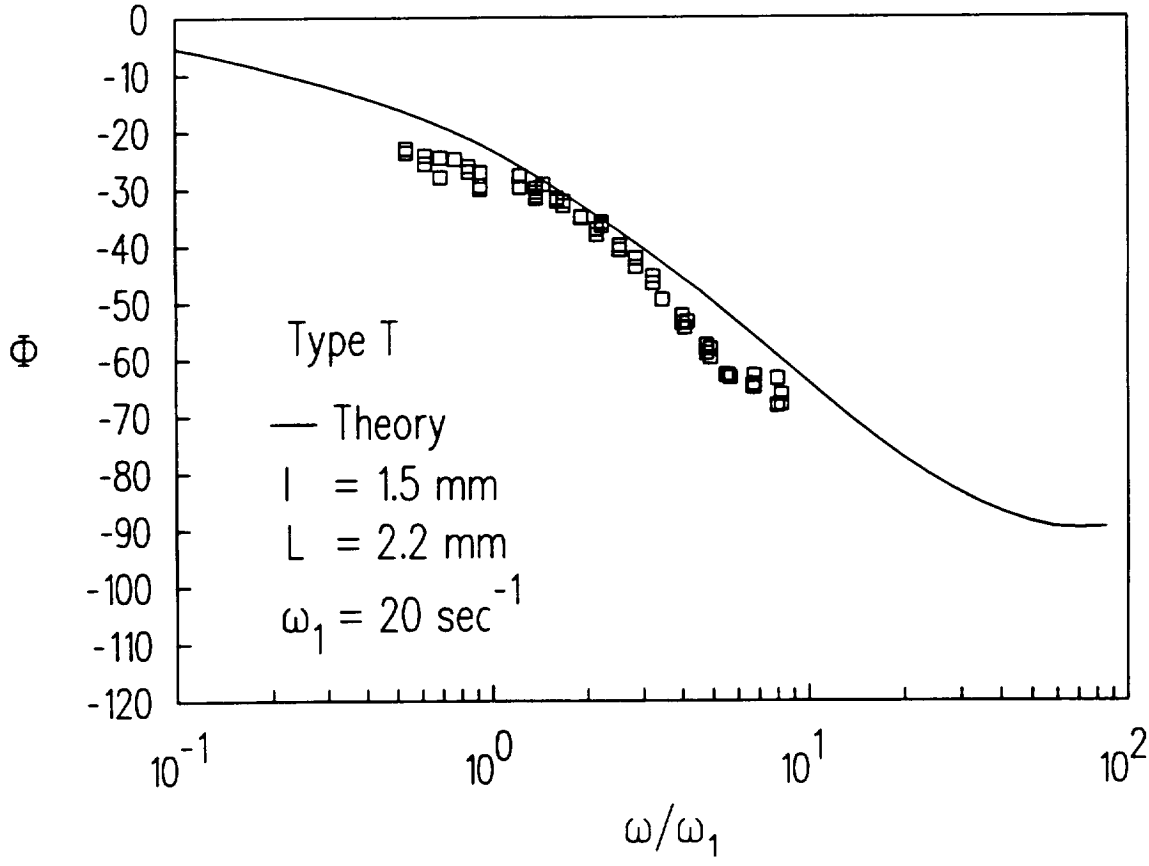

8. Amplitude Ratio and Phase Angle vs. Gas Temperature Frequency. Junction formed by Omega Engineering. Actual wire length:1 = 1.25 mm

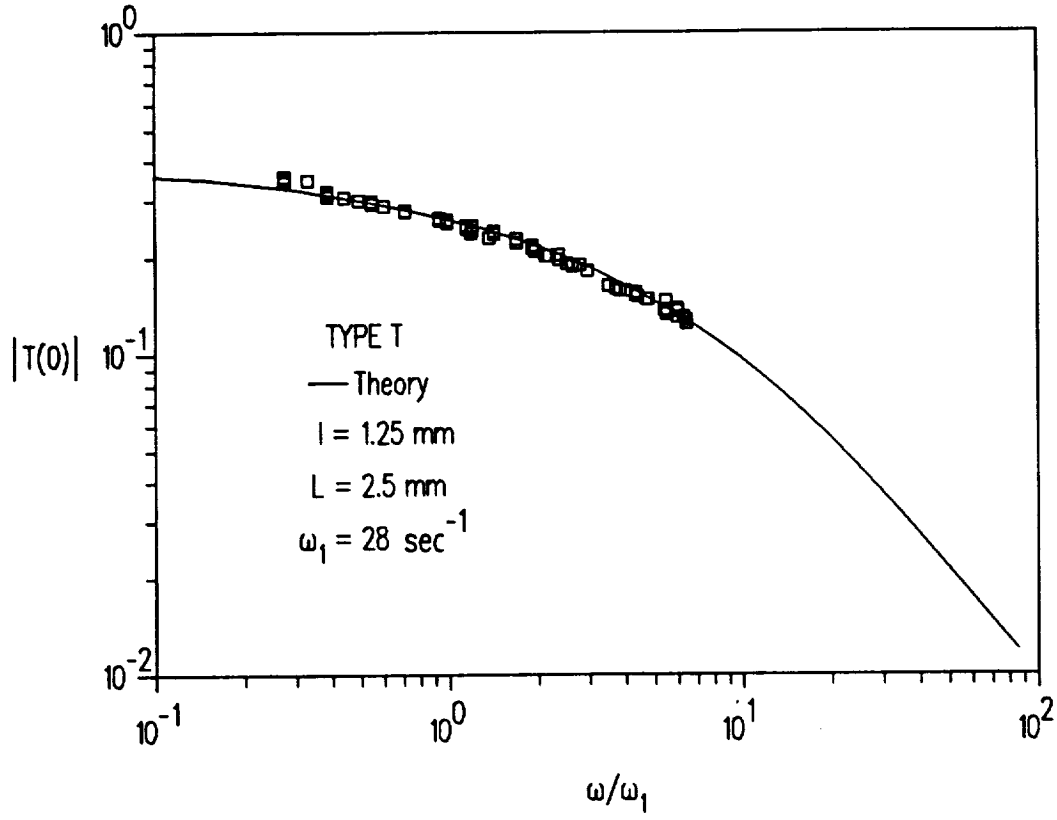

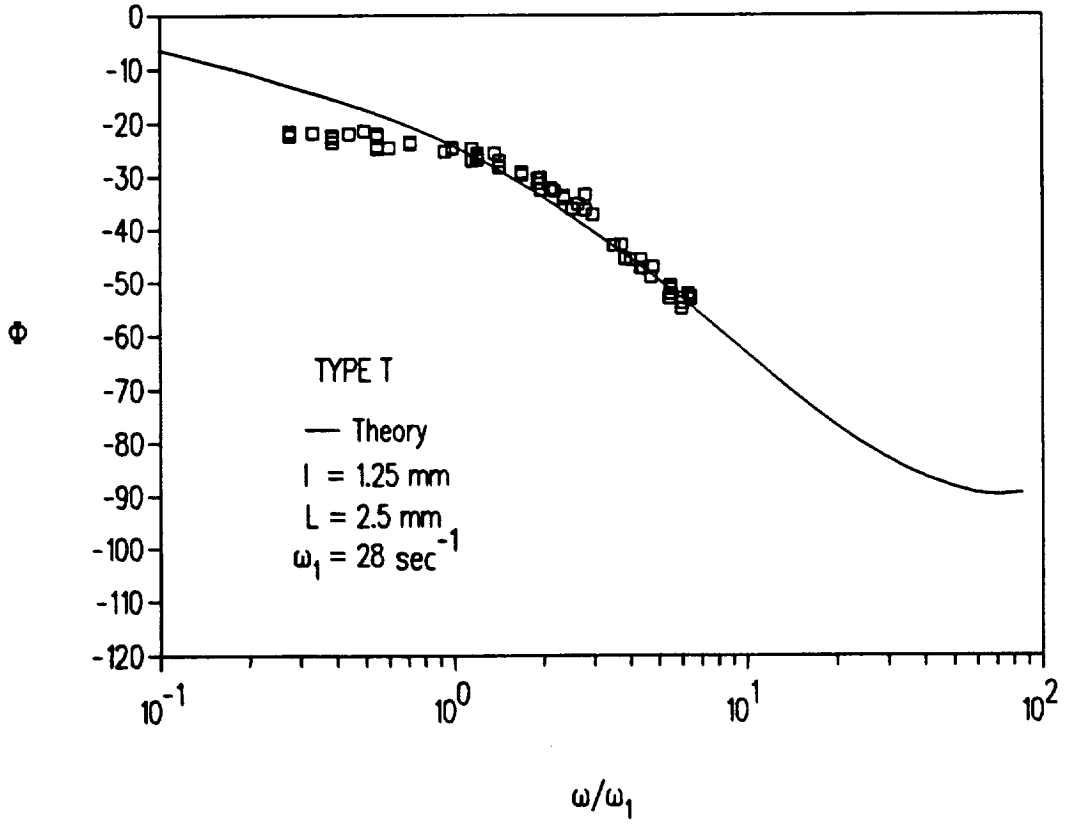

9. Amplitude Ratio and Phase Angle vs. Gas Temperature Frequency. Junction formed by laser heating. Actual wire length: l = 1.25 mm.

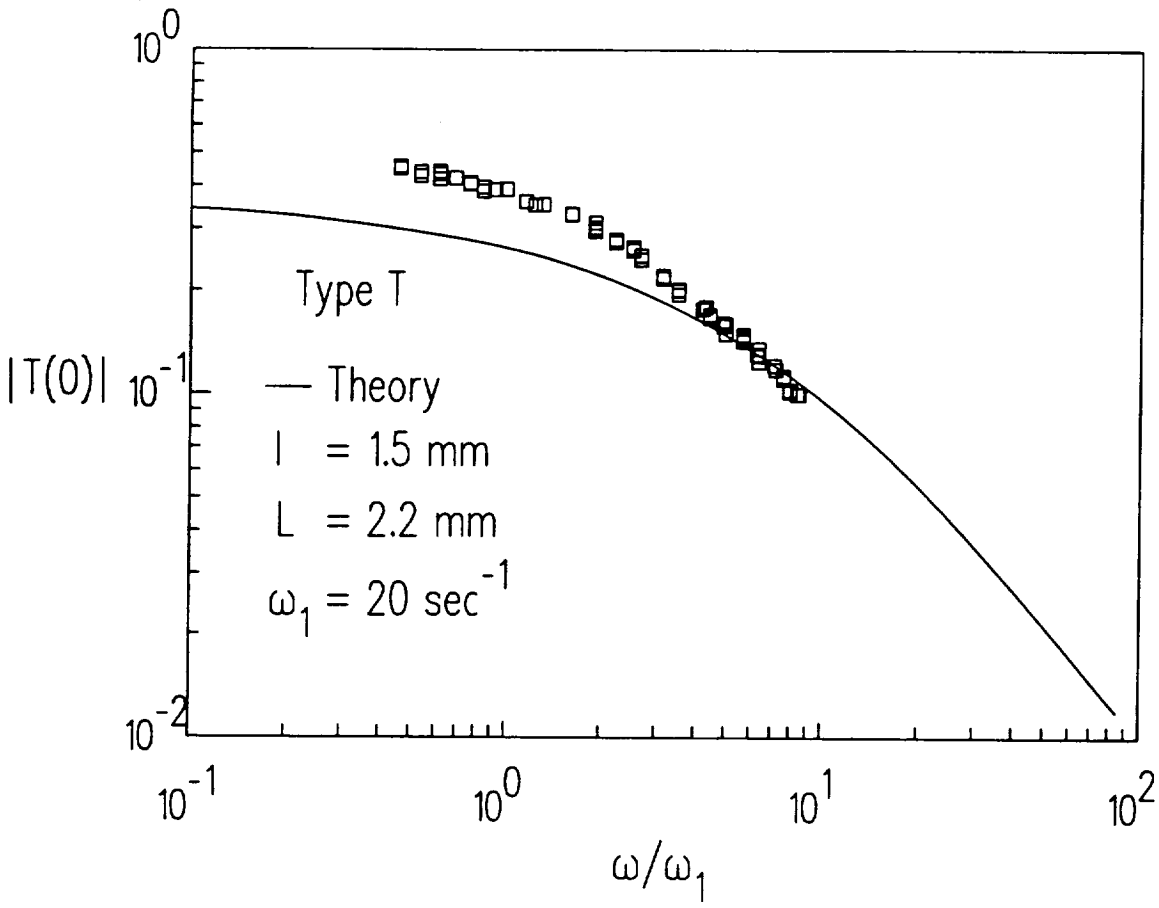

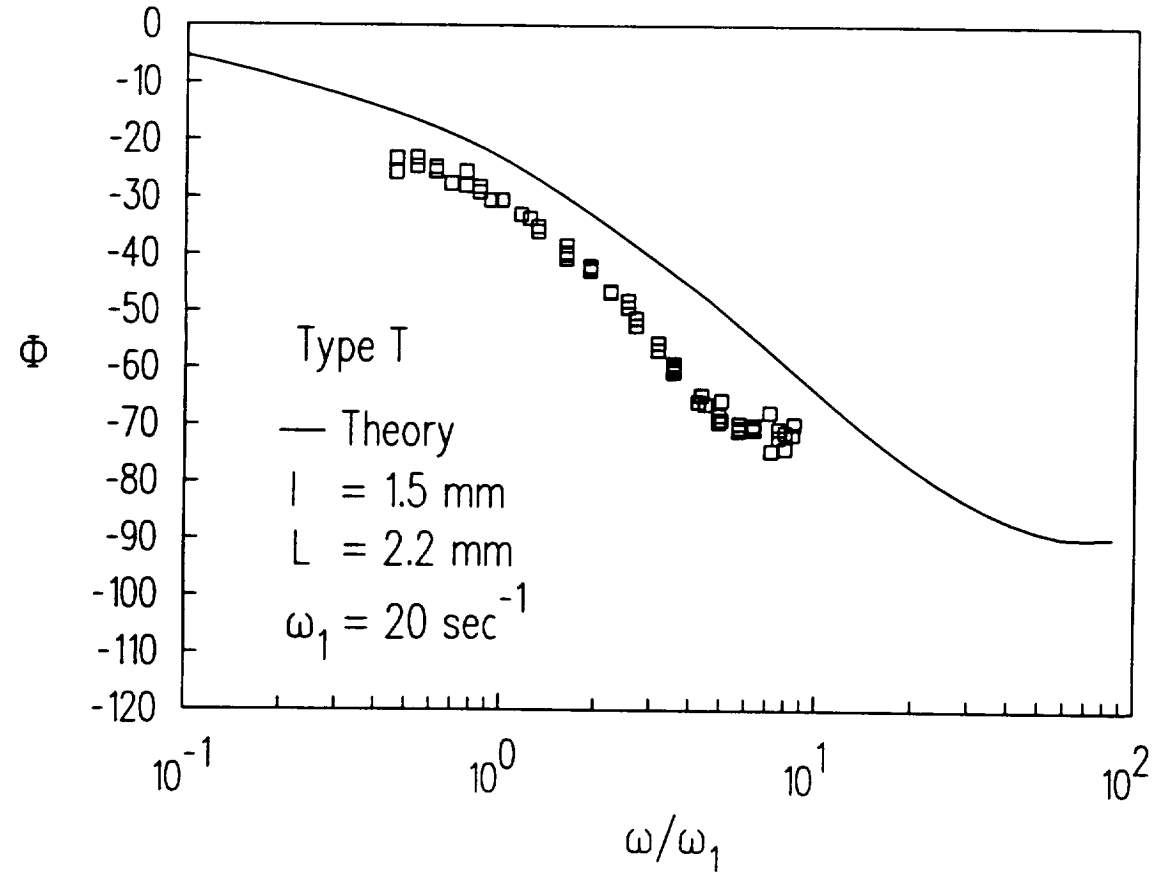

10. Amplitude Ratio and Phase Angle vs. Gas Temperature Frequency for Thermocouple with Large Bead. Actual wire length: l = 1.3 mm

118